Norwegian University of Life Sciences

Master's Thesis 2022 30 ECTS
Faculty of Science and Technology

Investigation of spatiotemporal variations in soil moisture in Søråsfeltet, Ås, applying different measurement techniques

Ida Lunde Naalsund
Environmental Physics and Renewable Energy

Abstract

Soil moisture is crucial in biological, hydrological, and meteorological processes. However, it is highly variable in both time and space, and understanding these variations is key to understand and accurately represent the related land-atmosphere interactions in numerical weather predictions (NWP). Despite increasing research on the topic, the spatiotemporal changes in soil moisture are not yet fully understood, and further research is needed for adequate representation of soil moisture in NWP.

As a part of the Norwegian Meteorological Institute's project Hydrometeorology to Operations (H2O), this thesis aims to broaden the understanding of spatiotemporal variations in soil moisture content and compare the performances of different measurement techniques. To this end, measurements of volumetric soil moisture content obtained from five different techniques applied in Søråsfeltet, Ås, have been analysed. The techniques include a manual soil sampling method, three different electromagnetic sensor types (ThetaProbe ML2, SoilVUE10, GroPoint Profile), and a cosmic-ray soil moisture probe. Time series from the manual soil sampling method and ThetaProbe ML2 were obtained during a manual measurement campaign from June to September 2021. The other sensors are permanently installed in the field, and from these, measurements from June to December 2021 have been used. In addition, a soil-specific calibration process of the GroPoint Profile sensors has been conducted and evaluated.

The different measurement techniques agreed upon the general soil moisture trends. Down to 60 cm depth, soil moisture closely followed the precipitation patterns, and precipitation was found to be a significant ($P < 0.05$) predictor of soil moisture down to 30 cm depth. At 75 cm depth, soil moisture increased only during larger precipitation events. At 100 cm depth, soil moisture only changed by 1.5 % throughout the research period.

On specific dates, the measurements from the ThetaProbe ML2 varied up to 20 % across Søråsfeltet. The spatial variability could be due to differences in soil texture or elevation across the field, but influence from buildings was also detected. However, a large variation is to be expected as over 100 ThetaProbe measurements were taken on each date. From these measurements, soil moisture variability seemed to increase with increasing soil moisture. Displaying the standard deviation of the cosmic-ray measurements as a function of the mean yielded an upward convex shape peaking around 41 %.

The SoilVUE10 sensor consistently measured lower values than the other sensors but exceeded them during heavy rainfall. The soil moisture peaks during rainfall are likely due to holes near the sensor, making the sensor come in direct contact with water and thus over-representing the soil moisture in the area. The unrealistically low values cannot be as easily explained but might partially be attributed to the sensor's location. Therefore, the sensor should be moved before any conclusion on the sensor's performance is drawn. Also, more physically sound quality controls of the permanently installed sensors are recommended to ensure reliable measurements.

The soil-specific calibration process provided for the GroPoint Profile sensors was deemed too inaccurate to give satisfactory results. In general, it is not suitable for soils with high clay content. Instead, performing the calibration on-site is recommended.

Samandrag

Fuktinnhaldet i jord er avgjerande i biologiske, hydrologiske og meteorologiske prosessar. Men, dette fuktinnhaldet er høgst variabelt i både tid og rom, og det å forstå desse endringane er essensielt for å kunne forstå og nøyaktig representere dei tilhøyrande land-atmosfære-samhandlingane i numeriske værmodellar. Trass i aukande forsking på feltet, er endringane i jordfukt i tid og rom endå ikkje heilt forståtte, og meir forsking er naudsynt for å opppnå betre representasjon av jordfukt i numeriske værmodellar.

Som ein del av Meteorologisk Institutt sitt prosjekt Hydrometeorology to Operations (H2O), har denne oppgåva som mål å utvide forståinga av endringar i fuktinnhald i jord i både tid og rom og å samanlikne ytinga til ulike målemetodar. For å oppnå dette har jordfuktmålingar frå fem ulike målemetodar anvendte på Søråsfeltet, Ås, blitt analyserte. Målemetodane inneber ein manuell målemetode, tre ulike elektromagnetiske sensorar (ThetaProbe ML2, SoilVUE10, GroPoint Profile) og ein "cosmic-ray"-sensor. Tidsseriar frå den manuelle målemetoden og ThetaProbe ML2 vart samla inn under ein manuell målekampanje frå juni til september 2021. Dei andre sensorane er installerte i feltet, og målingar frå juni til desember 2021 er henta frå desse. I tillegg har ein jordspesifikk kalibreringsmetode for GroPoint Profile-sensorane blitt utført og evaluert.

Dei ulike målemetodane var samstemde om dei generelle trendane i jordfukt. Fuktinnhaldet i jorda fulgte regnmønstra ned til 60 cm djupn, og nedbør var ein signifikant ($P < 0.05$) prediktor av fuktinnhaldet ned til 30 cm djupn. Ved 75 cm djupn auka fuktinnhaldet berre etter større nedbørhendingar. Ved 100 cm djupn varierte fuktinnhaldet berre med 1.5 % gjennom forsøksperioden.

På spesifikke datoar varierte målingane frå ThetaProbe ML2 med opp til 20 % på tvers av Søråsfeltet. Denne romlege variasjonen kan skuldast ulikskapar i jordtekstur eller høgdeforskjellar på feltet, men påverknaden av bygningar hadde også utslag på fleire av målingane. Men, ein stor variasjon innad i desse målingane er forventa, ettersom det vart teken over 100 ThetaProbe-målingar på kvar måledato. Frå ThetaProbe-målingane såg det ut til at variasjonen i fuktinnhaldet i jorda auka med aukande fuktinnhald. Ved å framstille standardavviket til "cosmic-ray"-målingane som ein funksjon av gjennomsnittleg fuktinnhald, såg ein ei konveks form med topp rundt 41 %.

SoilVUE10-sensoren målte konsekvent lågare verdiar enn dei andre sensorane, men opplevde størst auking i fuktinnhald ved store nedbørhendingar. Toppane i fuktinnhald etter nedbør skuldast mest sannsynleg hól i bakken nær sensoren som leier vatnet ned langs sensoren og dermed overrepresenterer jordfukten i området. Dei urealistisk låge verdiane kan ikkje forklarast like lett, men kan delvis skuldast plasseringa av sensoren. Difor bør sensoren flyttast før det kan trekkast konklusjonar om ytinga til han. I tillegg bør tilstrekkelege kvalitetskontrollar vere på plass for sensorane på Søråsfeltet, for å forsikre at målingane er pålitelege.

Den jordspesifikke kalibreringsprosessen gjeven for GroPoint Profile-sensorane var ikkje nøyaktig nok til å gi tilfredsstillande resultat. Generelt egnar ikkje denne metoden seg for jord med høgt innhold av leire. I staden anbefalast det at kalibreringa skjer på staden der sensoren skal installerast.

Preface and aknowledgements

This master thesis marks the end of my studies in Environmental Physics and Renewable Energy and time as a student at the Norwegian University of Life Sciences (NMBU). The thesis is a part of the Norwegian Meteorological Institute's project Hydrometeorology to Operations (H2O).

First and foremost, I want to thank Mareile Wolff and Laura Ehrnsperger for their guidance and support. Your curiousness and enthusiasm have encouraged me to go further and dig deeper into the realm of soil moisture which was completely unknown to me before starting this thesis. Therefore, a very special thanks to Attila Nemes is also due. Your expertise in soil physics and hydrology has been of invaluable help. Thank you for always taking the time and for sharing your knowledge with me.

Signe Kroken also deserves a big thanks for being the institute of physics' go-to person. Thank you for providing data, equipment and encouraging words.

Thanks to Zelalem Mengistu for providing information on the cosmic-ray sensor.

And to friends, boyfriend and family: As always, thank you for believing in me. And my dear classmates, who I've not only shared the last months with but five years here in Ås. I am so proud of us for never giving up, taking care of each other, and becoming the people we are today. I wish you all the best of luck.

Ida Lunde Naalsund

Ås, 15.05.2022

“ *We know more about the movement of celestial bodies than about the soil underfoot.* ”

Leonardo da Vinci

Contents

List of Figures

List of Tables

List of Acronyms

ADR	Amplitude domain reflectometry
H2O	Hydrometeorology to Operations
MET Norway	The Norwegian Meteorological Institute
NVE	The Norwegian Water Resources and Energy Directorate
NWP	Numerical weather prediction
TDR	Time domain reflectometry
VMC	Volumetric soil moisture content

1 Introduction

1.1 Background

Although it only constitutes 0.001 % of global water stocks, soil moisture is essential in the hydrological cycle (Shiklomanov, 1993). It controls energy and water exchange between the atmosphere and the land surface and is thus a key parameter in numerical weather prediction (NWP). It is also important in flood and landslide modelling and prediction, as antecedent soil moisture is a controlling factor of infiltration, surface run-off and soil erosion (Brocca et al., 2017). Further, soil moisture measurements can forewarn drought and floods before more standard indicators are triggered (National Oceanic and Atmospheric Administration, 2022). Soil moisture is highly variable in both time and space, and knowledge of this variability is key to understanding and predicting the aforementioned processes.

In the last 40 years, research aiming to understand the spatial and temporal variability of soil moisture from the local to global scale has increased (Brocca et al., 2017). Precipitation and evapotranspiration have been found to be the main drivers of temporal soil moisture variability on large scales (Porporato et al., 2004). However, this variability is also a function of soil characteristics, vegetation, topography and groundwater (Grayson et al., 1997; Brocca et al., 2017). The same meteorological factors, i.e., precipitation and evapotranspiration, also clearly impact spatial soil moisture variability at regional to continental scales. However, at smaller scales, static factors such as land cover, topography and soil texture and structure are more important influences on soil moisture spatial variability (Crow et al., 2012; Vereecken et al., 2007).

Today, a wide range of commercially available techniques for measuring soil moisture exists. The gravimetric method of determining soil moisture content was for long the most widely used method, despite being the simplest (Johnson, 1962). As it is the only direct way of measuring soil moisture, it is used for calibrating the equipment used in other methods. In the 1980s, sensors determining soil moisture content indirectly from the dielectric properties of soil were introduced (Topp et al., 1980). They serve as a good alternative to the gravimetric method for point measurements of soil moisture, as they are less invasive and labour-demanding. Also, these low-cost instruments facilitate soil moisture measurements at different depths. Radiological techniques, such as gamma absorption and neutron scattering, address the issue of low spatial representativeness faced by the gravimetric method and electromagnetic sensors. More recently, such sensors have been used to form regional networks providing near-real-time soil moisture data for use in various applications (UK Centre for Ecology & Hydrology; Zreda et al., 2012).

In the last two decades, remote sensing of soil moisture has been an active research area, and microwave and optical/thermal infrared sensors have been successfully used to retrieve surface soil moisture (Peng and Loew, 2017). Remote sensing provides a unique capability to obtain soil moisture observations at global and regional scales that help satisfy the science and application needs in agriculture, hydrology, and climate sciences. Satellites dedicated to soil moisture observations have been launched (Kerr et al., 2001; Entekhabi et al., 2010), and missions such as SENTINEL-1 pro-

vide long-term perspectives for land surface monitoring (Choker et al., 2017). The spatiotemporal resolution and accuracy of the products have been continuously improved; however, authenticity verification of the satellite-based products still remains a challenge (Peng et al., 2021).

1.2 Motivation and research questions

Despite the research efforts in the last decades, the temporal and spatial variations in soil moisture are not yet fully understood, and there is still a deficiency of conclusive methods of soil moisture measurement worldwide (Zhu et al., 2012; Civeira, 2019). Little effort has been made to compare different measurement techniques and evaluate them under field conditions (Walker et al., 2004). Increasing the understanding of soil moisture and the measurement techniques will be crucial for better representation of soil moisture in NWP and increasing reliability of forecasts.

In their project Hydrometeorology to Operations (H2O), the Norwegian Meteorological Institute aims to "develop world-leading capacity in regional NWP integrated across the land-atmosphere (L-A) domain" in order to deliver accurate and reliable hydrometeorological forecasts (Norwegian Meteorological Institute, 2020). Special emphasis is put on L-A processes and soil hydrology, with soil moisture as a key parameter. As a part of the H2O project, this thesis aims to broaden the understanding of spatiotemporal variations in soil moisture and investigate the performances of different measurement techniques.

In order to achieve this, three research questions will be answered in this thesis:

1. How does soil moisture change in time and space across Søråsfeltet from June to December 2021?

2. How do different soil moisture measurement techniques perform and compare?

As an extent of the latter research question, a soil-specific calibration method will be conducted and evaluated in this study, leading to the last research question:

3. Is the soil-specific calibration process provided for the GroPoint Profile sensors feasible for the case of Søråsfeltet, and does it increase sensor accuracy?

2 Theory

Soil moisture cannot be seen in isolation, as it is a product of interconnected processes in the atmosphere, soil and vegetation. Soil has inherent properties crucial in determining soil water flow and constitutes complex eco-systems together with the vegetation that grows in it, which have equally complex interactions with soil moisture and the atmosphere. Understanding the processes which determine the soil moisture content and how soil moisture in return influences plant growth, groundwater quality, drought, floods and the thermal climate of soils requires a holistic view of land-atmosphere interactions. This again requires combined knowledge from fields such as soil physics, pedology, hydrology, plant physiology and meteorology.

This chapter starts by giving an introduction to soil and how its properties govern the movement of soil water before explaining the role of soil moisture in both the water and energy balance in the earth-atmosphere system.

Unless stated otherwise, the theory in this chapter is based on Hillel (1982), Hanks and Ashcroft (1980), Kutilek and Nielsen (1992), Weil and Brady (2004), Novák (2012) and Oke (1987).

2.1 Soil

Soil is what we call the outer layer of the Earth's surface. It is initially formed through the breaking down of rocks in physical and chemical processes throughout hundreds of years. After this initial weathering of rocks, mineral and organic matter is produced. These processes form a characteristic soil profile consisting of several layers of different properties, called horizons. Each horizon has characteristics that differ from the layer above and beneath. These characteristics can be visible, such as colour, texture, structure and thickness. Others are not visible to the naked eye but include chemical and mineral content and electrical properties.

The number of horizons present in a specific soil varies according to the area in which it is formed, but in theory, there are five main horizons (Figure 1). The O horizon is formed in undisturbed ecosystems from organic matter such as plant and animal remains which accumulate on the surface. This organic matter undergoes physical and biochemical processes creating layers of decomposed material, and some of it is transported downwards by soil water and animals. The A horizon is the layer of mineral particles darkened by the organic matter transported downwards from the O horizon. In some soils, some of the components in the A horizon are soluble and move downward. This washing out of solutes creates a lighter horizon at the base of the A horizon, denoted the E horizon. The layers beneath the O and A horizons contain less organic matter and are often called the subsoil. Clay minerals, carbonates and oxides are washed down from the horizons above or created in place through weathering and accumulate in the B horizon. As this horizon contains little organic material, the colour is mainly due to the iron oxides, giving a red hue (Wikipedia, 2022). Below the B horizon, we find the C horizon, which is the least weathered of the horizons. This layer consists of partially weathered or unweathered rocks situated above the bedrock (R horizon).

A vertical section of soil is called a soil profile and consists of a combination of the five main horizons. The order and combination of horizons vary for different soil profiles; some contain all five while others contain only one or a few. The boundaries between the horizons may be irregular. However, they are mainly horizontal, as they are formed through the influence of air, water and solar radiation originating at the soil-atmosphere interface.

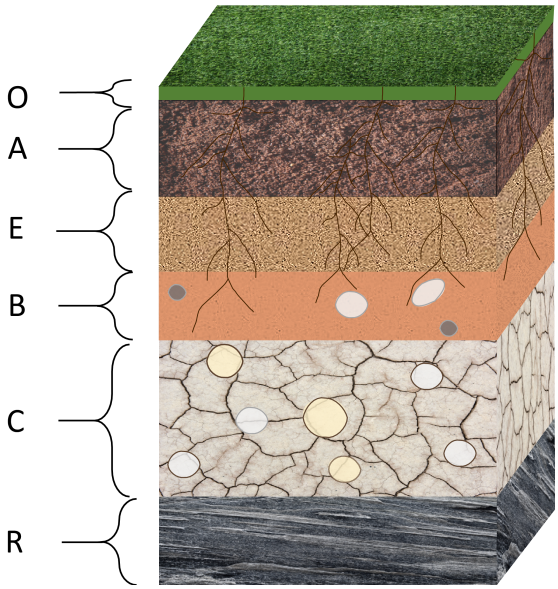

Figure 1: Schematic representation of the different soil horizons. Adapted from Weil and Brady (2004) and Wikipedia (2022).

2.1.1 Soil texture

Soil texture refers to the size range of the particles in the soil and is of crucial importance as it governs the general physical properties of the soil. The size range of soil particles is traditionally divided into three ranges known as textural fractions, namely sand, silt and clay. Sand includes the largest soil particles, with size ranges from 20 to 2000 μm. The smallest particles (< 2 μm) fall under the clay category. All particles between the sand and clay size ranges are denoted as silt. Based on the textural fractions mentioned above, soils can be divided into different textural classes. The textural classes are determined by the mass ratio of the three textural fractions, sand, silt and clay.

Loam is a group of soils which are mixtures of the three textural fractions. According to Weil and Brady (2004), "an ideal loam may be defined as a mixture of sand, silt and clay which exhibits the properties of those separates in about equal proportions". However, if a type of loam is dominated by, for example, sand, it will be classified as sandy loam.

Of the three textural fractions, clay has the most considerable influence on soil behaviour. This is because clay "exhibits the greatest specific surface area and is, therefore, most active in physicochemical processes" (Hillel, 1982). The properties of clay are also very different depending on the degree of hydration; "clay particles

adsorb water and thus cause the soil to swell and shrink upon wetting and drying" (Hillel, 1982). Also, under normal circumstances, clay is never dry. The water associated with the clay can be held so tightly that it can be considered a part of the clay itself.

One feature essential for the movement of water in soil that differs greatly between the textural classes is the permeability, also called hydraulic conductivity. According to Soil Science Society of America (1997), permeability is "the ease with which gases, liquids or plant roots penetrate or pass through a bulk mass of soil or a layer of soil". It is a measure of length per time and is often expressed in cm/s when regarding soil water movement. For sandy soils, it ranges from 10^{-2}-10^{-3} cm/s, while for clay soils it ranges from 10^{-4}-10^{-7} cm/s. This means that a coarse sandy soil with permeability 10^{-2} cm/s would facilitate the transport of 10 m of water per day, while a clay soil with a permeability of 10^{-6} cm/s would only lose 1 mm/day.

2.1.2 Soil composition

Soil generally consists of mineral and organic matter, air and water. A simple representation of the volume fractions of these soil components is shown in Figure 2 for soil conditions optimal for vegetation growth. From the figure, we see that half of the soil consists of solids in the form of mineral and organic matter, while the other half consists of pore spaces filled with air and water. The fraction of air and water is highly variable in both time and space.

The pore space, or total porosity of the soil, sets the maximum physical limit of soil water. The porosity can be estimated from the following formula,

$$\text{soil porosity} = (1 - \frac{\text{bulk density}}{\text{particle density}}) \cdot 100, \tag{1}$$

where the particle density is the density of the solid components of the soil, i.e., the mineral and organic matter, for which 2.65 g/cm^3 is a commonly used value (Blake, 2008). The bulk density of soil is defined as the mass of dry soil per unit volume, and this volume includes both the solids and pores in the soil.

The bulk density is affected by any factor that influences the pore space of the soil. Such factors might be external, such as compaction, or inherent to the specific soil at hand. Soil texture is one such inherent factor that influences bulk density, as different textures imply different organisation of solid particles and thereby differences in pore spaces. Fine-textured soil types such as loam and clay generally have lower bulk densities than coarser, sandy soils. This is because finer soils have pore spaces both within and between particles called micro- and macropores. Table 1 contains the ideal bulk densities for plant growth for the three textural classes, according to the United States Department of Agriculture.

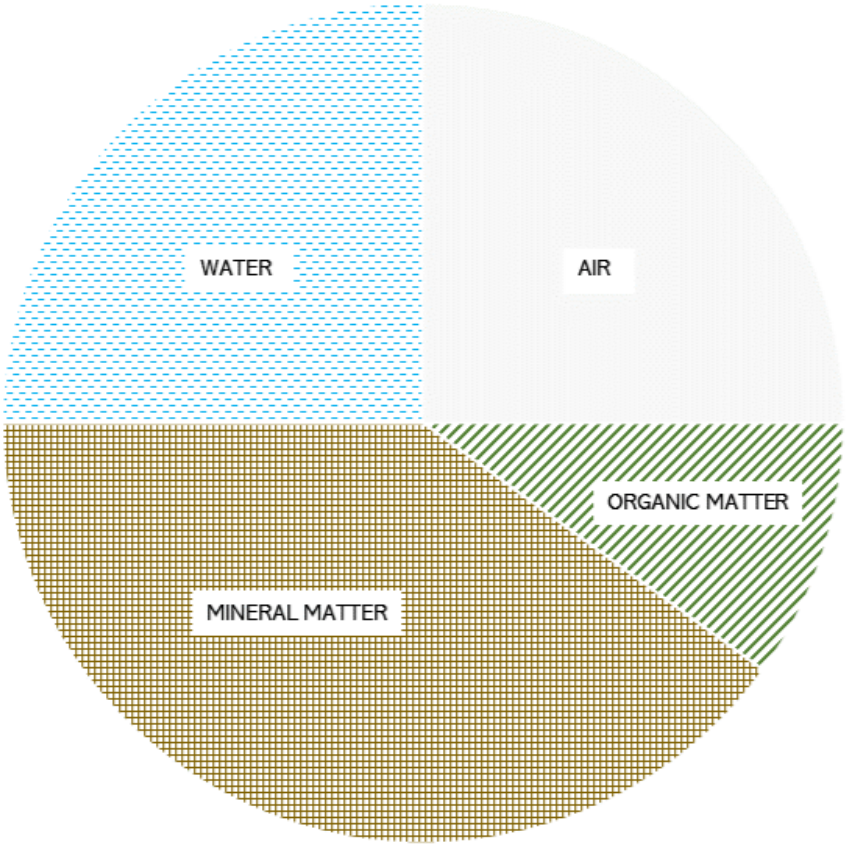

Figure 2: Schematic composition of soil components by volume in conditions optimal for plant growth. Adapted from Hillel (1982).

Table 1: Ideal bulk densities for plant growth for the three main textural classes sand, silt and clay. From United States Department of Agriculture (2008).

Soil texture	Ideal bulk density
Sandy	< 1.60
Silty	< 1.40
Clayey	< 1.10

Another factor influencing the bulk density is the soil sample's depth. As explained in Section 2.1, deeper soil layers contain less organic material than the shallower layers, which, together with the compaction caused by the weight of the overlying layers, causes the bulk density to increase with increasing depth.

2.2 Soil water content

The amount of water present in a volume of soil is a crucial parameter which determines, for example, plant growth, thermal properties of the soil, transport of chemicals and groundwater recharge.

The fractional content of water in soil can be expressed in terms of either mass or

volume,

$$w = \frac{M_{\mathrm{w}}}{M_{\mathrm{s}}} \tag{2}$$

$$\theta = \frac{V_{\mathrm{w}}}{V_{\mathrm{t}}} \tag{3}$$

where w is the gravimetric water content determined from the mass of water, M_{w}, and the mass of soil, M_{s}. θ is the volumetric water content, given as the ratio of the volume of water, V_{w}, present in the total volume, V_{t}, of soil, water and air. w and θ are usually multiplied by 100 and reported as percentages of volume and mass. This thesis will represent soil moisture as volumetric moisture content (VMC).

Soil moisture content can be determined through both direct and indirect methods, both of which will be utilized in this thesis. Direct methods determine soil moisture from the weight difference between moist and dry soil, while indirect methods exploit the relationship between soil moisture and other soil properties. The theory and workings behind some of the most prevalent measurement methods, which have been used in this thesis, are presented in Section 3.3.

2.2.1 Infiltration

When water falls on the soil surface, by precipitation or irrigation, some of it will be absorbed by the soil, while parts may fail to penetrate the soil and flow on the surface. This excess water is called surface run-off. The partitioning of precipitation into infiltration and run-off is determined by the soil's infiltration capacity.

The infiltration capacity is the rate at which the soil can absorb incoming water. When precipitation or irrigation rates exceed the infiltration rate, water accumulates on the surface and runs off. The infiltration capacity depends on several factors, which are properties of both the soil and the incoming water. For example, it depends on the time since the onset of precipitation or irrigation and soil properties such as antecedent soil moisture, permeability, number and size of pores, and surface conditions such as compaction.

The infiltration rate is defined as the volume of water flowing into the soil per unit of soil surface area and time. Like infiltration capacity, the infiltration rate depends on the time since the onset of the rain or irrigation, as it is often high at first and decreases with time. It also depends on the antecedent water content, as wetter soil will absorb water more slowly than dry soils. This is illustrated in Figure 3. We see that the curve for the infiltration rate is steeper at the beginning for the dry soils, but with time the infiltration rate is equal for the two soils.

Soils can, in some cases, become hydrophobic, i.e. water-repellent, which impedes the infiltration rate and capacity (Hallett et al., 2011). In this state, water is less able to penetrate the soil and is gathered on the soil surface, leading to increased surface run-off. Hydrophobicity is caused by water-repellent organic compounds that coat the soil particles and is enhanced by soil drying, fires, fertilization or input of

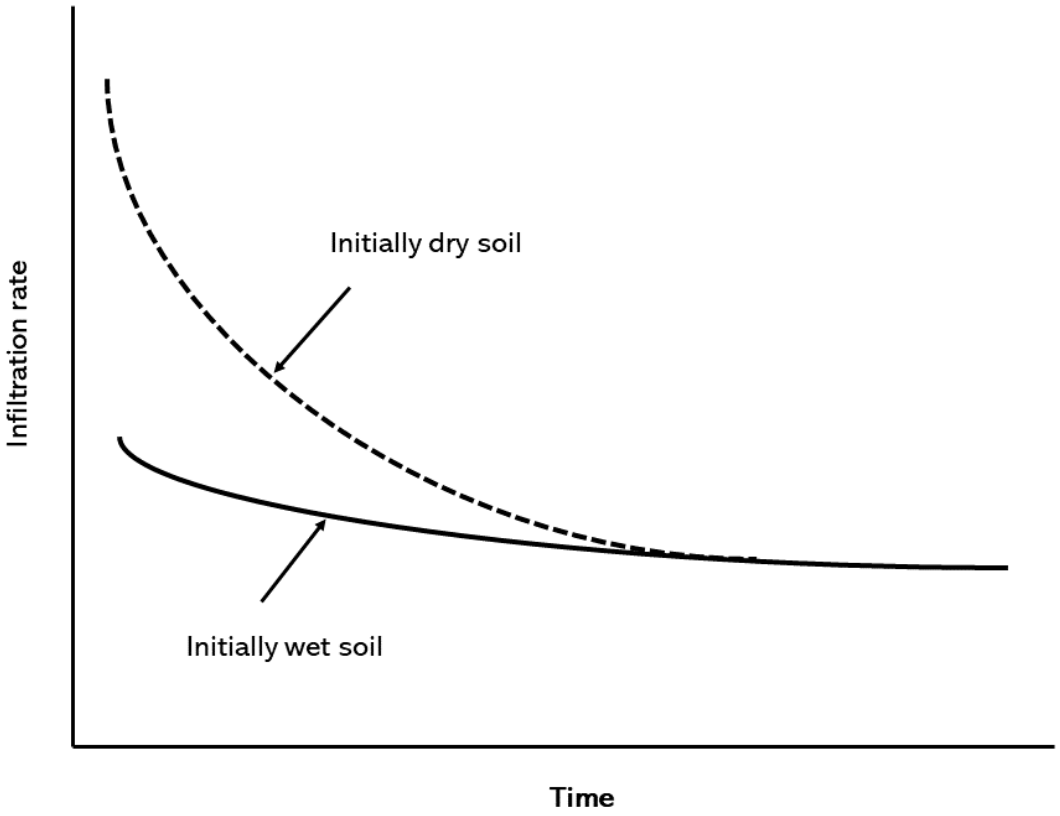

Figure 3: Infiltration rate as a function of time for initially dry and wet soil. Adapted from Hillel (1982).

organic material. Sandy textured soils are more prone to hydrophobicity, as they have a smaller surface area coated more extensively than clayey or silty textured soils.

2.3 Soil water potential

Soil water contains energy in different forms. In classical mechanics, energy is either classified as kinetic or potential. The kinetic energy of soil water is generally considered negligible, as the movement of water in soil is relatively slow. Therefore, potential energy due to position and internal condition is the main form of energy determining the energy level and thus movement of soil water. Differences in soil water potential between one point and another are what cause the flow of water within the soil, which is always in the direction of decreasing potential energy.

The difference in the energy level of soil water from water at a standard reference state is called the soil water potential. The reference state generally used involves a "hypothetical reservoir of pure water, at atmospheric pressure, at the same temperature as that of soil water (or at any other specified temperature), and at a given and constant elevation." (Hillel, 1982). The soil water potential is the sum of the difference in energy levels due to the gravitational, pressure and osmotic forces be-

tween the soil water and reference water and can be used to predict the movement of water in soil. The total soil water potential can therefore be expressed as

$$\phi_{\mathrm{t}} = \phi_{\mathrm{g}} + \phi_{\mathrm{o}} + \phi_{\mathrm{p}}, \tag{4}$$

where ϕ_{t} is the total potential, ϕ_{g} is the gravitational potential, ϕ_{o} is the osmotic potential and ϕ_{p} is the pressure potential.

Like any other body on Earth, soil water is subject to gravitational forces which pull it towards the centre of Earth. The gravitational potential in terms of potential energy per unit mass is

$$\phi_{\mathrm{g}} = gz, \tag{5}$$

where g is the gravitational acceleration and z is the height above a reference.

Osmotic potential comes from the attraction of water to ions and other solutes in the soil, and reduces the soil water's potential energy. This potential generally does not affect soil water flow significantly, as it only occurs when there is a membrane present which transmits water more readily than salts.

Pressure potential refers to the soil water potential attributable to other factors besides gravity and solutes. It is influenced by capillarity, adsorption, submergence, and air pressure and can be either positive or negative, depending on whether the hydrostatic pressure of the soil water is greater or less than atmospheric pressure. The matric potential ϕ_{m} is an important subcategory of pressure potential, which attracts and binds water in the soil and lowers its potential. According to Hillel (1982), the matric potential "denotes the total effects resulting of the affinity of the water to the whole matrix of the soil, meaning its pores and particle surfaces together".

2.3.1 Types of soil water flow

There are two main types of liquid water movement in soil, dependent on the amount of water present in the soil: Saturated and unsaturated flow. Saturated flow occurs when the soil's pores are completely filled with water and are said to have reached saturation or maximum retentive capacity. Soil saturation usually takes place after a heavy precipitation event or irrigation. The driving force of saturated flow of soil water is the gradient of a positive pressure potential. In unsaturated soils, on the other hand, only the finest pores are filled with water. Therefore, water movement is mainly driven by gradients in matric potential during unsaturated flow.

Soil water flow can also be distinguished between matrix and preferential flow, where the relative importance of the two types depends on soil type and rainfall intensity. Matrix flow refers to the even and relatively slow flow of water through the soil, whereas preferential flow is a non-uniform flow where the water moves through preferred pathways in soil, bypassing most of the soil. Water infiltrating the soil surface often flows through these pathways during intense precipitation, including cracks and subsurface channels such as worm-holes and root channels. Even though these channels consist of a relatively small percentage of the total pore volume, they may

be responsible for most of the moisture and solute transport, facilitating rapid transport of water and solutes into the deeper layers of the soil. This type of flow may be initiated well below saturation. Preferential flow of water has, in several locations, led to groundwater contamination as pesticides and other solutes have been guided through these channels and directly into the groundwater, which can directly impact drinking water.

2.4 Water balance

Soil moisture accounts for about 0.001 % of the global water reserves, which is more than the sum of water stored in the atmosphere, rivers and living organisms (Shiklomanov, 1993).

Driven by solar energy, water travels across the globe through the atmosphere, land surface, vegetation, water bodies and soil, changing between the solid, liquid and gaseous forms in a never-ending cycle called the hydrological cycle. In this cycle, illustrated in Figure 4, water vapour enters the atmosphere through evaporation from bare soil and water bodies and evapotranspiration from vegetation. The water vapour is convected through the atmosphere, condensates and forms clouds of water droplets or ice crystals. When heavy enough, the water falls as precipitation on the ground, which flows into rivers and streams or infiltrates into the soil. Some of the water in the soil will be taken up by vegetation, and some will flow deeper into the ground and become groundwater, which will eventually flow into the surface water bodies. The hydrological cycle is a closed cycle, meaning that the water balance is restored, as no water is created or destroyed.

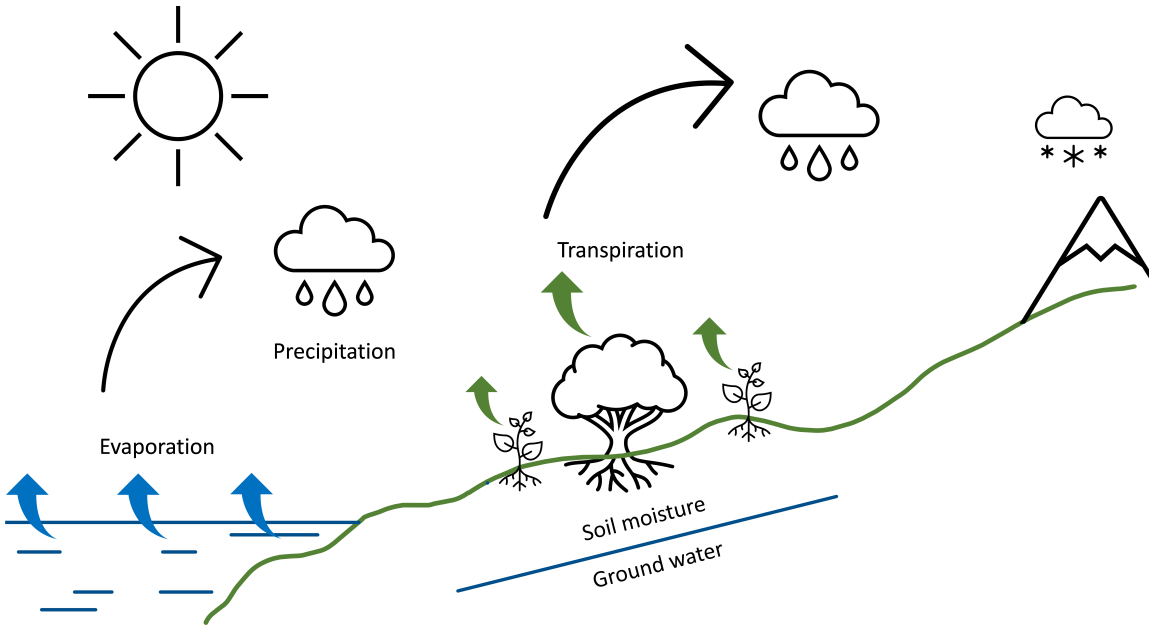

Figure 4: Schematic representation of the hydrological cycle. Adapted from Hillel (1982).

Water balance denotes the sum of water fluxes in and out of a system. The basic

water balance for an arbitrary volume of soil states that the difference in water added (W_{in}) and water withdrawn from the soil (W_{out}) equals the change in water content of the soil (δW), i.e.,

$$\delta W = W_{\text{in}} - W_{\text{out}} \tag{6}$$

The components of the water balance in the soil-plant-atmosphere system are shown in Figure 5. For soil moisture, precipitation is generally the largest source, while evaporation and transpiration are the greatest sinks.

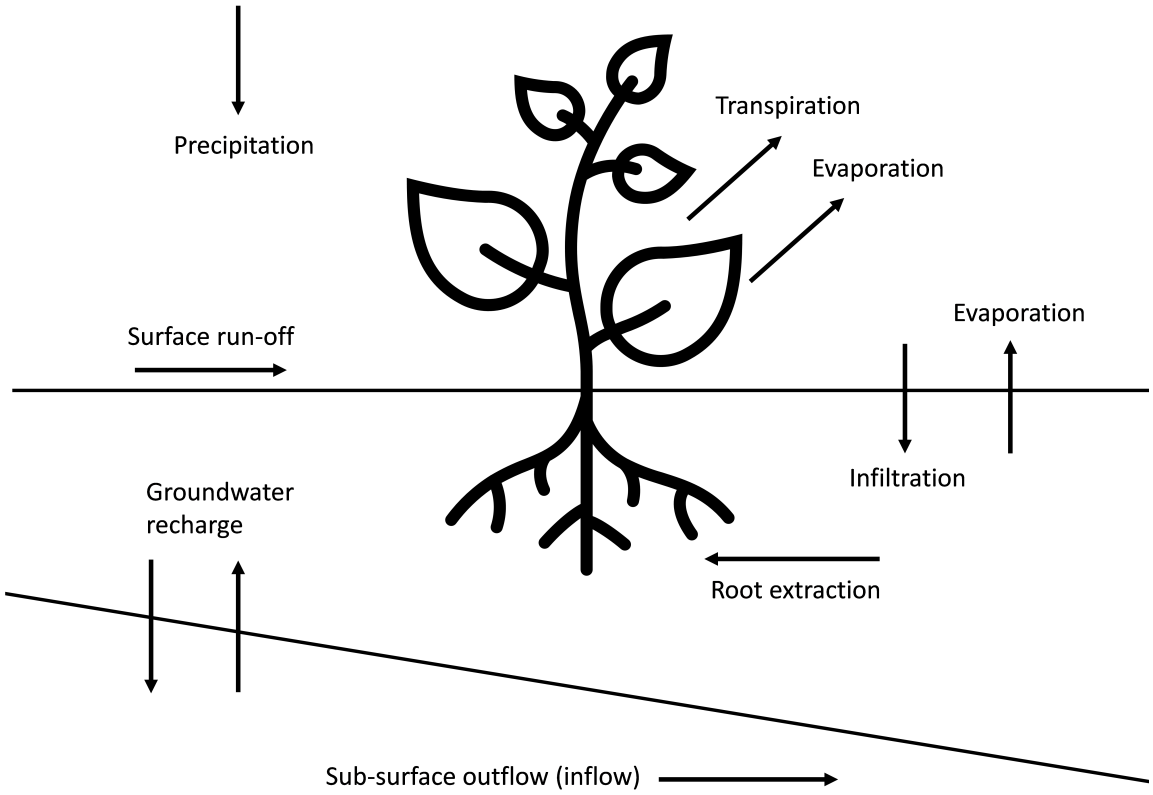

Figure 5: Schematic representation of the water transport processes in the soil-plant-atmosphere system. Adapted from Novák (2012).

Evaporation is the transport of water from the soil and plant surfaces to the atmosphere, while transpiration is the water loss through the plant's stomata during photosynthesis. Transpiration is caused by a vapour pressure deficit between usually water-saturated leaves and the relatively dry atmosphere. Vapour pressure deficit, d, is the difference between saturation vapour pressure and the actual water pressure at the same temperature. This gradient can be thought of as the evaporative demand of the surrounding climate.

The two processes are often combined into the single term evapotranspiration, a common term in the water and energy balance equations.

2.5 Soil moisture and surface energy balance

Analogous to the hydrological cycle presented in the previous section, where water is transported through the earth-atmosphere system by different modes, changing between its three physical states, the energy driving these processes also changes form.

In the earth-atmosphere system, energy enters in the form of short-wave solar radiation. It leaves through scattering and reflection of the incoming radiation and the long-wave emission from Earth and the atmosphere. Since the incoming and outgoing radiative terms are equal, the whole system is in equilibrium. However, if we consider smaller sub-systems within the earth-atmosphere system, the input and output terms generally do not zero out. One such sub-system of particular interest is the Earth's surface, where soil moisture plays a crucial role in partitioning the surface energy budget.

The net radiation at the Earth's surface (Q_*) is the sum of the incoming and outgoing radiative streams,

$$Q_* = K_\downarrow - K_\uparrow + L_\downarrow - L_\uparrow, \tag{7}$$

where $K_\downarrow$ and $K_\uparrow$ are incoming and outgoing short-wave radiation and $L_\downarrow$ and $L_\uparrow$ are incoming and outgoing long-wave radiation, respectively. At night, terms $K_\downarrow$ and $K_\uparrow$ vanish, as solar radiation is absent and the net radiation is negative. During daytime, Q_* is typically positive. The respective energy deficit and surplus must then be partitioned through a combination of conduction, convection, phase-change and energy storage. The conduction, convection and phase-change are facilitated through the ground heat flux Q_G, sensible heat flux Q_H and latent heat flux Q_E, respectively. The latent heat flux can be written as

$$Q_\mathrm{E} = \lambda E, \tag{8}$$

where λ is the latent heat of vaporisation and E is the evaporation rate.

The surface energy balance can thus be written as

$$Q_* = Q_\mathrm{H} + Q_\mathrm{E} + Q_\mathrm{G} + \Delta Q_\mathrm{S}, \tag{9}$$

where ΔQ_S is the energy storage. The heat fluxes are defined as positive away from the surface. Evaporation from the surface creates a positive latent heat flux, while condensation on the ground creates a negative flux.

The partitioning of the net radiation between the terms in Equation 9 depends on several factors, among them soil moisture content. Soil moisture acts as a source of water which facilitates the conversion of radiative energy into latent heat through evapotranspiration. When the soil is dry, Q_E decreases and the energy budget must be balanced through Q_H.

The heat and moisture states of the land and the atmosphere are intertwined and highly influenced by soil moisture. Soil moisture influences the thermal properties of the soil, such as heat capacity and thermal conductivity (See Oke (1987)). Also,

fluxes of water and energy from the land surface alter the water vapour and temperature profiles in the atmosphere, which impacts atmospheric downward and upward longwave radiation. This again affects the net radiation received at the land surface. The interactions between the heat and moisture state parameters and their impacts on land-atmosphere interactions are further described by Brubaker (1995).

3 Methods

This chapter is split into two parts, and the first part focuses on the soil moisture instrumentation and the research area from which the data used in the analysis is obtained. The different soil moisture measurement techniques and their locations are presented in Sections 3.1 to 3.4. Section 3.2 provides a brief climatological background for the field site, and Section 3.5 outlines the steps taken in the data processing prior to the analysis. Part two presents the methods used in the analysis of the data through Sections 3.6 to 3.11, where Section 3.11 describes the soil-specific calibration of one of the soil moisture sensors.

Part 1

3.1 Materials and research area

In this analysis, five different methods have been used for measuring soil moisture, from which continuous time series of soil moisture measurements have been obtained. Two of the time series were obtained during a manual measurement campaign from June to September 2021, from the volumetric method and ThetaProbe ML2 sensor. The ThetaProbe will be referred to as the ADR method. The measurement campaign is elaborated in Section 3.4. The remaining time series are derived from soil moisture sensors which are permanently installed in Ås. Four sensors are installed in Søråsjordet: Three GroPoint Profile sensors and one SoilVUE 10 sensor. The GroPoint Profile sensors will be called IoT sensors from here on, and the SoilVUE 10 will be abbreviated to SoilVUE. One last sensor is installed in Kjerringjordet, which will be further mentioned as the COSMOS sensor. Figure 6 shows the locations of the permanently installed sensors. The workings and specifications of the different instruments will be outlined in Section 3.3.

The lengths of the time series from the different instruments are shown in Table 2.

Table 2: Measuring periods of the different instruments and methods.

Method	**Measuring period**
Volumetric	22.06.2021 - 28.09.2021
ADR	22.06.2021 - 05.08.2021
COSMOS	01.06.2021 - 17.12.2021
IoT	04.08.2021 - 17.12.2021
SoilVUE	01.06.2021 - 17.12.2021

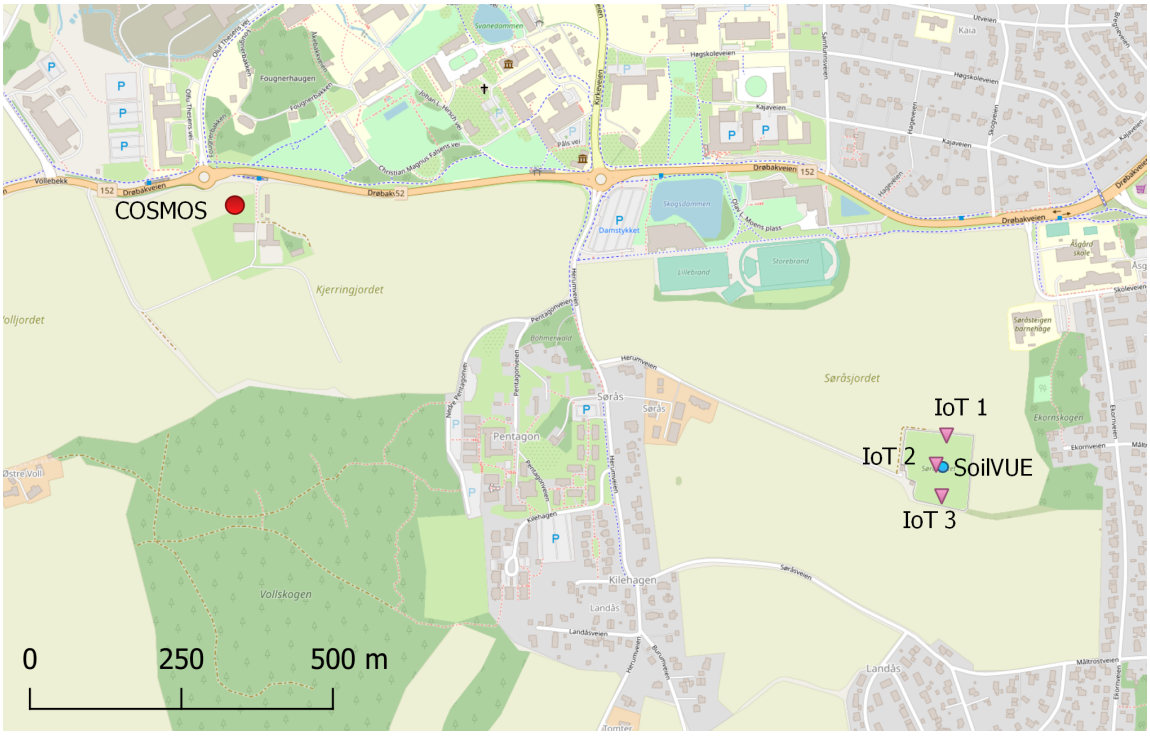

Figure 6: Approximate positions of all the permanently installed soil moisture instruments used in this analysis. The COSMOS sensor is placed in Kjerringjordet, while all the other instruments are in Søråsfeltet. The SoilVUE and IoT 2 sensors are within 1 meter apart. Image from OpenStreetMap, edited in QGIS.

Since most of the soil moisture time series have been obtained from Søråsfeltet, this becomes our main area of research. Søråsfeltet is an agricultural site in Ås, Viken county, Norway (Figures 7 and 8). Its coordinates are N59°39'37" E10°46'54" and it is located 93.9 m above sea level (Norwegian University of Life Sciences, 2021).

The field site in Søråsfeltet is relatively homogeneous, as the whole are is covered by grass and only has a slight slope of < 1 % to the southwest (Norwegian University of Life Sciences, 2021). Although the short grass coverage (canopy height ~ 10 cm) is relatively homogeneous across the field (Ehrnsperger, personal communication, 2022-03-22), there are several installations that may impact the soil moisture measurements. These include the meteorological instruments seen in Figure 7 and other structures, such as the buildings and solar panels seen in Figure 8.

The soil texture around Søråsfeltet is 48 % clay, 42 % silt and 10 % sand (Nemes, personal communication, 2022-03-18). When using Equation 1 and a bulk density of 1.03 g/cm^3, the porosity of the soil in Søråsfeltet is found to be 61 %.

The COSMOS sensor is located in Kjerringjordet at N59°39'51.9" E10°45'42.8", approximately 1 km northwest of Søråsfeltet, which is also an agricultural site. The sensor is operated by The Norwegian Water Resources and Energy Directorate (NVE).

Figure 7: Photo of Søråsfeltet, showing some of the meteorological instruments installed on the site. The tower seen to the left marks the centre of the field. The photo is taken in the southeasterly direction. Photo: Ida Lunde Naalsund.

Figure 8: An aerial photo of Søråsfeltet. The larger installations in the field can be seen in the photo, such as the two houses in the upper right corner and the solar panels in the lower right corner. Source: Kartverket.

3.2 Meteorological conditions during the research period

The months from June to November 2021 were all warmer than the long-term average temperature of the last 30 years (Wolff and Grimenes, 2021). In November 2021, a new temperature record was set: 14.9 °C was the warmest temperature recorded in November in Ås since 1874. During the research period, December was the only month where the monthly average temperature was below the climate normal. The recorded monthly average was -3.8 °C, while the climate normal for December is -1.9 °C.

2021 was a dry year compared to the long-term normal. The annual total precipitation was 612 mm, which is far lower than the normal value of 892 mm. August was the driest month of the year, with only 4 mm of precipitation.

Precipitation data from the Norwegian Meteorological Institute (MET Norway) for our research period is shown in Figures 9a and 9b. We see that after the relatively dry summer and the drought period in August, precipitation peaks at the start of October. The total monthly precipitation in October was 155 mm, of which 99 mm fell on the first three days.

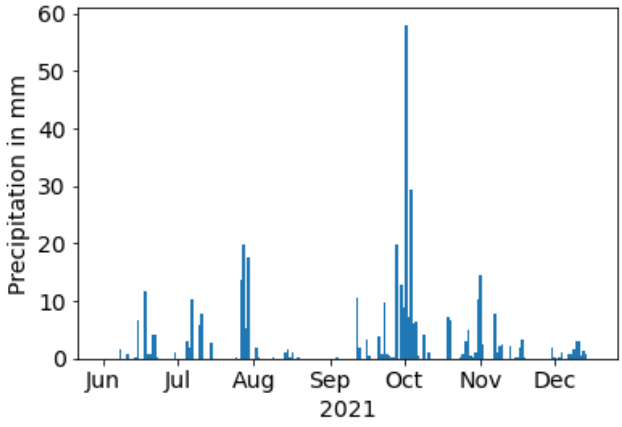

(a)

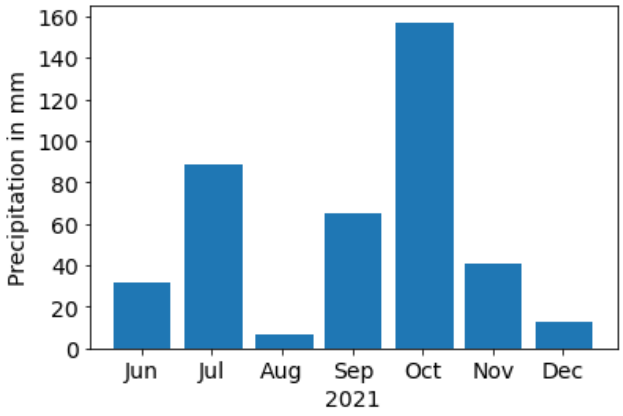

(b)

Figure 9: a) Daily and *b)* monthly precipitation from June to December 2021. Based on data from MET Norway.

3.3 Instrumentation

Soil moisture measurement methods can be divided into direct and indirect methods (Little et al., 1998). Direct methods use weight to determine how much water is present in a sample of soil. In contrast, indirect methods estimate soil moisture by a calibrated relationship with some other measurable variable. Such variables include soil water suction and dielectric and electric properties of the soil. When calibrating the sensors using indirect methods to a specific soil type, these measurements will be compared to a direct method of measuring soil moisture.

All theory and information on the operating modes of all instruments and methods used is taken from Muñoz-Carpena (2004) unless stated otherwise.

3.3.1 Volumetric method

One of the methods used is the volumetric method, which is a direct method of measuring soil moisture. This approach involves gathering soil samples of a known volume, as illustrated in Figure 10. The samples are weighed before they are placed in an oven and dried at 105 °C for 24 hours. A temperature of 105 °C is preferable, as organic material can decompose at higher temperatures than this, which leads to additional weight loss (Hillel, 1982). After the samples have been dried, they are weighed again. The weight difference between the wet and dry soil samples gives us the mass of water, which is used to determine the soil moisture content from the following equation:

$$\theta_v = \frac{V_w}{V_s} = \frac{M_w}{\rho_w \cdot V_s}, \tag{10}$$

where θ_v is the volumetric water content, $\mathrm{V_w}$ is the volume of water, $\mathrm{V_s}$ is the volume of soil, $\mathrm{M_w}$ is the mass of water and ρ_w is the density of water (Little et al., 1998).

When taking soil samples for the volumetric method, it is important to extract samples that are large enough to be representative of the whole mass. Generally, large samples give more reliable results, and according to Reynolds (1970), a sample size of at least 100 g is recommended.

Although simple, this method can give an accurate measure of volumetric water content within 1 % soil moisture content and is often used as a "ground truth" to which other methods are compared (Little et al., 1998; Sharma, 2018). Disadvantages of this method are that it is invasive, time and labour consuming, and it does not allow for several measurements in the exact same location. This method is also sensitive to changes in the bulk density of the soil, as higher bulk density means more soil, and thereby water, can be packed into the cylinder, giving higher values of soil moisture. When the soil is very dry and crumbling, gathering an exact volume of soil can be challenging.

3.3.2 Electromagnetic sensors

Electromagnetic sensors indirectly measure soil moisture by utilizing the electric and dielectric properties of the soil (Sharma, 2018). Soil generally consists of soil parti-

Figure 10: A 100 cm^3 cylinder used in the field for gathering soil samples for the volumetric method.

cles, air and water (Section 2.1). All these soil components have different dielectric constants, κ. The dielectric constant is defined as the ratio of the permittivity of a medium to the permittivity of free space and is a measure of how much electric energy can be stored in the medium. κ of soil ranges from 2-5 while κ of air and liquid water are 1 and 81, respectively (Muñoz-Carpena, 2004). Since the dielectric constant of water is far greater than that of the other components in the soil, the total dielectric constant of the soil will be governed by the amount of water in the soil (Sharma, 2018).

By using empirical equations, the relationship between the dielectric constant of the soil and soil moisture can be determined. Topp et al. (1980) developed the following equation between the dielectric constant of soil and soil moisture:

$$\theta = -5.3 \cdot 10 - 2 + 2.92 \cdot 10 - 2\kappa\text{–}5.5 \cdot 10 - 4\kappa^2 + 4.3 \cdot 10 - 6\kappa^3, \qquad (11)$$

where θ is soil moisture and κ is the dielectric constant of the soil (Krzic et al., 2010).

ThetaProbe ML2 One of the electromagnetic sensors used in this analysis is the ThetaProbe ML2 Soil Moisture Sensor from Delta-T Devices. The sensor was connected to an HH2 Handheld Meter from Delta-T Devices, which displays the soil moisture readings (Figure 11).

The ThetaProbe operates through the amplitude domain reflectometry (ADR) method, which translates the impedance of the soil to its soil moisture content (Delta-T Devices Ltd, 1998). A signal is sent through a transmission line whose impedance changes as the impedance of the soil changes. According to Delta-T Devices Ltd (1998), "this impedance has two components; the apparent dielectric constant and the ionic conductivity. The signal frequency has been chosen to minimise the effect of ionic conductivity, so that changes in the transmission line impedance are dependent almost solely on the soil's apparent dielectric constant." The difference in the

Figure 11: The ThetaProbe ML2 connected to the HH2 Handheld Meter.

produced wave and wave reflected back from the prongs of the sensor is used to find the dielectric constant of the soil. This constant is then used to determine the soil moisture content in the soil.

The prongs of ThetaProbe ML2 are 6 cm long, its outside diameter is 4 cm, and the soil sampling volume is approximately 30 cm^3 surrounding the central prong (Delta-T Devices Ltd, 1998).

This instrument is sensitive to roots, stones, air pockets and variation in soil density and composition (Little et al., 1998). Therefore, soil moisture measurements in natural ecosystems might be disturbed to a certain degree (Ehrnsperger, personal communication, 2022-03-22). It is important to take the degree of variability of these parameters into account when deciding on the number of measurements to take at any particular location. If the soil is known to be very heterogeneous, it will be necessary to take measurements from at least three closely-spaced locations (Delta-T Devices Ltd, 1998).

The specifications for the sensor are presented in Table 3.

Table 3: Instrument specifications for ThetaProbe ML2. From Delta-T Devices Ltd (1998).

Instrument	ThetaProbe ML2
Manufacturer	Delta-T Devices
Measurement range	0-100 %
Accuracy	±2 %

SoilVUE 10 The SoilVUE 10 sensor from Campbell Scientific utilizes time domain reflectometry (TDR) for determining soil moisture content (Campbell Scientific, Inc.,

Figure 12: SoilVUE10 soil moisture sensor. TDR measurements are taking at the silver areas along the column. Used with permission from Campbell Scientific, Inc. (2022).

2021). This method relates the time taken for a signal to travel through a transmission line and be reflected back to the dielectric constant of the soil, which again is used to determine the soil moisture content through an empirical relation. The dielectric constant is derived from

$$\kappa = \left(\frac{ct}{2L}\right)^2, \tag{12}$$

where κ is the dielectric constant, c is the speed of an electric signal in vacuum, t is the transmission time and L is the length of the transmission line (Krzic et al., 2010).

The SoilVUE sensor installed in Søråsfeltet is operated by MET Norway. It measures soil moisture together with permittivity, electrical conductivity, and temperature at 5, 10, 20, 30, 40, 50, 60, 75 and 100 cm depth (Campbell Scientific, Inc., 2021). The sensor is displayed in Figure 12.

The specifications for the sensor are presented in Table 4.

Table 4: Instrument specifications for SoilVUE 10. From Campbell Scientific, Inc. (2021)

Instrument	SoilVUE10
Manufacturer	Campbell Scientific
Measurement range	0-100 %
Accuracy	±1.5 %

GroPoint Profile The last type of electromagnetic sensors used in this analysis is the GroPoint Profile sensor. Three of these sensors are installed in Søråsfeltet, and are operated by the Norwegian University of Life Sciences (NMBU).

These sensors utilize what is called the time domain transmission (TDT) method. It is similar to the TDR method, but measures only the time of transmission of a signal through a transmission line, and not reflection. As with the TDR method, the transmission time is related to the dielectric constant of the soil, which again is used to determine the volumetric soil moisture content in the soil.

The specifications for the sensors are presented in Table 5.

Table 5: Instrument specifications for GroPoint Profile. From GroPoint (2010).

Instrument	GroPoint Profile
Manufacturer	GroPoint
Measurement range	0-100 %
Accuracy	±2 %

The GroPoint Profile sensors used in this analysis are of type GPLP-2, which have two soil moisture segments and four temperature sensors. The soil moisture measurements are taken at 5 and 25 cm, while the temperature measurements are taken at 0.35, 10, 20 and 30 cm (GroPoint, 2010). A schematic drawing of the sensor is shown in Figure 13.

The sensors are connected to loggers of type SM5039 from Scanmatic.

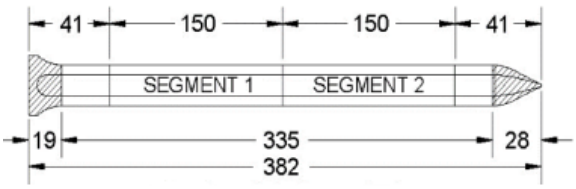

Figure 13: Schematic drawing of the GroPoint Profile sensor used in this analysis. All numbers are in mm. Taken from GroPoint (2010), with permission.

3.3.3 COSMOS

The last sensor used is a cosmic-ray sensor of type CRS-2000/B from Hydroinnova, referred to as the COSMOS sensor. The sensor is operated by NVE.

Unlike the other instruments, this sensor provides footprint measurements, i.e. measurements from a larger, spherical area, instead of point measurements. Fast neutrons are emitted from a radioactive source. When these neutrons meet protons, i.e. H^+ ions, they are slowed down drastically and form a "cloud" of slowed-down or thermalized neutrons. Since water is the primary source of hydrogen in soil, the volume of these thermalized neutrons is approximately proportional to the volume of water in the soil.

The sensor in Kjerringjordet is seen in Figure 23. It measures soil moisture at 15 and 30 meters distance from the sensor and at 25 and 50 cm depth (Mengistu, personal communication, 2022-03-08).

Figure 14: The CRS-2000/B sensor (COSMOS) installed in Kjerringjordet. Photo: Ida Lunde Naalsund.

3.4 Measurement campaign summer 2021

From 22 June to 28 September 2021, a manual measurement campaign was conducted in Søråsfeltet, Ås. During the campaign, soil moisture measurements were taken using the volumetric and ADR method, introduced in Section 3.3.

The dates on which the measurements were taken are presented in Table 6. The ADR measurements ceased on 05 August due to malfunction of the ThetaProbe sensor. Also, after 05 August, the measurements were carried out by a different person than in the first leg of the campaign.

The measurements from the two methods were carried out in a specific pattern each time, illustrated in Figure 15. The ADR measurements were taken in eight transects in different cardinal directions. The transects are named after the cardinal direction in which it lies, i.e., N is north and NE is northeast. Each transect started by the fence and ended in the centre of the field, marked by the tower seen on the left of Figure 7. The point locations in which measurements were taken were approximately five meters apart, and at each of these locations, three measurements were taken, 5-10 cm apart (Figure 16b).

Even though the HH2 Handheld Meter has a ”store” function for storing the measurements, the measurements had to be noted down manually, as the RS232 output of the meter was not compatible with modern computers. This made the ADR mea-

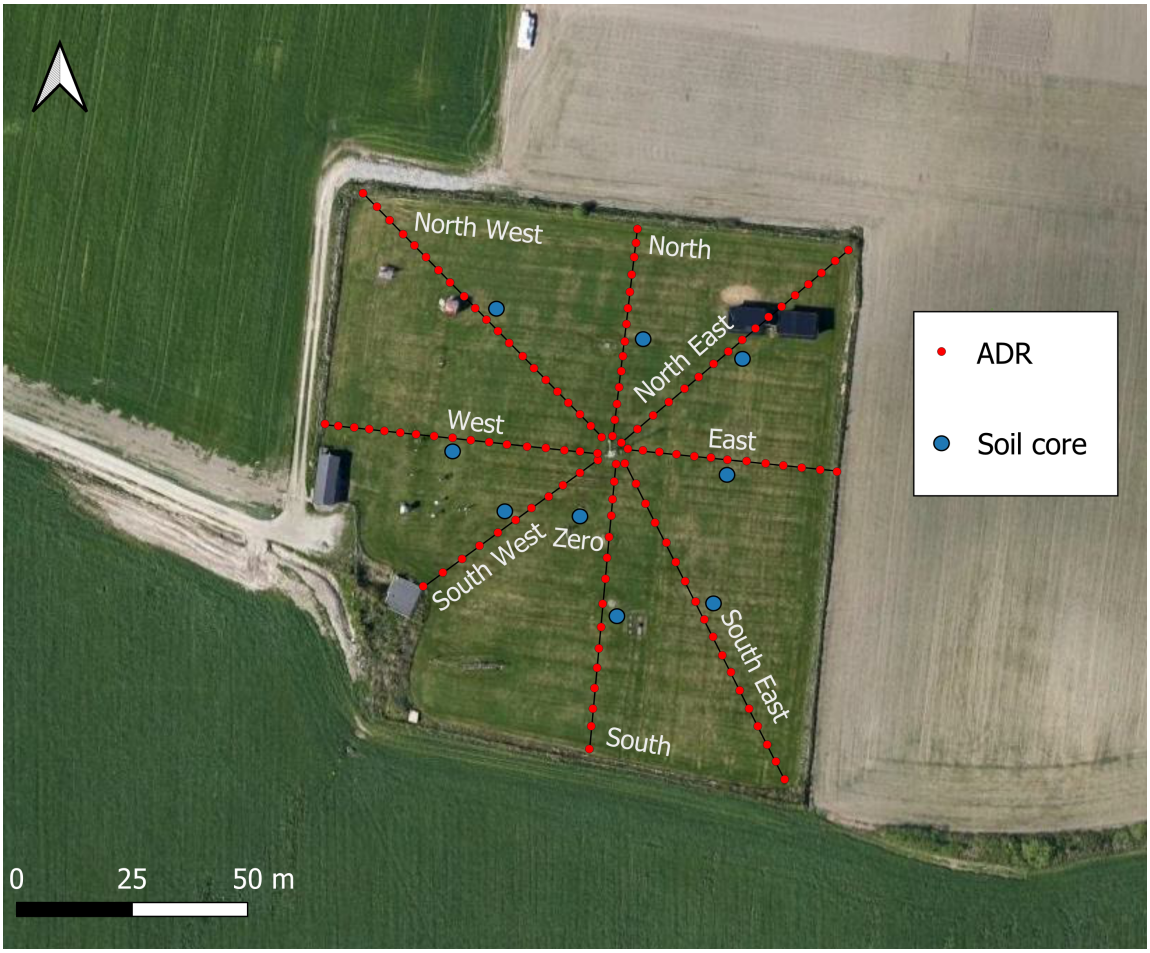

Figure 15: Søråsfeltet, the main research area, with the point locations where the ADR and volumetric method measurements were taken during the manual measurement campaign. Satellite image from Google Maps, edited in QGIS.

surements slightly more time consuming, especially during precipitation, since the notes had to be kept dry. The manual transcript of measurements also introduced the potential risk of erroneous notes.

Soil samples for the volumetric method were taken near the centre of every transect (Figure 16a). One additional soil sample was taken in point location ZERO, which is close to the SoilVUE and IoT 2 sensor. The soil samples were taken by hammering a cylinder of 100 cm^3 into the ground until it was filled with soil, as seen in Figure 10. Any excess soil was scraped off with a knife. The content of the cylinder was transferred to an airtight plastic bag inside a cooling bag to avoid evaporation. After all nine soil cores were gathered, the samples were brought to a laboratory where they were weighed and further dried at 105 °C.

Table 6: Dates of measurements and which methods were used in the measurement campaign in the summer of 2021.

Date	Method
22.06.2022	Volumetric and ADR
28.06.2022	Volumetric and ADR
09.07.2022	Volumetric and ADR
16.07.2022	Volumetric and ADR
23.07.2022	Volumetric and ADR
31.07.2022	Volumetric and ADR
05.08.2022	Volumetric and ADR
11.08.2022	Volumetric
18.08.2022	Volumetric
25.08.2022	Volumetric
01.09.2022	Volumetric
09.09.2022	Volumetric
17.09.2022	Volumetric
22.09.2022	Volumetric
28.09.2022	Volumetric

(a) Digging in the ground before extracting the soil samples for the volumetric method. Photo: Private.

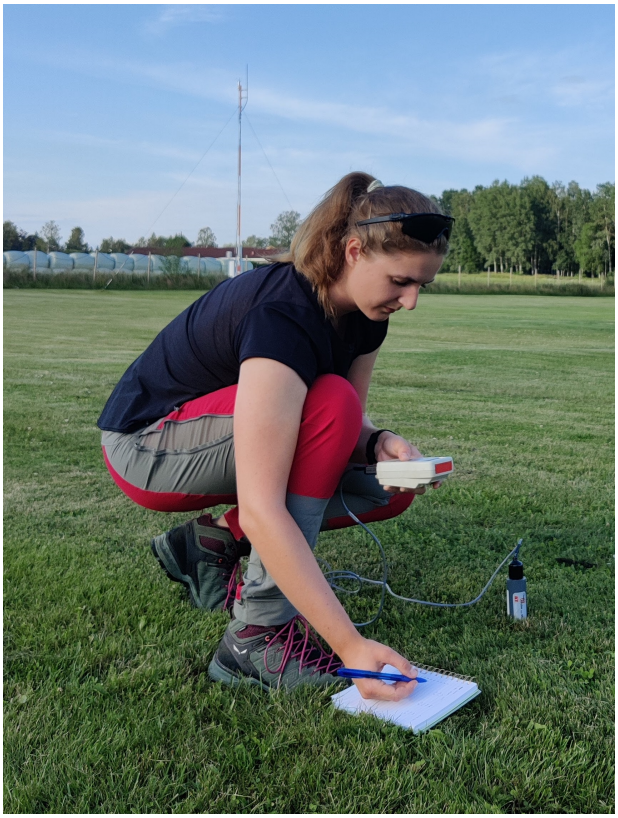

(b) Noting down readings from the HH2 meter when taking measurements with the ThetaProbe. Photo: Private.

Figure 16: Manual measurements taken in the campaign summer 2021.

3.4.1 Accuracy of volumetric method

After the volumetric method measurements were taken, the accuracy of the method was quantified (Table 7). First, the average bulk density for each location was found. This was used to calculate the "average" soil moisture content for the location. Then, the deviations between the soil moisture content measured on each date and this average soil moisture content were found and averaged for every location. Finally, a single deviation for the method was found by averaging all deviations.

Table 7: Accuracy of the volumetric method at each of the locations, calculated as the deviation from soil moisture content found using an average bulk density specific to each location.

Location	**Deviation (%)**
SW	2.42
W	2.72
NW	2.11
N	2.16
NE	3.49
E	2.38
SE	3.70
S	2.64
Z	2.18
Average	2.64

3.5 Data processing

Soil moisture measurements were initially visualised in order to detect values outside of the physical limits of 0-100 % and other unrealistic values. Some of the data sets were further processed before the analysis began.

3.5.1 IoT sensors

Data from the IoT sensors was quality checked before the analysis begun. Firstly, data outside the physical limits of soil moisture of 0-100 % was discarded. After that, the data was despiked using the interquartile range (IQR) of the data. Data points which lie outside of $Q1-1.5\cdot IQR$ and $Q3+1.5\cdot IQR$ were removed, where Q1 and Q3 are the first and third quantiles of the data (Ehrnsperger, personal communication, 2022-03-22). These terms will be further explained in Section 3.8.

3.5.2 SoilVUE sensor

The SoilVUE data was retrieved via MET Norway's Frost API. Data uploaded to MET Norway's server is run through a quality control system, and the quality of the data is summed up by a quality code stored together with the data. Quality code 0 means "OK", 1 means "OK, value is controlled and corrected, or value is missing and interpolated", while code 2 means the quality of the data is slightly uncertain and has not been controlled (Norwegian Meteorological Institute). If an instrument

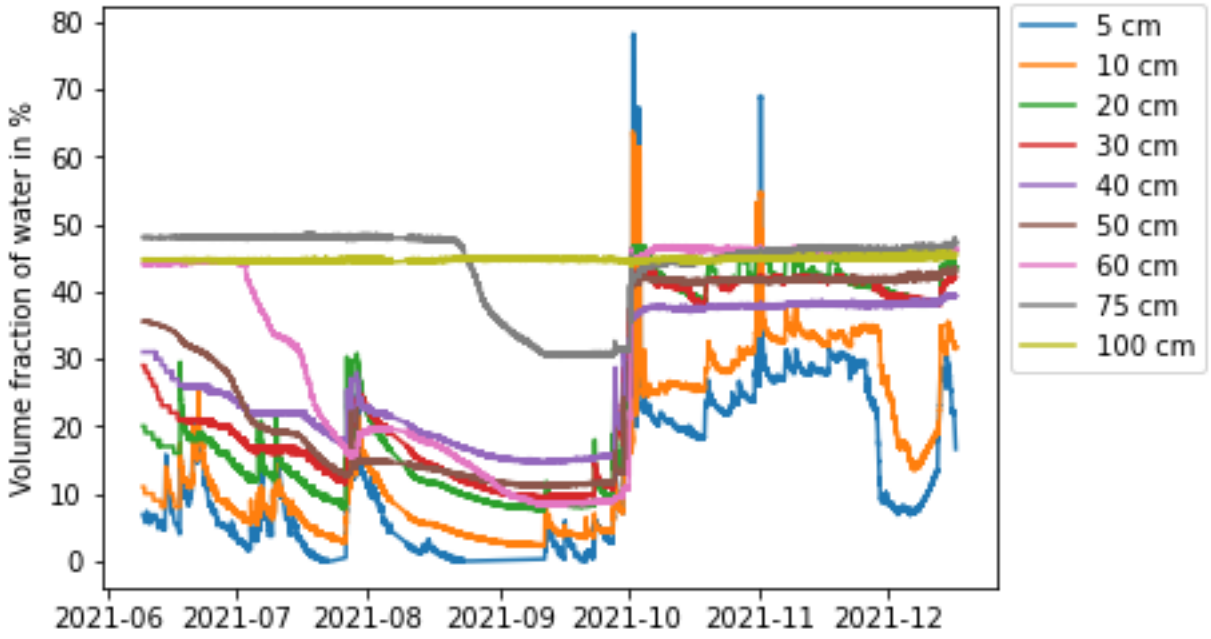

Figure 17: Original time series from all segments of the SoilVUE sensor.

measures at several depths, only data from the standard height will be run through the quality control (Wolff, personal communication, 2022-04-09). This was confirmed when inspecting the SoilVUE data retrieved from Frost, as only the values from the 5 cm segment of the sensor were marked with quality code 0, while the rest were marked with quality code 2.

When displaying the SoilVUE data, we see that the 5 and 10 cm segments of the sensor report values of soil moisture over 70 % and 60 %, respectively (Figure 17. From Section 2.1, we know that the maximum theoretical soil moisture level is determined by the soil's porosity, which is 61 % for Søråsfeltet (Section 3.1). This means that both the 5 and 10 cm segments of the SoilVUE sensor occasionally report physically impossible values. Therefore, these values were filtered out before starting the analysis.

The threshold for filtering out values from the SoilVUE sensor was determined from the maximum values of the IoT sensors. From Table A.2, we see that the IoT sensors have maximum values from 48.3 to 51.9 %. This indicates the saturation level of the soil in the area, and the threshold for filtering out high values from the SoilVUE sensor was therefore set to 50 %.

In Figure 17, we also see a distinct dip in soil moisture at the beginning of December for the 5 and 10 cm segments. This is most likely due to the freezing of the soil water, which changes its dielectric constant, thus leading to incorrect sensor readings (Nemes, personal communication, 2022-03-17). Soil temperature measurements from MET Norway show that from 26 November, the soil temperature at 5 cm depth was below zero, and temperatures at 10 cm depth were close to zero. Data from 26 November and onward will therefore be discarded.

Part 2

3.6 Temporal and spatial variability in soil moisture measurements

In order to investigate the temporal variability in soil moisture measurements from Søråsfeltet, the time series from the different measurement techniques were displayed. Since we know precipitation to be an important driver of soil moisture changes, the occurrence of precipitation events is also indicated in these plots.

ADR method and IoT measurements were further investigated in order to assess the spatial variability in soil moisture across Søråsfeltet.

3.7 Statistical hypothesis tests

Statistical tests were carried out to investigate the data distribution and compare the data from the different instruments. The tests used were statistical hypothesis tests which test a hypothesis about the properties of the different data sets. The statistical tests used in this analysis are presented in Table 8. All tests were conducted at a 95 % significance level, meaning that a p-value less than 0.05 leads to the null hypothesis being rejected. An example is the Shapiro-Wilk normality test where

$$H_0\text{: The variable is normally distributed}$$

and

$$H_1\text{: The variable is not normally distributed,}$$

where H_0 and H_1 are the null and alternative hypothesis. If the p-value from this test is lower than 0.05, we can reject the null hypothesis, meaning that is it unlikely that the data comes from a normal distribution.

The Shapiro-Wilk test was run on each data set individually and was the first test to be performed. This was because other tests, such as Fischer's f-test, assume that the data comes from a normal distribution (bioCEED, University of Bergen). The Shapiro-Wilk test was then used to assess whether the Fischer's f-test or Levene's test, which does not assume a normal distribution, should be used when testing for similar means.

The Shapiro-Wilk test was supported by histograms which give a visual representation of the data distribution.

All statistical tests were carried out using functions from the scipy.stats package in Python 3.8.

Table 8: Statistical tests used in the analysis to compare the different data sets.

Test	**Use**	**Note**
Shapiro-Wilk test	Test for normality	No normally distributed data required
Fischer's f-test	Test for similar variances	Assumes normally distributed data
Levene's test	Test for similar variances	No normally distributed data required
Kolmogorov-Smirnov test	Test for similar distributions	No normally distributed data required

3.8 Box plots

Box plots were made to visually present the range and distribution of the soil moisture measurements from the different methods and instruments. This makes for easy comparison between the different methods and locations.

The components of a box plot are shown in Figure 18. 50 % of the data from the data set is contained within the box, called the interquartile range (IQR) (Galarnyk, 2018). The median is marked as a straight line through the box. The outliers, defined as values further away from the box than 1.5 times the length of the box, are displayed as circles in the box plot.

The box plots were made using the Pandas package in Python 3.8.

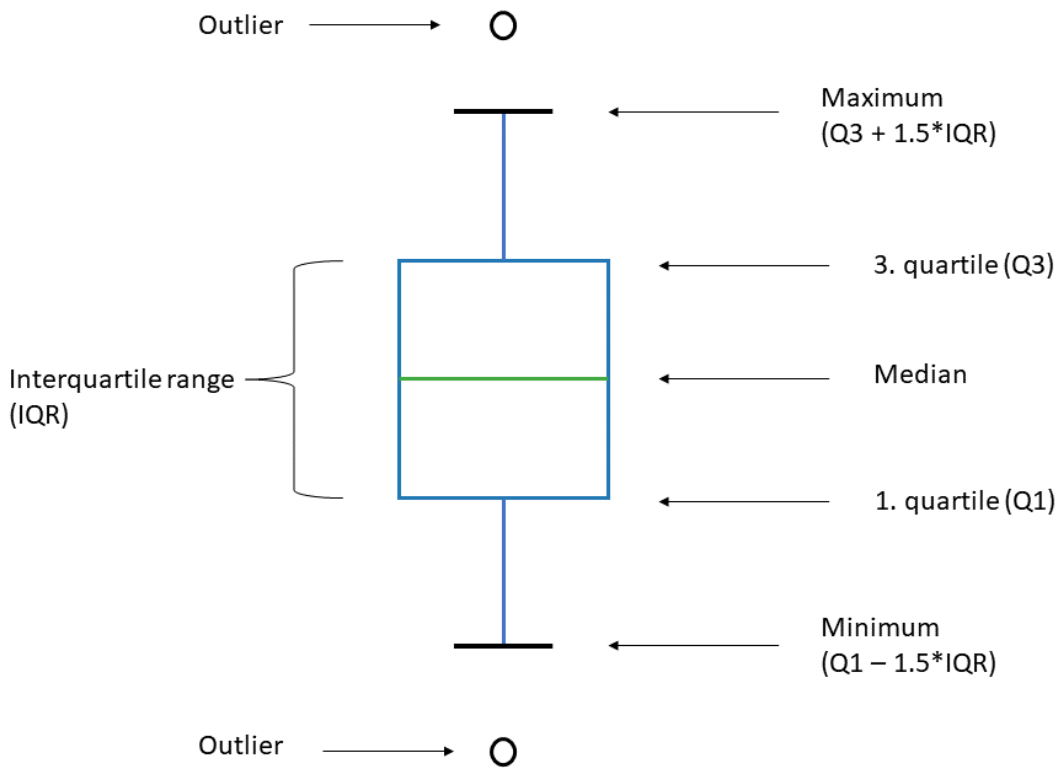

Figure 18: Illustration of the components in a box plot. Adapted from Galarnyk (2018)

3.9 Comparison of IoT and SoilVUE sensors

In order to compare the data from different instruments while diminishing the spatial variability of soil moisture across Søråsfeltet, a small case study of the SoilVUE and IoT 2 sensors, which are installed within 1 m apart, was conducted. The investigation includes calculating the absolute difference between the two sensors and assessing how the difference changes with different levels of precipitation.

3.10 Effect of precipitation on soil moisture

Precipitation is known to have a great influence on soil moisture. The effect of precipitation on soil moisture at different depths was quantified by calculating Pearson's correlation coefficient and conducting a simple linear regression between daily rainfall and daily averages of soil moisture from the SoilVUE and IoT sensors at the different depths. From the linear regression, we can determine whether precipitation is a significant predictor of soil moisture.

The precipitation on 12 September marked the end of a long drought period (Figure 9a). The infiltration rate of the soil in this period was investigated by finding the time taken for soil moisture to increase after the first precipitation event. The change

in soil moisture was investigated both across Søråsfeltet and at different depths by finding this time for all three IoT sensors at both depths and the SoilVUE sensor at all nine depths.

3.11 Calibration of GroPoint Profile sensor

The three GroPoint Profile sensors used in this analysis had not been specifically calibrated for the soil in Søråsjordet before installation. The GroPoint Profile sensors are calibrated in fine sand by the manufacturer, and even though the errors from the difference in soil conductivity between the soil types are deemed to only be a few percent, GroPoint recommends soil-specific calibration when high accuracy is valued (GroPoint, 2010). Therefore, one GroPoint Profile sensor was calibrated specifically to the soil in Søråsfeltet. This way, the errors due to no calibration of the three operating GroPoint sensors and the importance of calibration before field installation can be assessed.

The GroPoint Profile sensor was calibrated according to the user manual from GroPoint (2010), with a few minor adaptations. In this process, we start off with dry soil at less than 5 % soil moisture and increase the soil moisture by around 5 % in seven to eight calibration steps until the soil reaches saturation. At each soil moisture step, readings are taken from the sensor and compared to the actual soil moisture content. The actual soil moisture values are obtained through the volumetric method explained in Section 3.3.1. The relationship between these two sets of measurements will be fitted to a second or third-order polynomial which will give coefficients with which the sensor's calibration coefficients can be updated.

The calibration process started by extracting soil from the Søråsfeltet. This soil was left to air dry for 13 weeks. The soil at this stage is shown in Figure 19a, at which the soil moisture was 4.2 %.

Since the soil in Søråsfeltet has a high clay content, the soil forms lumps, as seen in Figure 19a. From the manual, lumps with diameter over 2 mm should be dissolved, by hand. In our case, the soil had been left out for too long before the lumps were dissolved, and at this point they were too hard to be dissolved by hand. Therefore a hammer was used to break up the lumps and make the soil as uniform as possible. However, not all lumps could be reduced to less than 2 mm diameter, as illustrated in Figure 19a. When the soil was made uniform, the total volume of soil was measured to be 17.6 liters. The volume was measured by adding soil to a 5 liter container in 0.5 liter increments and settling the soil by tapping the bottom of the cup on the table. After these initial preparations were done, the soil was ready for calibration.

Half of the soil was transferred to an acrylic box with dimensions 40 cm x 20 cm x 50 cm which was specifically constructed for the calibration. This type of box was preferred over a wooden box, as a wooden box would have to be lined with plastic in order to prevent water loss to the wood. The sensor was then placed in the box and covered with the rest of the soil. The sensor and box containing half the soil are seen in Figure 19b. The soil should be uniformly and tightly packed around the sensor to avoid air pockets. The soil should furthermore cover the sensor by at least 7 cm in all directions, including the tip, sides, top and bottom.

(a) The soil after air drying for 13 weeks and dissolving lumps.

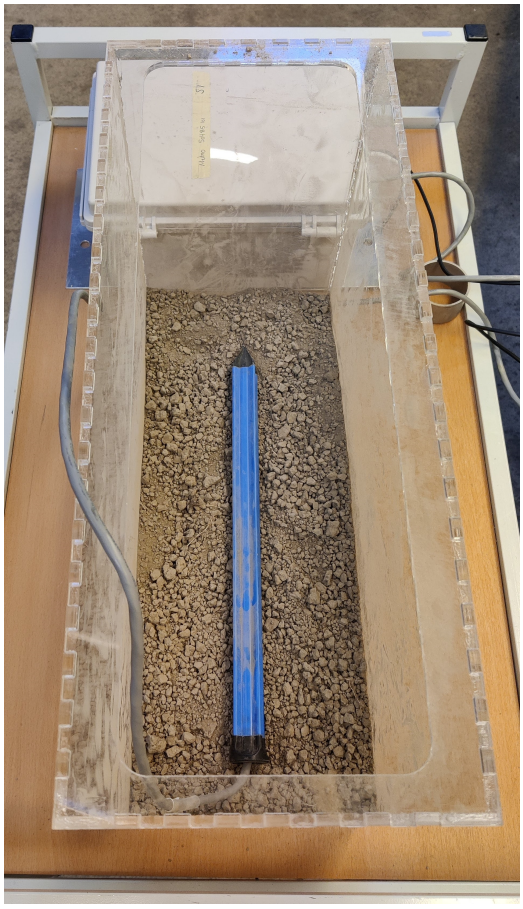

(b) The sensor placed in the acrylic box on top of half of the soil.

Figure 19: Initial stage of calibration process.

When the sensor was placed in the box and covered with soil, five sensor readings were taken at two minute intervals. These five readings were used to make an average for each soil moisture level. After the sensor readings were taken, the sensor was removed from the box and the actual soil moisture level was measured using the volumetric method. This was done by taking three soil samples from different parts of the box with a 100 cm^3 cylinder. The samples were transferred to ovenproof containers and weighed. The samples were then placed in a oven at 105 °C for at least 24 hours.

After the sensor readings and soil samples were taken, water was added to the soil to increase the soil moisture by approximately 5 %. The amount of water to add at each stage is determined by the saturation level of the soil. From United States Department of Agriculture (2019b), the saturated water content of clay is 45.9 %. In our case, we had 17.6 liters of soil, which means that the total amount of water that should be added to the soil in the calibration process was $0.459 \cdot \ 17.6\text{l} = 8.2\text{l}$. Since the process should be repeated eight times, the amount of water to add each time was $8.2\text{l}/8 \approx 1\text{l}$. Water was added to the soil using a spray bottle and evenly sprayed on the top layer of soil before exposing the next layer of soil. The soil was mixed with a trowel, and when all the water had been sprayed on and the soil was well mixed, the soil was left to equilibrate for several hours. The acrylic box was covered with plastic sheeting which was taped around the box, in order to eliminate any evaporation. From the manual, a waiting time of minimum two hours is recommended for loam and clay soils. In our case, the soil was left for minimum four hours as longer equilibrium times are beneficial for the water to uniformly spread throughout the soil (Nemes, personal communication, 2022-02-10).

As the soil moisture increased, the properties of the soil changed drastically. Between 10 and 20 % soil moisture, the soil formed lumps which were increasingly time-consuming to dissolve. More and larger lumps lead to more air pockets forming, which will affect the sensor readings. The soil no longer formed lumps or aggregates at higher moisture levels but became one large body. At this stage, it was important not to pack the soil around the sensor too tightly, as this would push some of the water out of the soil. Another disadvantage at this stage was that the soil stuck to everything, including the cylinder used for taking soil samples in the volumetric method. This loss of soil led to the three soil samples having slightly different volumes, not all precisely 100 cm^3. The amount of soil stuck inside the cylinder at soil moisture over 40 % is shown in Figure 20. Getting all the soil out was not possible. The difference in soil moisture measured with and without adding soil corresponding to the loss seen in Figure 20 was found to be around 2 to 3 %.

After the eight stages of the calibration were finished, the results were analysed in Microsoft Excel (version 2204). Two scatter plots were made, one for the 5 cm segment and one for the 25 cm segment, where the average sensor readings were on the x-axis and the actual soil moisture content on the y-axis. A trend line was added to the plots, and a third-order polynomial was chosen as line type. From this, the equation and R^2 values were obtained by choosing "Display equation on chart" and "Display R-squared value on chart". The R^2 is a goodness-of-fit measure; the closer it is to 1, the better the fit between the two variables. The coefficients from the third-order equations can be used to update the sensor.

Figure 20: Cylinder soiled from soil sampling at high soil moisture levels.

3.11.1 Comparison with permanently installed IoT sensors

The coefficients in the third-order polynomial equations were used to create corrected time series of the IoT sensors which are permanently installed at Søråsfeltet. The new, corrected time series were compared to the original time series.

3.11.2 Calibration with constant bulk density

In order to assess the sensitivity to bulk density of the volumetric method, one experiment where the bulk density of the soil was kept constant at 1.2 g/cm^3 was carried out. A bulk density of 1.2 g/cm^3 was chosen as it is a reasonable estimate for soil with our texture (Nemes, personal communication, 2022-03-17).

4 Results

This study aims to investigate the spatial and temporal variations in soil moisture in Søråsfeltet, Ås, and how different soil moisture instrumentation compare. In addition, the importance of soil specific calibration of the GroPoint Profile sensors is aimed to be assessed.

In this chapter the main results obtained from the methods outlined in Sections 3.6 to 3.11 are presented. The temporal variability of soil moisture measurements on different scales is presented in Section 4.1, while the spatial variations in the ADR measurements obtained during the manual measurement campaign and the measurements from the IoT sensors from August to December 2021 are presented in Sections 4.2.1 and 4.2.2. In Section 4.3, the results obtained from three statistical hypothesis tests are presented, while the spread of the data from the different methods and instruments are further illustrated through box plots in Section 4.4. Section 4.5 presents the comparison of the SoilVUE and IoT 2 sensors, which are located within 1 meter apart. In Section 4.6, the effects of precipitation on soil moisture at different depths are quantified through linear regression and correlation coefficients, and the response time to precipitation is found from time series of precipitation and soil moisture displayed together. Lastly, Section 4.7 presents the findings from the calibration of one GroPoint Profile sensor performed in the laboratory.

4.1 Temporal variability

In order to understand how soil moisture changes on different temporal scales and how this variability is captured by the different measurement techniques, time series from the techniques are presented in this section. In Section 4.1.1, time series plots over the entire measurement period of the instruments are presented, while diurnal variations in soil moisture are investigated in Section 4.1.2. Since we know precipitation to be an important driver of soil moisture changes, the occurrence of precipitation events is also indicated in these figures. In order to compare the accuracies of the different instruments, plots containing the 10-day running means of the permanently installed sensors with their standard deviations are displayed in Section 4.1.3.

4.1.1 Time series from the different instruments

Time series of the soil moisture measurements from all methods and instruments are shown in Figures 21 to 25. As listed in Table 2, the measuring periods differ between some of the instruments.

The readings from the SoilVUE sensor at all depths are seen in Figure 21, together with the occurrence of daily precipitation over 4 mm. We see that in the period June to November 2021, the measured soil moisture at 100 cm is approximately constant at around 45 % and varies with less than 1.5 % throughout the research period. The measurements at 75 cm depth are also fairly constant, around 48 % from June until 15 September, when it decreases to 30.5 %. The largest fluctuations are seen for the shallower depths; soil moisture at 5 and 10 cm depth varies between 0 and 47.5 %

and 2.3 and 49.5 %, respectively. Soil moisture at 60 cm is stable at around 44 % in June and the beginning of July but reaches its minimum of 8.4 % on 11 September, which is lower than what is measured at all depths except 5 and 10 cm. Between 30 September and 01 October, a rapid rise in soil moisture is seen at all depths over 100 cm depth. This is a period of several consecutive days of precipitation, and the largest precipitation event of the year occurs in this period (Figure 9a). At this time, soil moisture values of around 47 and 45 % are seen at depths 5 and 10 cm, respectively. These two depths also experience a peak in soil moisture again around 01 November.

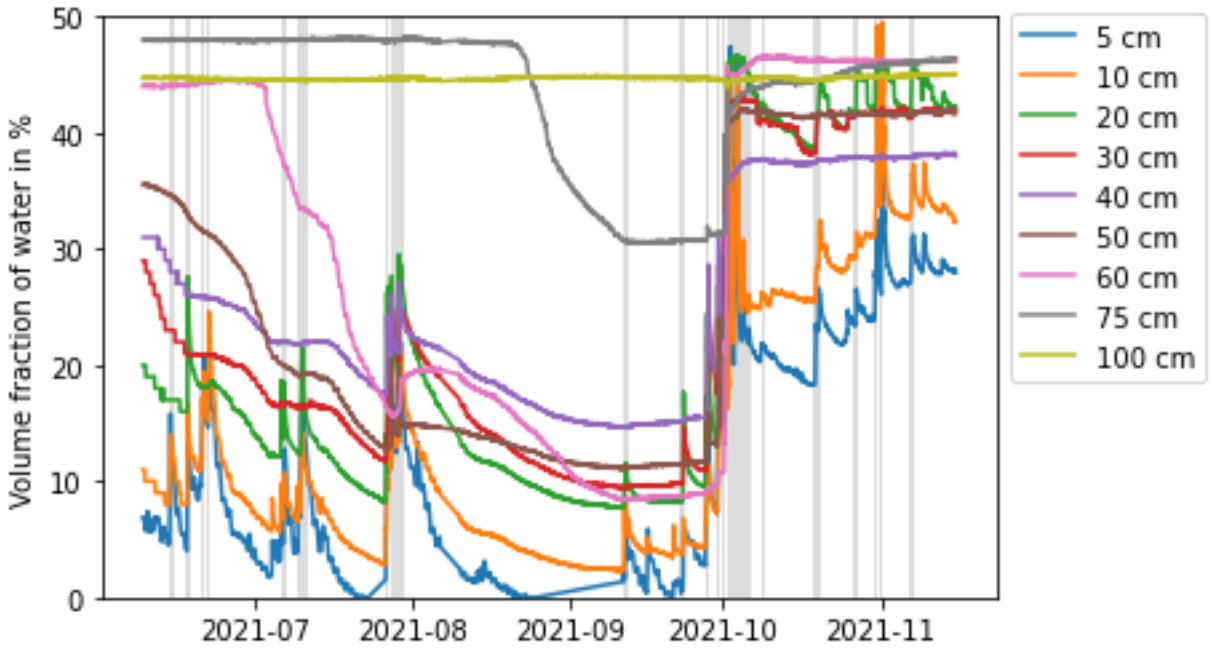

Figure 21: Soil moisture measurements from the SoilVUE sensor at all depths from June to November 2021. The occurrence of daily precipitation over 4 mm is indicated by the vertical grey lines.

Soil moisture measurements from the three IoT sensors, at depths 5 and 25 cm, are shown in Figure 22. We see that soil moisture is declining at both depths for all sensors from 05 August to 11 September, a period with almost no precipitation. On 11 September, all sensors experience an abrupt increase in soil moisture. The soil moisture levels then decrease until a new rapid increase is seen on 21 September and again on 27 September, before the soil moisture levels stay relatively high and steady until the end of December. The measurements from the 25 cm segments generally report higher values and have smaller fluctuations than the 5 cm segments. The 5 cm segment of the IoT 2 sensor reports the lowest values for most of the measurement period but also has the highest peaks in soil moisture during the precipitation events, reaching up to 51.9 %.

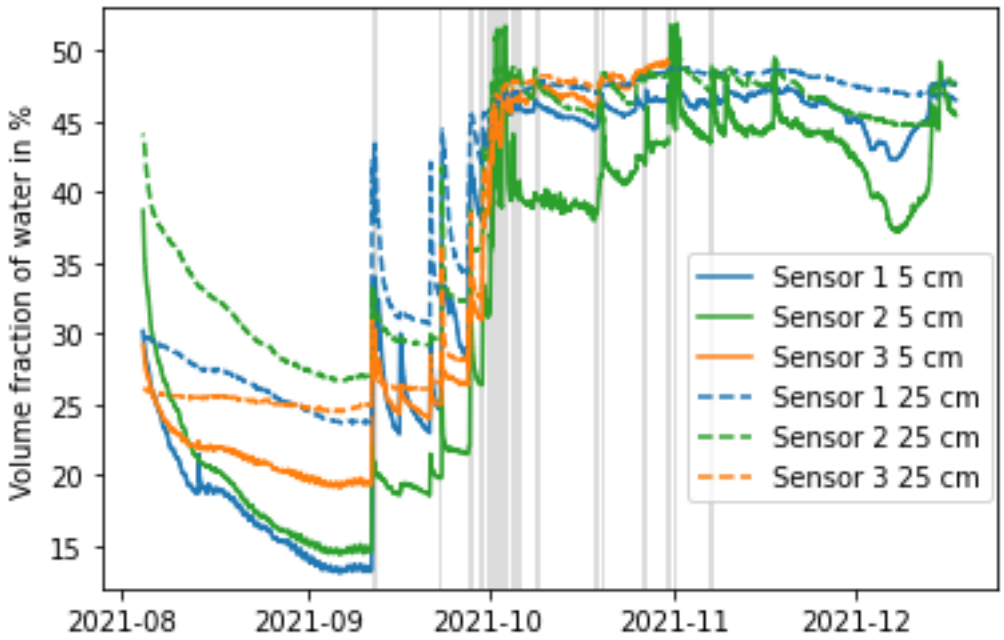

Figure 22: Soil moisture measurements from the three IoT sensors at both depths from August to December 2021. The occurrence of daily precipitation over 4 mm is indicated by the vertical grey lines.

Figure 23 shows the soil moisture measurements from the COSMOS sensor from 01 September to 16 December 2021. There is a relatively large variation between measurements within the same period; from 01 June to 28 September, the daily variation in soil moisture is on average 11.4 %, while from 28 September to 16 December, this variation is on average 17.4 %. The increases in soil moisture generally correspond to precipitation events, but on 09 December, soil moisture increases even though there is very little precipitation in this period. The maximum value was 54.8 %, recorded on 12 October, while the lowest value was 8.6 %, on 10 September, toward the end of the drought period starting on 31 July.

The manual measurements obtained from the measurement campaign from June to September 2021 are presented in Figures 24 and 25. The general trend of increase and decrease in soil moisture corresponding to precipitation is similar for all locations and transects, both for the volumetric and ADR method. For example, all locations and transects experience an increase in soil moisture from 23 to 31 July 2021.

However, we see that the variability in soil moisture measurements differs both between the dates and transects of the ADR measurements. For example, on 23 July, the ADR measurements on the northeast transect vary between 1.3 and 17.1 %, while they vary between 6.7 and 3.0 % soil moisture on the east transect (Figure 25). On 09 and 16 July and 05 August 2021, the average measurements from point location NE6 of the northeast transect are over 12 % higher than the rest of the locations along the same transect.

From Figure 24, we see that the variability in soil moisture during the dry period from 31 July to 09 September differs between the locations of the volumetric method.

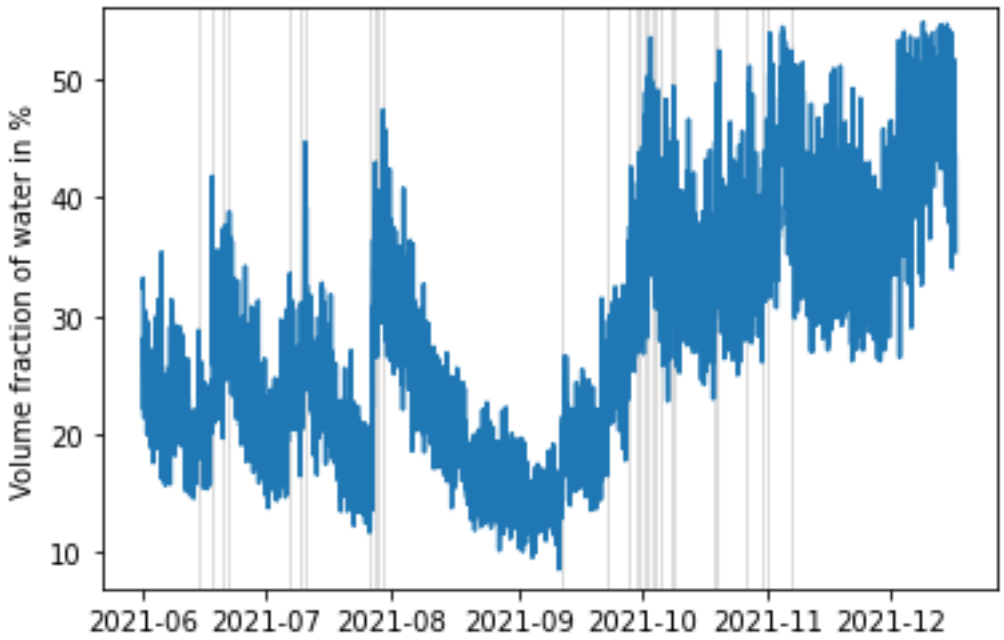

Figure 23: Soil moisture measurements from COSMOS from June to December 2021. The occurrence of daily precipitation over 4 mm is indicated by the vertical grey lines.

For location south, this variation is 20.8 %, but in location ZERO, soil moisture only varies with 3.4 % in this period. After the precipitation events between 23 and 31 July, location ZERO only experiences an increase of 2.43 % while several of the other locations experience an increase in over 10 % soil moisture. Also, location southwest experiences a large increase in soil moisture from 01 to 09 September, from 17.1 % to 29.5 %, which is not associated with a precipitation event or reflected in other locations.

In Figure 26, we see time series from the shallowest depths of all instruments from the period 01 June to 16 December 2021 displayed together. Since the IoT sensors started logging on 05 August, they only slightly overlap with the manual measurements. From the figure, we see that the general trends with increasing and decreasing soil moisture are similar for all methods, although the volumetric method is the only method reporting an increase in soil moisture from 22 June to 28 June. On 22 June, the difference in soil moisture between the average values of the volumetric and ADR method is 15.5 %.

The volumetric method, together with the IoT sensors, have measurements in the same range as the COSMOS sensor, while the ADR measurements and the SoilVUE sensor, in particular, report lower values for soil moisture than the rest. The SoilVUE sensor is always reporting lower values than the other instruments, and this difference is largest in the dry periods. For example, the difference in soil moisture measured by the SoilVUE and the volumetric method is, on average, 16.8 % in the period 31 July to 09 September.

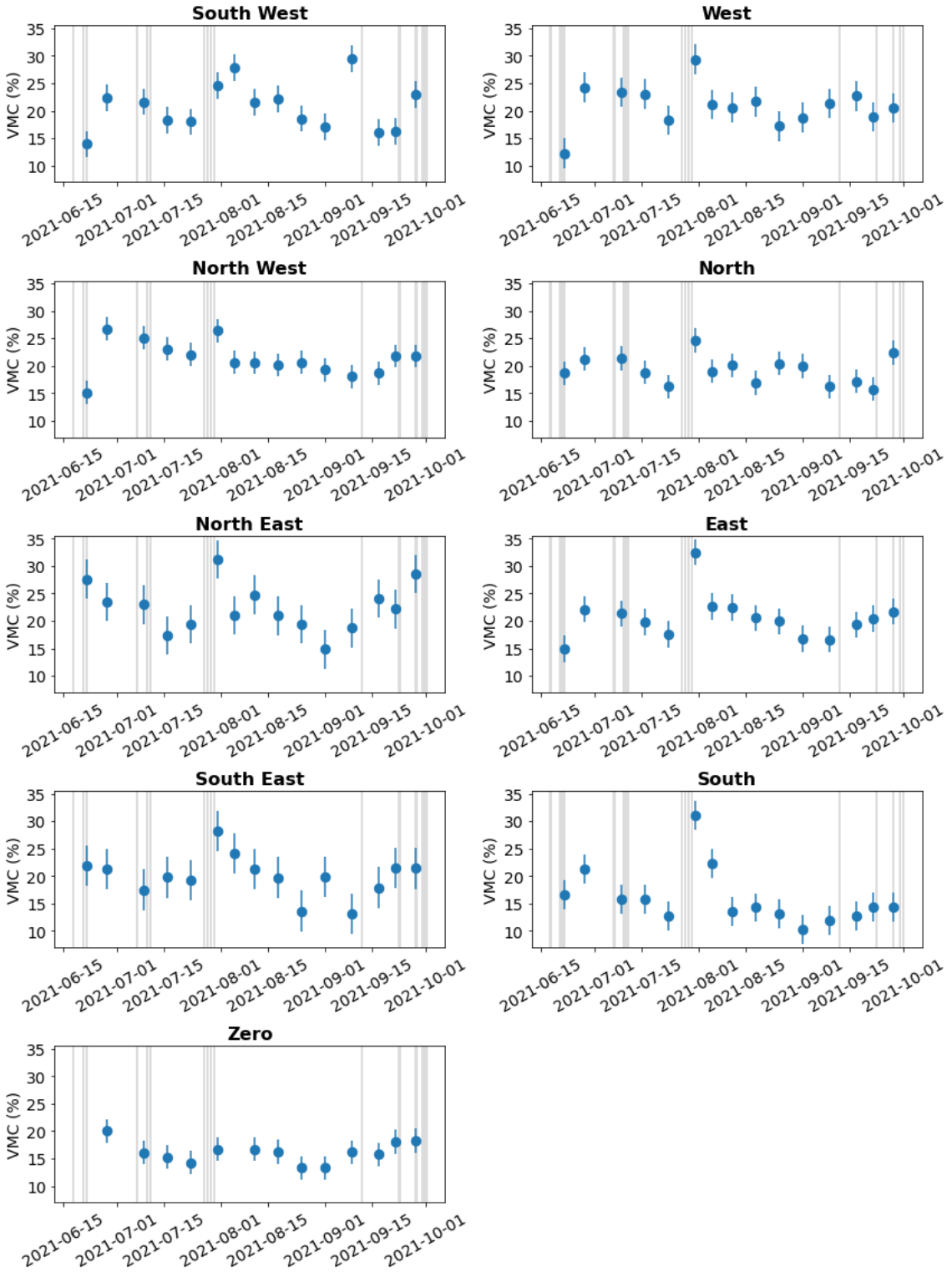

Figure 24: Volumetric soil moisture content (VMC) from the volumetric method from each of the locations seen in Figure 15. Error bars mark the deviation of the soil moisture measurements from soil moisture found when using a constant bulk density (from Table 7). The occurrence of daily precipitation over 4 mm is indicated by the horizontal grey lines.

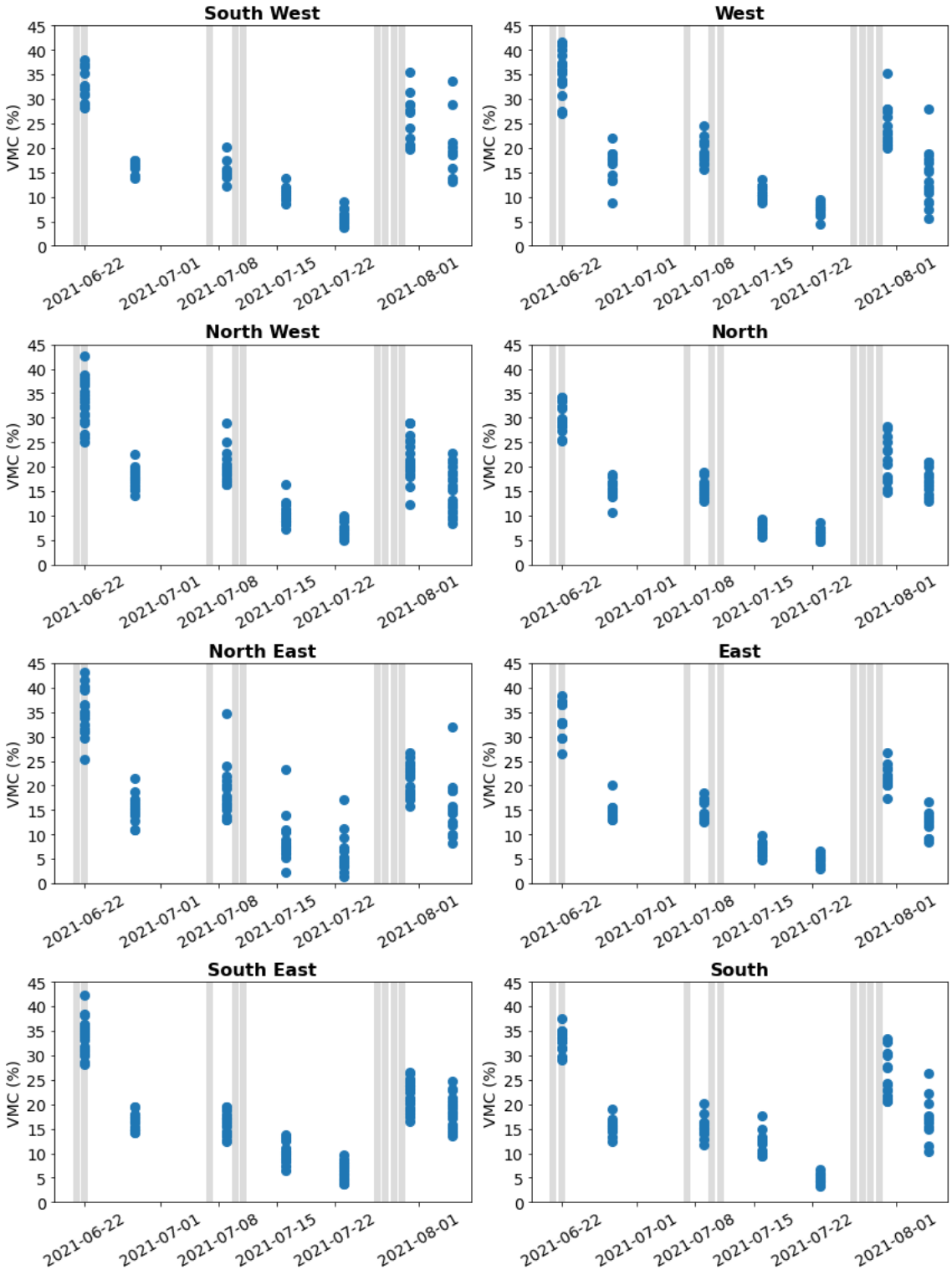

Figure 25: Average of the three ADR measurements taken at each point location in the different transects seen in Figure 15. The occurrence of daily precipitation over 4 mm is indicated by the horizontal grey lines.

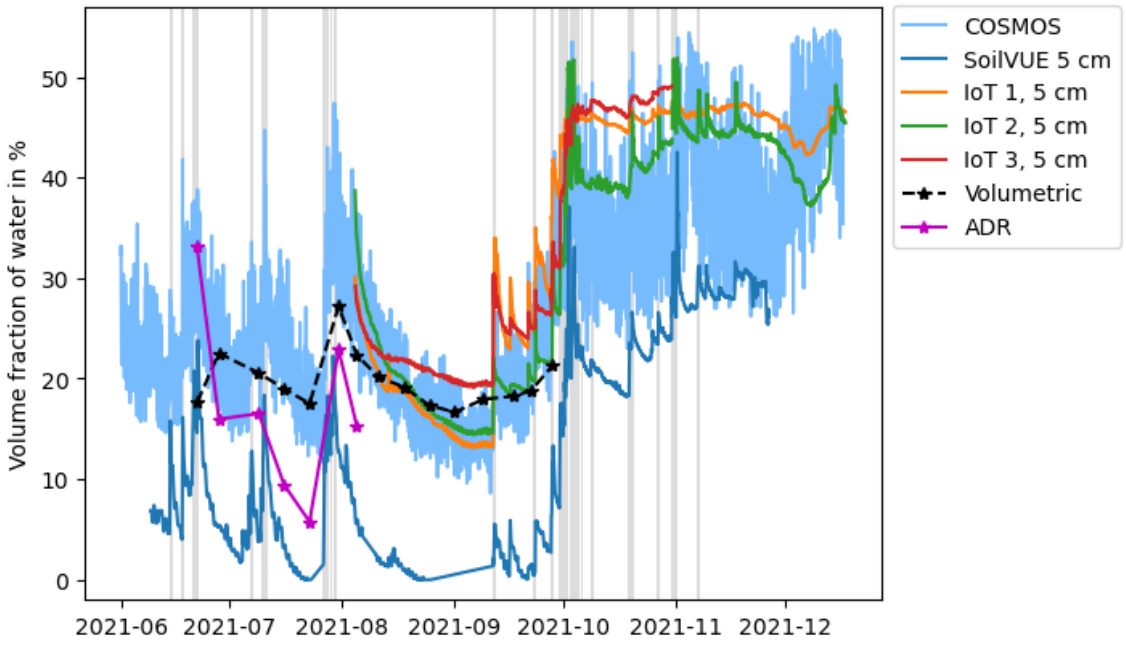

Figure 26: Time series from instruments in the period 22 June to 16 December 2021. 5 cm segments of IoT and SoilVUE sensors are used. For the volumetric method and ADR measurements, an average of all locations for each date has been used. The occurrence of daily precipitation over 4 mm is indicated by the horizontal grey lines.

4.1.2 Diurnal patterns

Soil moisture measurements from the IoT 1 sensor between 01 and 06 September 2021 are seen in Figure 27. Although the general trend shows decreasing values of soil moisture, there is a distinct diurnal pattern with increasing soil moisture from morning to noon and decreasing soil moisture from the early evening hours throughout the night. The diurnal variation in soil moisture lies between 0.2-0.8 %. The peaks in soil moisture occur around the same time each day, from about 1400 to 1900 UTC. The minima are more variable in length, but all occur around 0700 UTC.

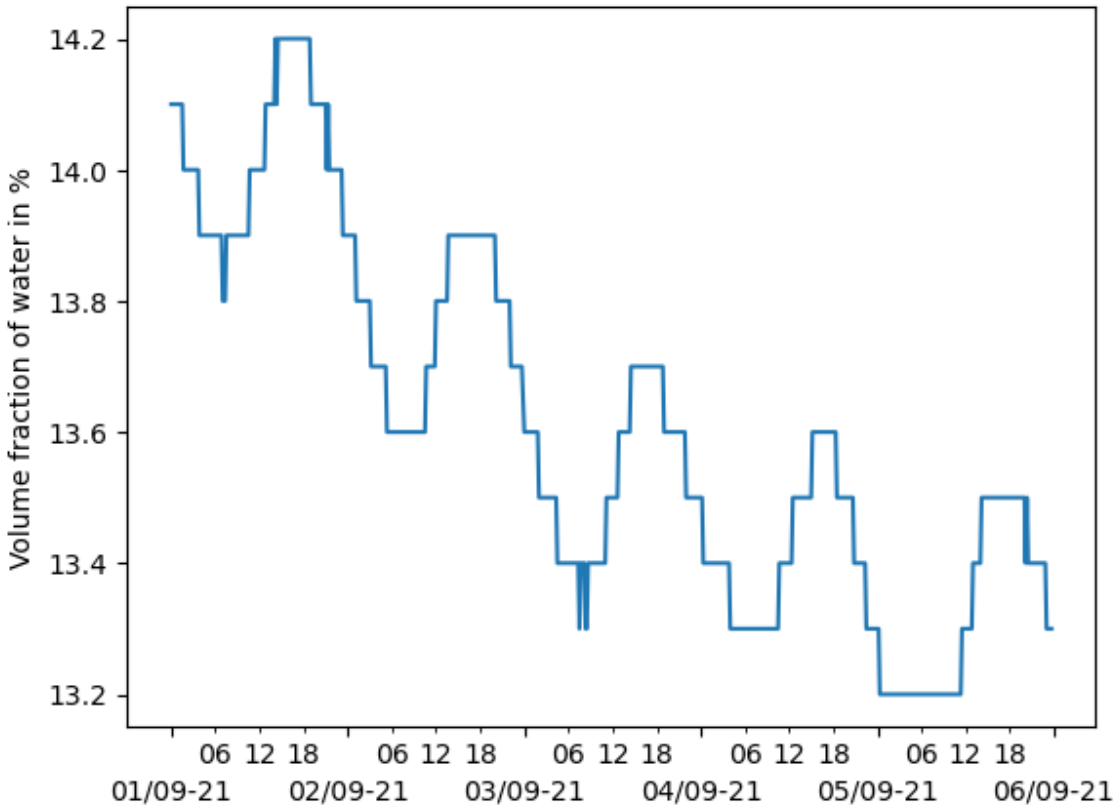

Figure 27: Diurnal pattern in soil moisture measured by the 5 cm segment of the IoT 1 sensor, between 01 to 06 September 2021. Times in UTC.

4.1.3 Standard deviations of permanently installed sensors

In Figure 28, we see the 10-day running means of the permanently installed instruments with standard deviation as the shaded area around the graph. From the figures, the standard deviations of the different instruments seem comparable and are higher in periods where the soil moisture is changing rapidly. All instruments have their peaks in standard deviation on 08 October, and the COSMOS sensor has an equally large peak on 04 August. The IoT 2 sensor shows the largest errors, with a standard deviation of 5.9 % on 08 October.

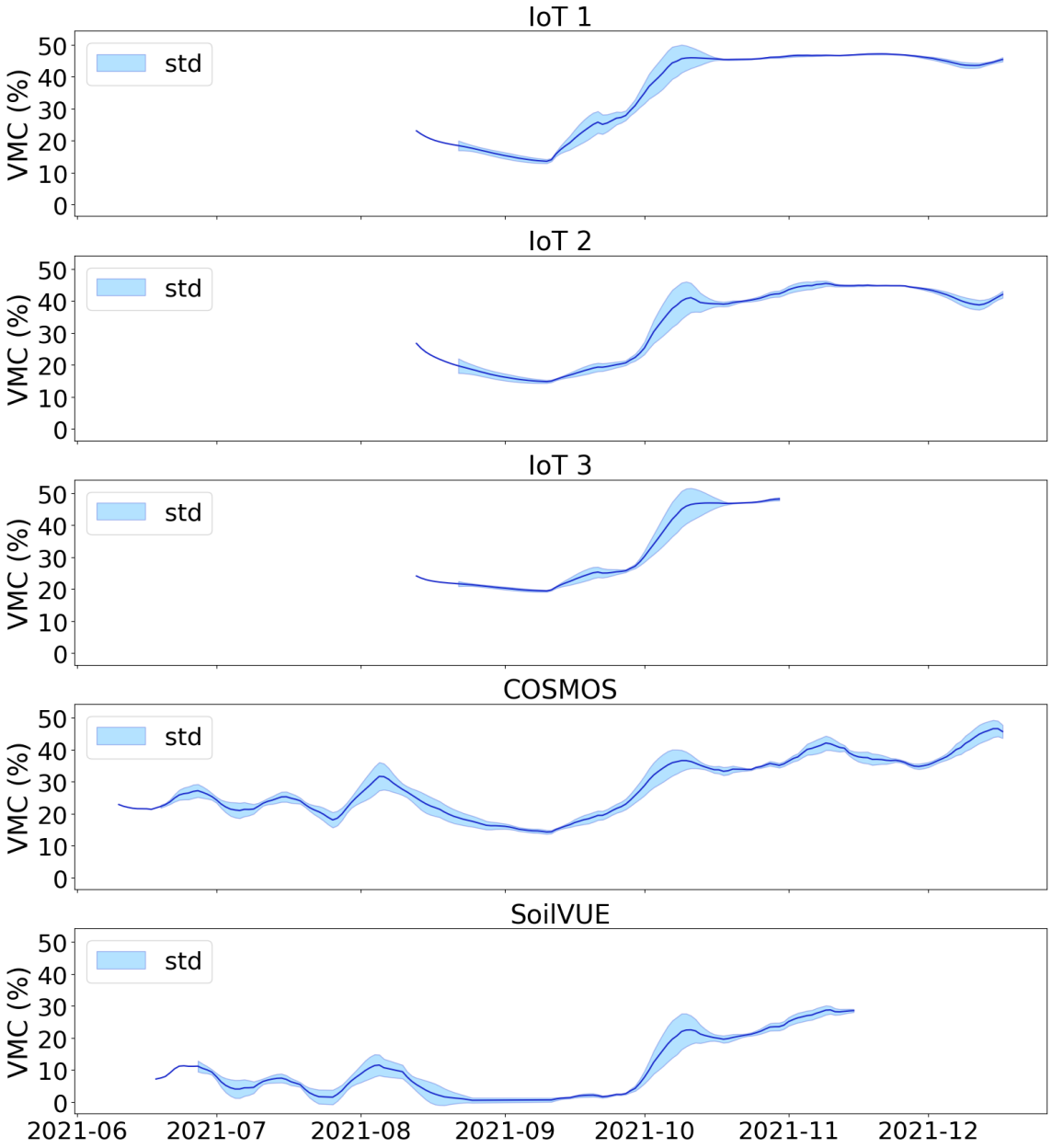

Figure 28: Running mean of volumetric soil moisture content (VMC) over ten days with standard deviation of the permanently installed sensors. Standard deviation is seen as the light, shaded area around the line.

4.2 Spatial variability in soil moisture across Søråsfeltet

In this section, the spatial variability in soil moisture across Søråsfeltet has been investigated by comparing the ADR measurements from the different transects (see Figure 15) and the measurements from the three IoT sensors, which are evenly spread out across the field.

In addition, the coefficient of variation (CV) has been calculated for the volumetric method measurement. The CV is defined as the standard deviation over the mean and is a useful measure in determining the spatial variability in soil moisture

measurements. The average CV of the volumetric method measurements was 0.19.

4.2.1 Variability across ADR transects

In Figure 29, we see how the ADR measurements vary between the different point locations on the different measurement dates. For some of the transects, we see that several maxima and minima in soil moisture on the different dates occur in the same point locations. The most remarkable example is location NE6 of the northeast transect, which consistently measures higher soil moisture values than its neighbouring location. At the most, its measured value was 17.6 % higher than NE5. In addition, locations N5 and N8 of the north transect show peaks in soil moisture for almost all dates, while N13 shows a dip in soil moisture for all dates.

Generally, when the soil moisture content is higher, the variation in soil moisture across the transect is higher. For example, in the northwest transect, soil moisture varies between 25.9 and 43.5 % on 22 June, while it varies between 5.4 and 10.0 % on 23 July. On the two days of least soil moisture, 16 and 23 July, the variations across most transects are about 5 %, except for the northeast transect, where the variation is over 15 %, due to the higher values in location NE6.

The order of the dates from highest to lowest soil moisture content is generally the same across the different transects.

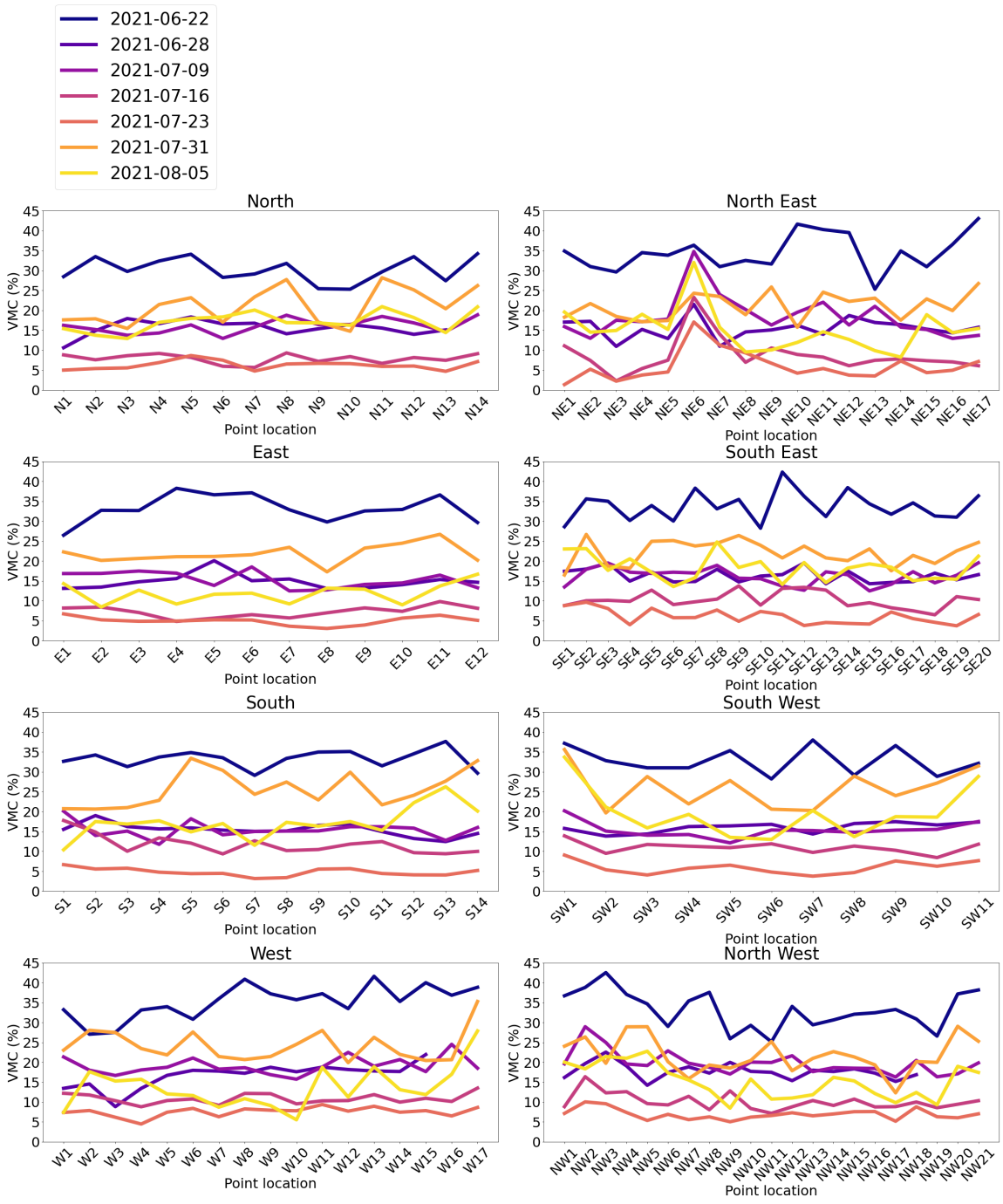

Figure 29: ADR measurements at every point location of every transect on the different measurement dates.

4.2.2 Variability between IoT sensors during heavy precipitation

In Figure 30, we see how soil moisture measured at 5 cm depth by the three IoT sensors changes from 01 to 03 October, during the largest precipitation event of the research period. The IoT 2 sensor is the one changing the most during this period. It starts off at 31.6 % soil moisture on the morning of 01 October, reaches 51.5 % at 1300 UTC on 02 October, and decreases to 38.9 % at 0610 UTC on 03 October before it increases again. In the same time period, the IoT 1 sensor ranges between 43.5 and 46.8 % and the IoT 3 sensor between 38.8 % and 47.1 %. The increases in soil moisture generally coincide for the three sensors, but the changes in soil moisture are larger and more rapid for sensor IoT 2. The sudden decrease around 14 UTC on 02 October is not reflected by the other sensors.

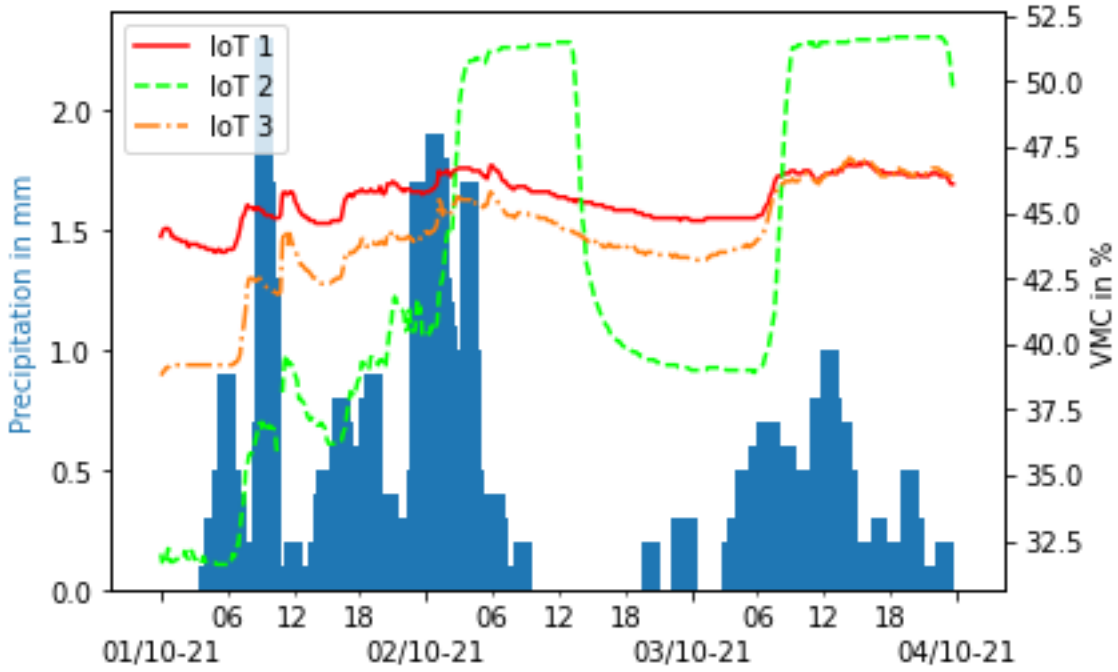

Figure 30: Volumetric soil moisture content (VMC) measured at 5 cm depth by the three IoT sensors in Søråsfeltet from 01 to 03 October 2021, during the heaviest rainfall of the year.

4.3 Statistical analysis

In this section, the results from the Shapiro-Wilk test for normality, Levene's test for equal variances and Kolmogorov-Smirnov test of equal distributions are shown. The distributions of the data sets are further investigated through histograms displayed in Section 4.3.1.

4.3.1 Normality test

From the Shapiro-Wilk test for normality, none of the p-values were over 0.05, meaning the null hypothesis, which stated that the data follows a normal distribution, was rejected. This is supported by the histograms shown below.

Histograms of the soil moisture measurements from the IoT sensors at depths 5 and 25 cm are shown in Figure 31, all showing bimodal distributions. For the 5 cm segments, most soil moisture values lie between 45 and 50 %, and there are few measurements between 35 and 40 %. The peaks in the 25 cm measurements are around 20 and 25 % and 40 and 50 % soil moisture.

Bimodal distributions are also seen in the SoilVUE measurements at depths 0-75 cm (Figure 32). Depths 5 and 10 cm have peaks between 0 and 10 % soil moisture and almost no measurements above 40 %. In contrast, the deeper depths have peaks between 35 and 45 %. Soil moisture measurements at 100 cm depth show a left-skewed distribution.

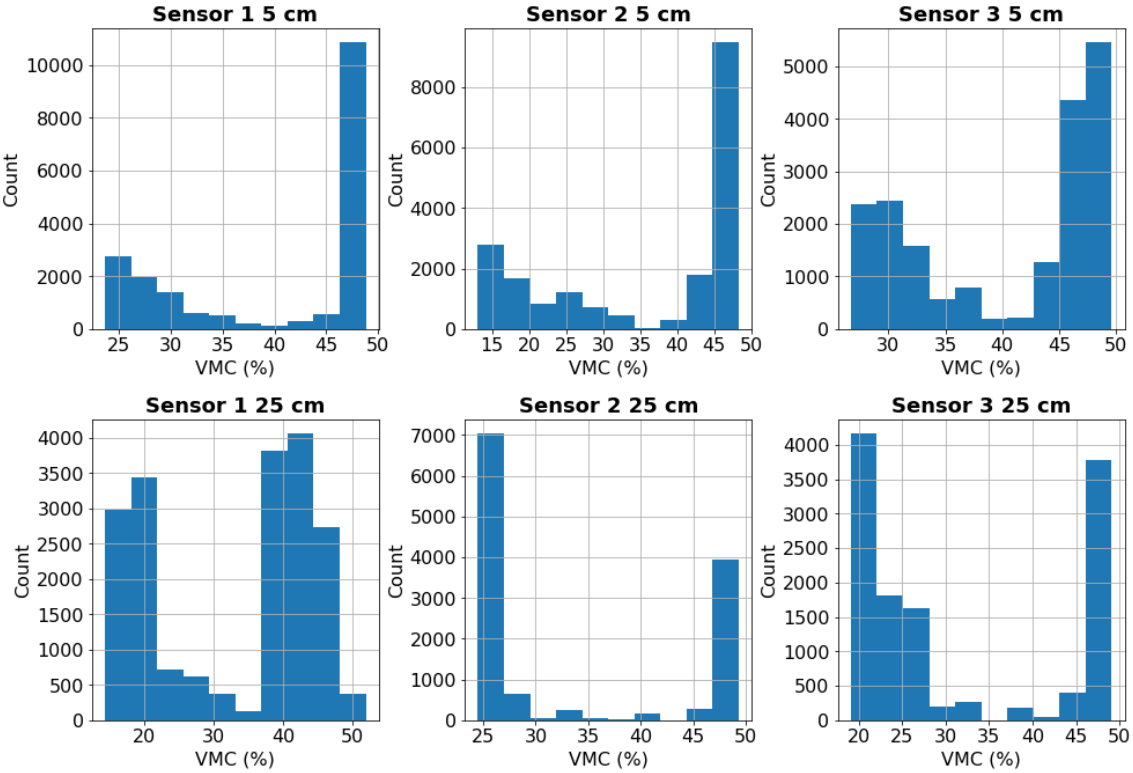

Figure 31: Histograms of measurements from 5 and 25 cm depths of the IoT sensors.

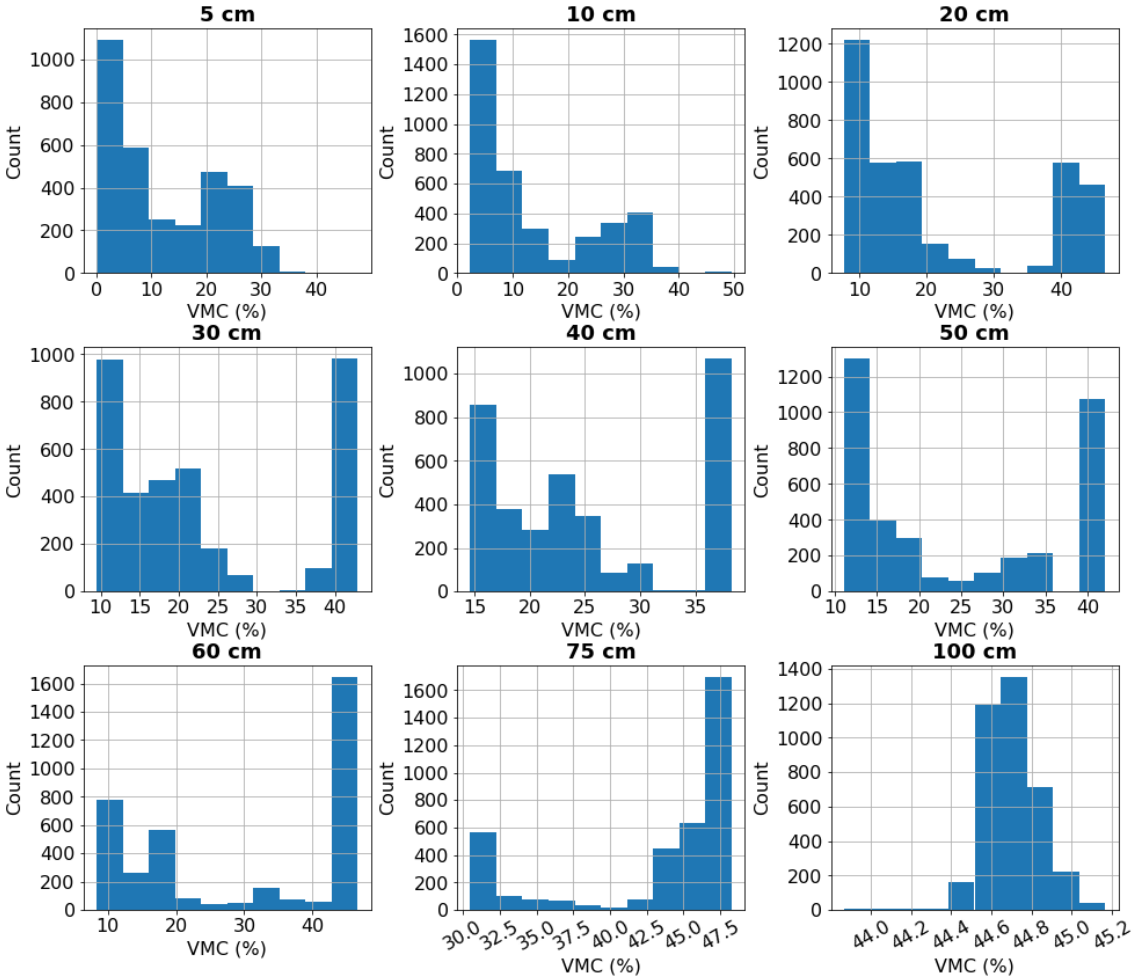

Figure 32: Histogram of measurements from all depths of the SoilVUE sensor.

The histograms of the soil moisture measurements from the COSMOS sensor, ADR and volumetric method are seen in Figures 33, 34 and 35, respectively. These data sets appear closer to following a normal distribution than the SoilVUE and IoT data, but we see that the distribution of the COSMOS and ADR data sets are right-skewed.

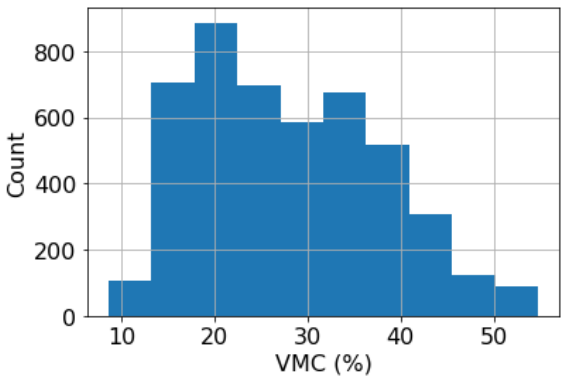

Figure 33: Histogram of measurements from the COSMOS sensor.

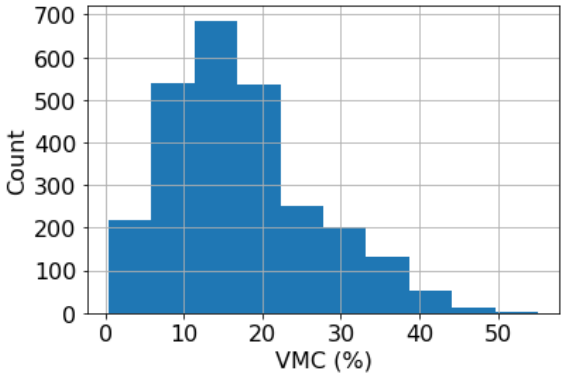

Figure 34: Histogram of all ADR measurements.

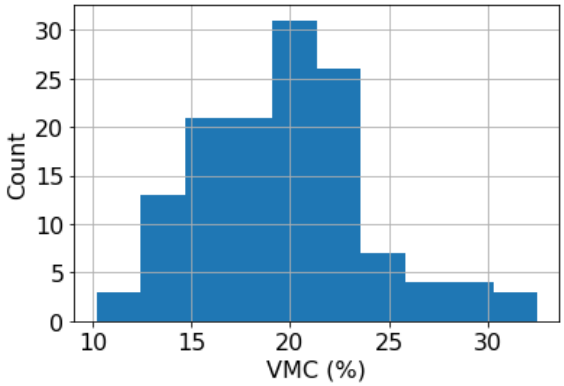

Figure 35: Histogram of the volumetric method measurements.

From the results of the Shapiro-Wilk test and the histograms, the distributions of soil moisture measurements from all instruments are clearly not normally distributed, and therefore statistical tests adequate for non-normal distributions will be used further.

4.3.2 Test for similar distributions

In order to assess whether the measurements from the different methods show the same distribution, a Kolmogorov-Smirnov test was carried out. The null hypothesis of the test is that the two distributions are equal. Table 9 shows the p-values obtained from the test. From the table, we see that all p-values are below 0.05, meaning that we can reject the null hypothesis from all tests and conclude that none of the data sets come from the same distributions.

Table 9: p-values from Kolmogorov-Smirnov test.

	SoilVUE	**IoT 1**	**IoT 2**	**IoT 3**	**Volumetric**	**ADR**	**COSMOS**
SoilVUE		0	0	0	1.891×10^{-33}	7.921×10^{-46}	6.901×10^{-322}
IoT 1	0		0	0	2.601×10^{-48}	7.991×10^{-175}	0
IoT 2	0	0		0	6.661×10^{-43}	1.231×10^{-149}	0
IoT 3	0	0	0		2.111×10^{-28}	3.511×10^{-231}	3.071×10^{-224}
Volumetric	1.891×10^{-33}	2.601×10^{-48}	6.661×10^{-43}	2.111×10^{-28}		4.691×10^{-10}	1.871×10^{-26}
ADR	7.921×10^{-46}	7.991×10^{-175}	1.231×10^{-149}	3.511×10^{-231}	4.691×10^{-10}		5.651×10^{-90}
COSMOS	6.901×10^{-322}	0	0	3.071×10^{-224}	1.871×10^{-26}	5.651×10^{-90}	

4.3.3 Variance test

A variance test was carried out to see whether the variances of the data sets from the different instruments are equal or not. Levene's test was used, as it does not assume normally distributed data. The null hypothesis of this test is that the variances of the two data sets are equal. From Table 10, we see that the test yielded p-values below 0.05 for all pairs except SoilVUE and IoT 3, meaning that only these two data sets are deemed to have equal variances.

Table 10: p-values obtained from Levene's test for equal variances.

	SoilVUE	**IoT 1**	**IoT 2**	**IoT 3**	**Volumetric**	**ADR**	**COSMOS**
SoilVUE		2.891×10^{-9}	1.001×10^{-6}	0.14	1.861×10^{-33}	7.961×10^{-12}	2.171×10^{-22}
IoT 1	2.891×10^{-9}		3.231×10^{-6}	1.301×10^{-15}	3.381×10^{-13}	6.401×10^{-10}	9.311×10^{-44}
IoT 2	1.001×10^{-6}	3.231×10^{-6}		4.401×10^{-7}	2.371×10^{-21}	4.901×10^{-13}	5.961×10^{-52}
IoT 3	0.14	1.301×10^{-15}	4.401×10^{-7}		5.171×10^{-17}	3.141×10^{-8}	3.491×10^{-26}
Volumetric	7.961×10^{-12}	6.401×10^{-10}	4.901×10^{-13}	5.171×10^{-17}		5.071×10^{-14}	5.791×10^{-26}
ADR	7.961×10^{-12}	6.401×10^{-10}	4.901×10^{-13}	3.141×10^{-8}	5.071×10^{-14}		0.012
COSMOS	2.171×10^{-22}	9.311×10^{-44}	5.961×10^{-52}	3.491×10^{-26}	5.791×10^{-26}	0.012	

4.4 Visual statistical analysis of multiple soil moisture sensors

From Figure 36, we see that the range of soil moisture values differ between the different locations of the volumetric method. The medians of locations south and ZERO lie outside the interquartile ranges of all other locations, meaning that the measurements from these locations are likely to significantly differ from the measurements from the rest of the locations. Measurements from location north differ from locations northwest, northeast, south and ZERO. None of the locations have values of soil moisture lower than 10 % and the highest value is 32.5 % for location east.

The median values from the ADR transects lie within the interquartile ranges of all other transects, meaning it is not likely that the measurements significantly differ from each other (Figure 37). The ranges of the ADR measurements are greater than the volumetric method measurements, as seen from the larger IQR. In contrast to the volumetric measurements, all transects have values of less than 10 % soil moisture.

From Figure 38, we see that the median values of the 5 and 25 cm segments of the IoT 3 sensor lie outside the interquartile ranges of the 25 cm segments of sensors 1 and 2. The median values of the 5 cm and 25 cm segments of the IoT 3 sensor are 25.4 % and 26.3 %, respectively, while the median values of the other two sensors are all above 39 %. The IoT 3 sensor has the widest range of the sensors, with values between 19.1 % and 49.1 % soil moisture. We also see that the variances are greater at 5 cm than at 25 cm depth.

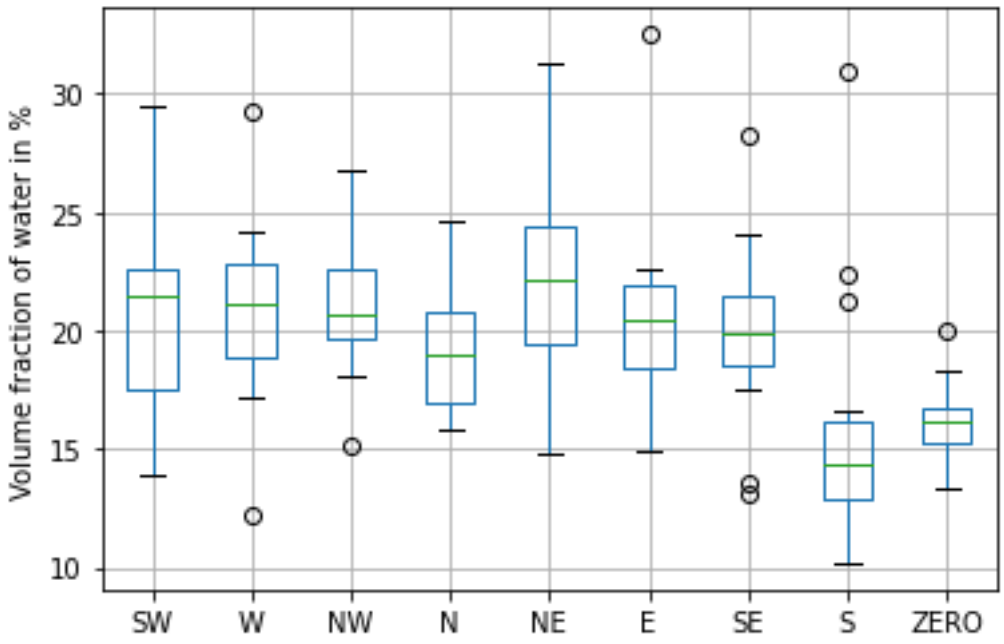

Figure 36: Box plot of the volumetric method measurements from each of the nine locations.

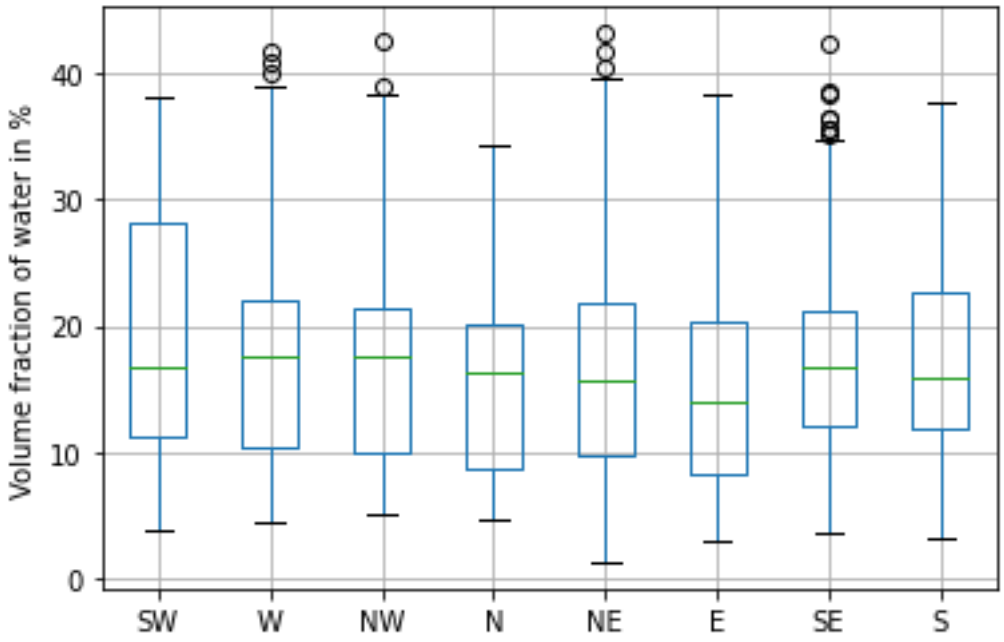

Figure 37: Box plots of ADR measurements from each of the eight transects. The box plots have been made from the average of the three measurements taken at each point location.

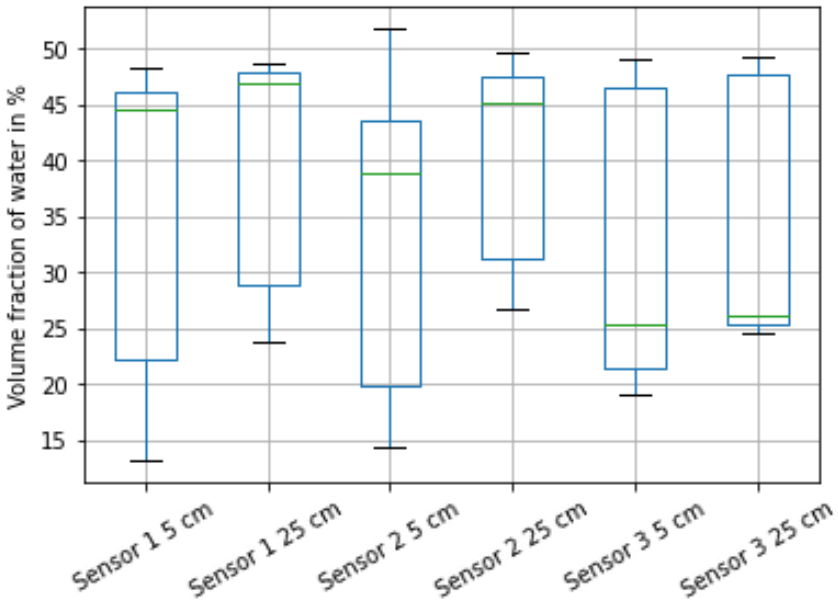

Figure 38: Box plot of measurements from the IoT sensors.

From Figure 39, we see that the medians of the 5 and 10 cm segments of the SoilVUE sensor lie outside the IQR of the other depths. This also applies to the 75 and 100 cm segments. The 5 and 10 cm segments have the largest variances, while the measurements at 100 cm depth only vary between 43.9 and 45.3 %.

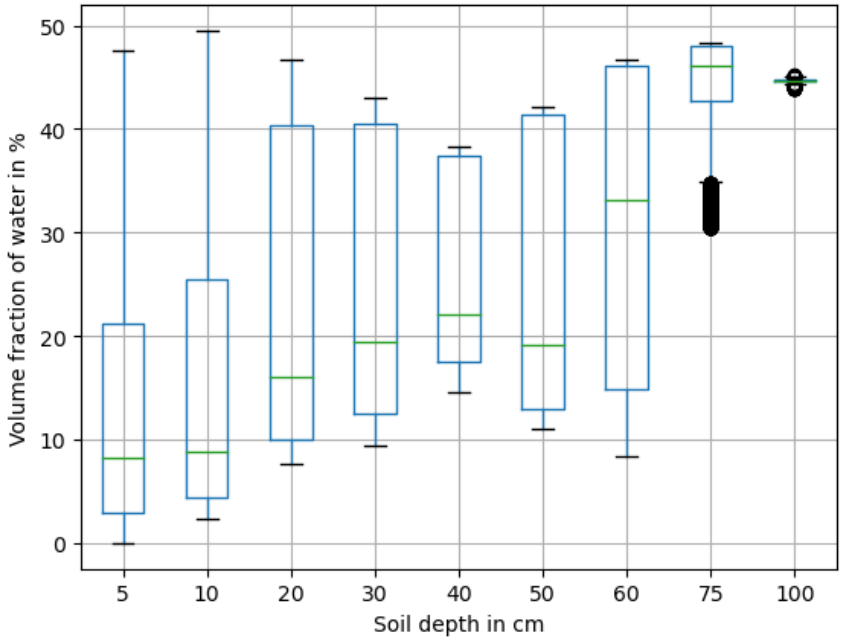

Figure 39: Box plot of SoilVUE measurements at all depths.

From Figure 40 we see that the values from the COSMOS sensor range between 8.6 % and 54.8 % soil moisture content, and the median value is 26.7 %. 50 % of the

measurements have values lower than around 35 % soil moisture content.

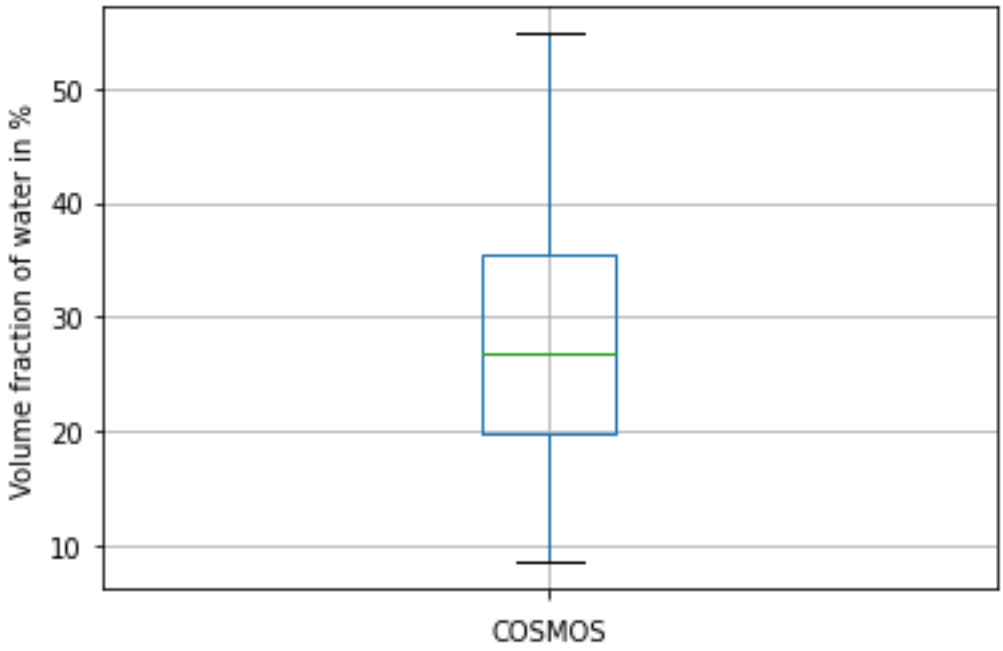

Figure 40: Box plot of measurements from the COSMOS sensor.

4.5 Comparison of SoilVUE and IoT sensor

The SoilVUE and IoT 2 sensors are located within 1 meter apart in the centre of Søråsfeltet. Comparing the measurements from these sensors thus enables intercomparison of instruments while diminishing the factor of spatial soil moisture heterogeneity.

In Figure 41, we see the soil moisture time series from the IoT 2 and SoilVUE sensors at 5 cm. The measurements follow the same patterns, and computing the Pearson's correlation coefficient between the two yielded $r = 0.98$, meaning the two time series are highly correlated.

We also see that the SoilVUE sensor consistently reports lower soil moisture values than the IoT sensor. In Figure 42, we see that most of the time, the difference between the two sensors is between 15 and 20 %. However, on 02 October, the difference is reduced to 4 %, and on 01 November, it is as low as 1.4 %, both of which are days with considerable amounts of precipitation (Figure 9a).

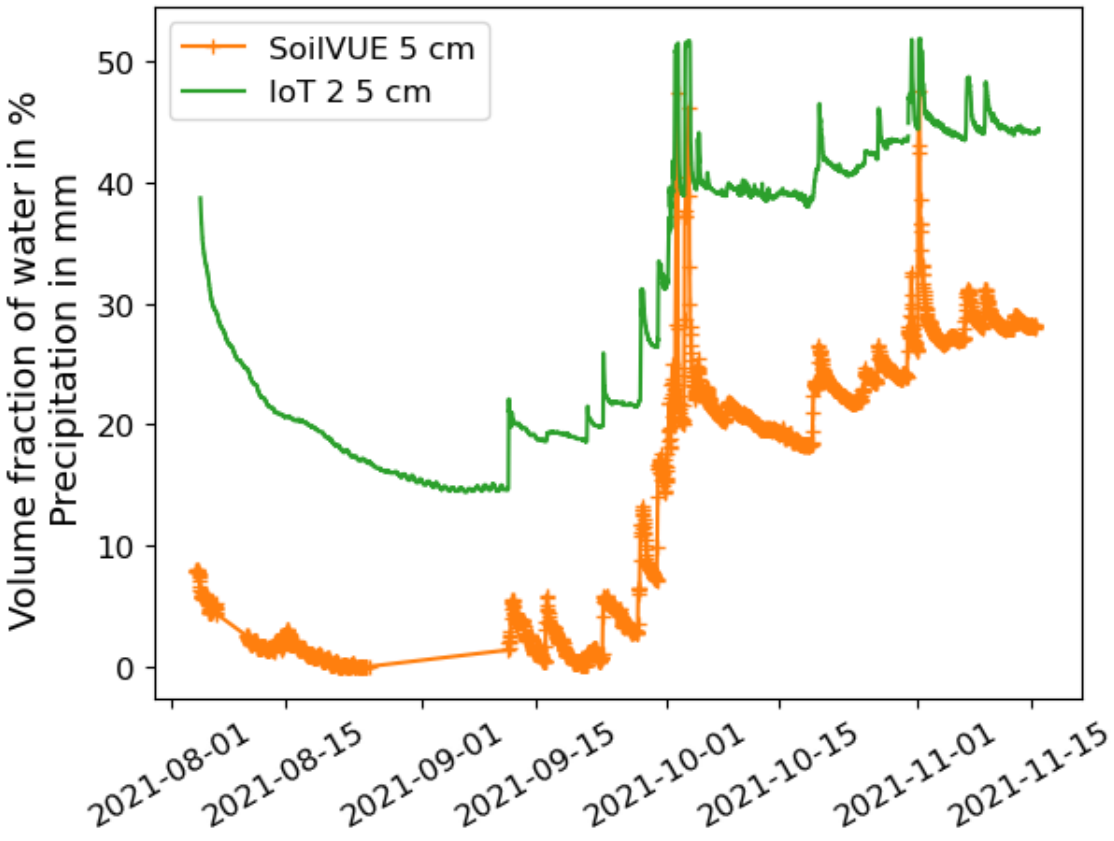

Figure 41: Soil moisture measurements from the 5 cm segments of the SoilVUE and IoT 2 sensor, which are located within 1 meter apart, in the center of Søråsfeltet.

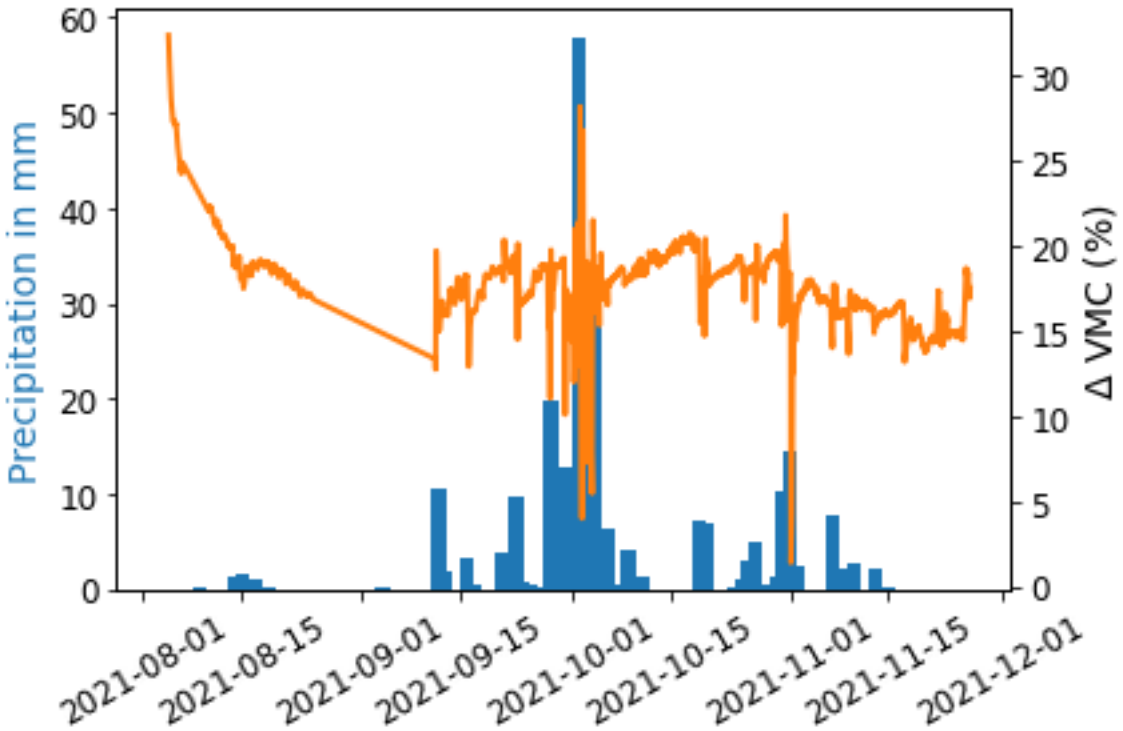

Figure 42: The absolute difference between soil moisture measurements from 5 cm segments of the SoilVUE and IoT 2 sensor together with daily precipitation. The difference in soil moisture is displayed as the solid orange line while precipitation is displayed as the dashed blue line. Precipitation is measured on the left y-axis, while the change in volumetric moisture content (Δ VMC) is on the right y-axis.

The same investigation was done for measurements from the IoT sensor at 25 cm and the SoilVUE sensor at 20 cm depth. We see from Figure 43 that the two sensors follow the same patterns at these depths also. We see that the difference between the two sensors is between 20 and 25 % for the first half of the measurement period and decreases to around 5 % after 01 October (Figure 44).

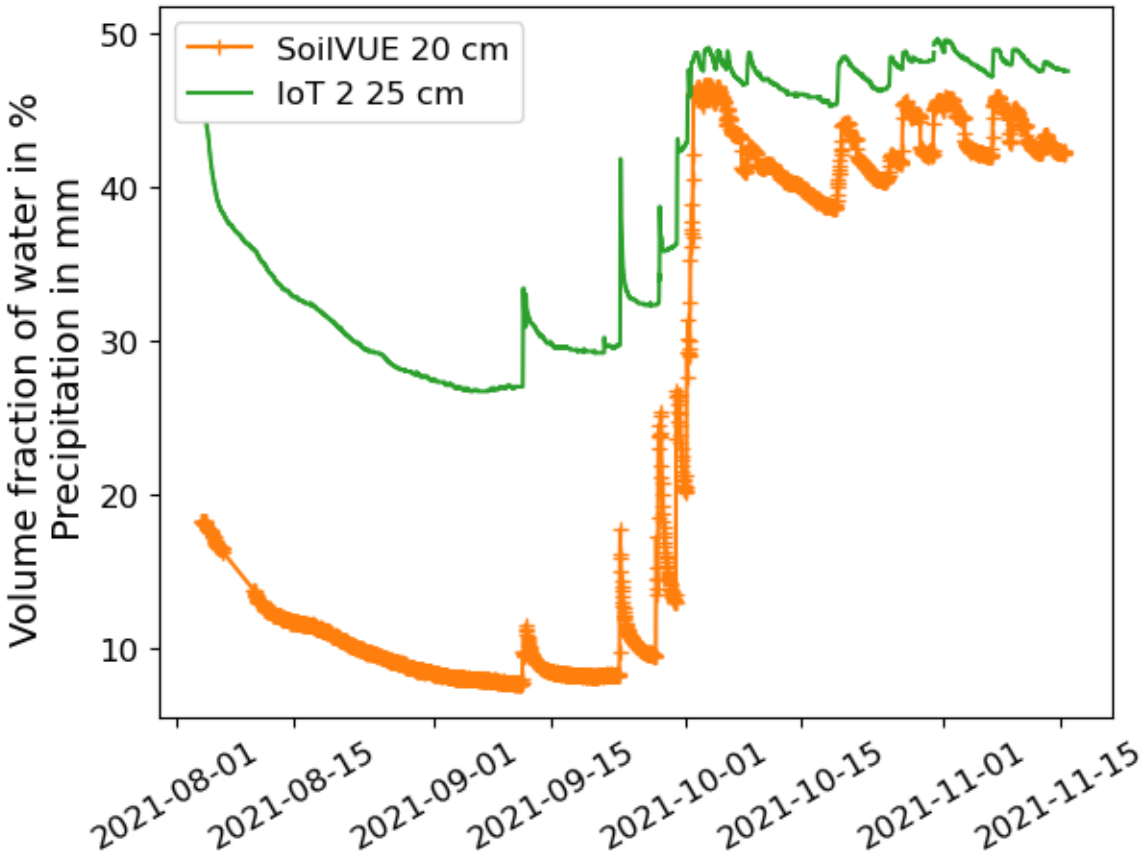

Figure 43: Soil moisture measurements from the 20 and 25 cm segments of the SoilVUE and IoT 2 sensors, respectively. The sensors are placed less than 1 m apart in the center of Søråsfeltet.

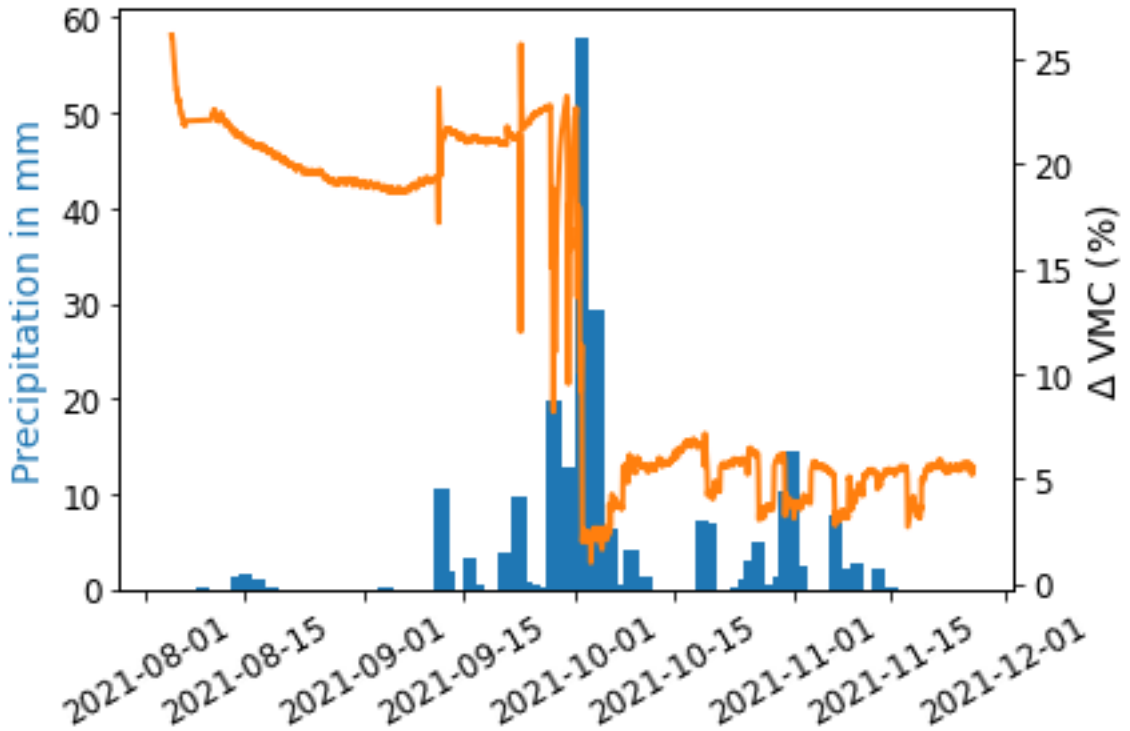

Figure 44: The absolute difference between soil moisture measurements by the SoilVUE (20 cm depth) and IoT 2 sensor (25 cm depth) together with daily precipitation. The difference in soil moisture is displayed as the solid orange line while precipitation is displayed as the dashed blue line. Precipitation is measured on the left y-axis, while the change in volumetric moisture content (Δ VMC) is on the right y-axis.

4.6 Effect of precipitation on soil moisture

Figure 45 shows daily precipitation together with daily soil moisture values of the different segments of the SoilVUE sensor. We see that for depths 5, 10 and 20 cm, soil moisture follows the variation in precipitation closely. Small peaks in precipitation around 18 June, 07 and 27 July lead to peaks in soil moisture for the three shallower depths. The 58 mm of precipitation on 02 October led to a rapid rise in soil moisture at all depths, except at 100 cm.

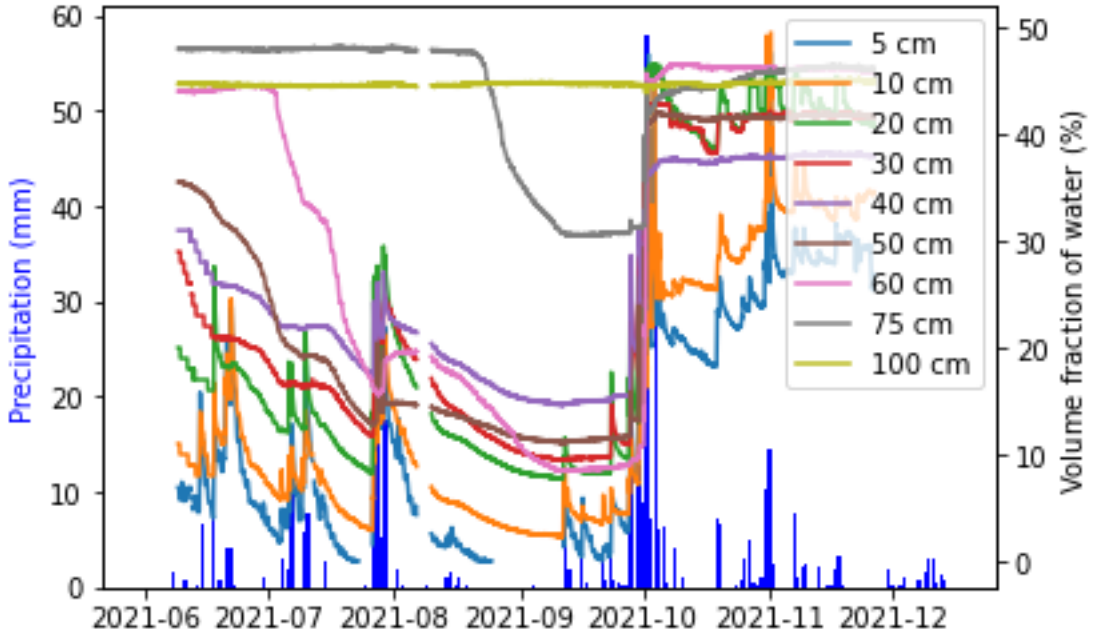

Figure 45: Daily precipitation together with soil moisture at different depths measured by the SoilVUE sensor. Soil moisture is represented by solid lines while precipitation is represented by the blue bars.

A linear regression was carried out to assess whether precipitation is a significant predictor of soil moisture measured at different depths by the SoilVUE sensor. The p-values are presented in Table 11, together with the correlation between precipitation and soil moisture at the different depths. From the table, we see that on a 95 % significance level, precipitation is a significant predictor of soil moisture at depths 5, 10, 20 and 30 cm. We also see that the correlation between precipitation and soil moisture is highest at these depths. However, at 75 and 100 cm depth, the two are negatively correlated.

Table 11: p-values obtained from linear regression from precipitation and soil moisture at different depths and the correlation between the two variables.

Depth (cm)	**Correlation**	**p-value**
5	0.26	0.0017
10	0.21	0.046
20	0.27	0.005
30	0.23	0.024
40	0.18	0.10
50	0.14	0.25
60	0.082	0.77
75	-0.042	0.19
100	-0.19	0.59

The p-values from linear regression and correlation coefficients between the IoT sen-

sor measurements and precipitation are shown in Table 12. Since all p-values are less than 0.05, precipitation is likely to be a significant predictor of soil moisture measured by all three sensors at both depths. We also see that the correlation between precipitation and soil moisture is similar between the 5 and 25 cm segments of the sensors and that sensor 3 has the highest correlation coefficients.

Table 12: Correlation and p-value from linear regression between daily sums of precipitation and daily averages of soil moisture measurements from the IoT sensors.

Sensor	**Depth (cm)**	**Correlation**	**p-value**
1	5	0.20	0.019
	25	0.19	0.0030
2	5	0.18	0.042
	25	0.18	0.0069
3	5	0.26	0.013
	25	0.27	0.011

4.6.1 Response time

The time from when a precipitation event occurs until soil moisture increases for all depths of the SoilVUE and IoT sensors is illustrated in Figures 46 to 50. The investigation period starts on 11 September, which marks the end of a 1.5 month dry period with little precipitation.

From Figure 46, we see that the 5 and 25 cm segments of all IoT sensors report a rise in soil moisture around two hours after the first precipitation falls at 1210 UTC on 11 September. All three sensors experience an increase in soil moisture at 1430 UTC at both depths.

At 5 cm depth, IoT 2 reaches its first soil moisture peak at 1510 UTC for IoT 2, IoT 3 at 1650 UTC and IoT 1 at 1750 UTC. At 25 cm depth, IoT 2 and 3 reach their first peak in soil moisture at 1510 UTC, while IoT 1 peaks at 1700 UTC.

The response time to the second precipitation event at 2040 UTC on 11 September was relatively similar to the first precipitation event. All sensors experience an increase in soil moisture at 2230 UTC, at both 5 and 25 cm depth.

The antecedent soil moisture levels and changes in soil moisture differed between the sensors. Sensor IoT 1 experienced the largest increase in soil moisture in this period at both depths. At 5 cm depth, the measured soil moisture increased from 13.3 % to 34 %, while at 25 cm depth, it increased from 23.7 to 43.5 %.

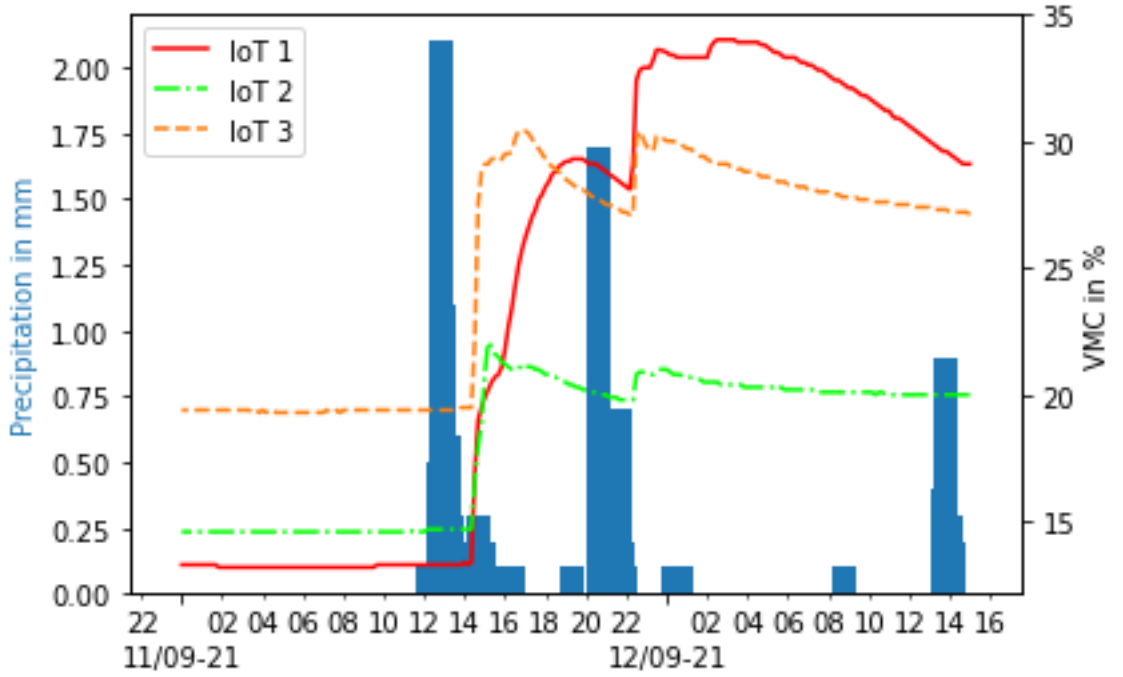

Figure 46: Precipitation and soil moisture at 5 cm depth measured by the three IoT sensors from 11 to 12 September 2021, after a long drought period. Precipitation is measured on the left y-axis, while volumetric soil moisture content (VMC) is on the right y-axis.

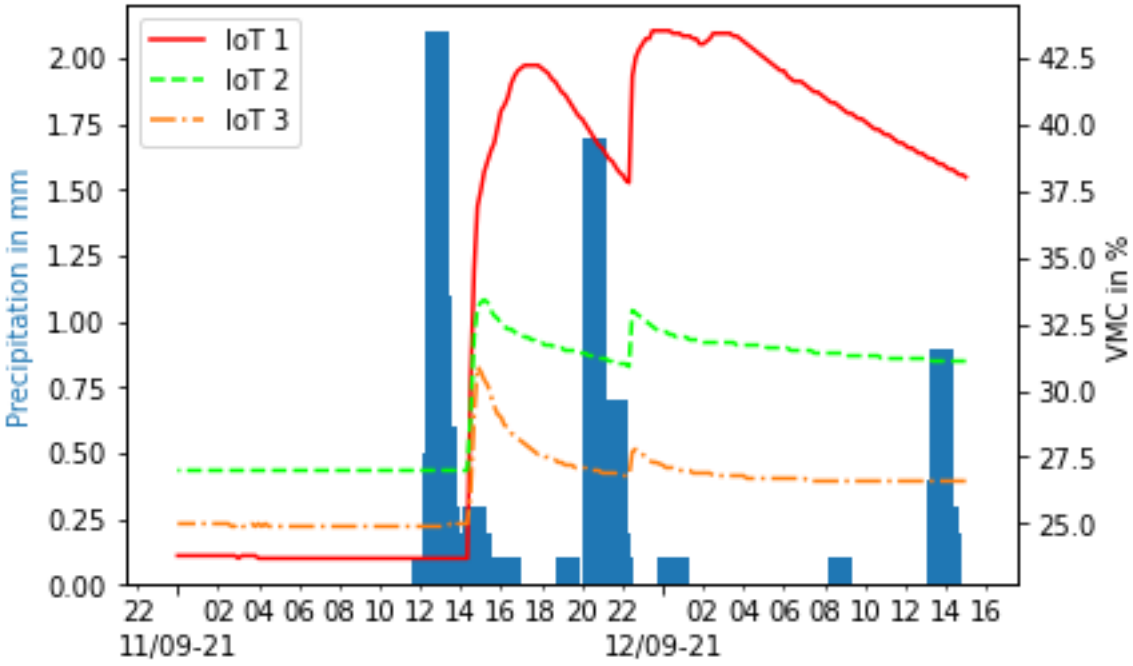

Figure 47: Precipitation and soil moisture at 25 cm depth measured by the three IoT sensors from 11 to 12 September 2021, after a long drought period. Precipitation is measured on the left y-axis, while volumetric soil moisture content (VMC) is on the right y-axis.

Figures 48, 49, and 50 show precipitation together with soil moisture from the SoilVUE sensor measured at the three shallower depths, the four intermediate depths and the two deepest depths, respectively.

Soil moisture measurements from the 5 cm segment are missing before the first precipitation event, but we see that soil moisture starts rising less than one hour after rainfall (Figure 48). The 10 and 20 cm segments respond within 30 minutes, as they experience an increase in soil moisture at 1240 UTC.

After the precipitation event at 2040 UTC on 11 September, an increase in soil moisture was seen at 2040 and 2050 UTC for depths 5 and 10 cm, respectively. This increase started at 2130 UTC at 20 cm depth. The peaks in soil moisture after the second precipitation event occur at 2200 and 2230 UTC for depths 10 and 20 cm, but not until 0150 UTC on 12 September for the 5 cm segment.

For the intermediate depths of 30 to 60 cm, the increase in soil moisture from 11 to 13 September is less than 0.5 % (Figure 49). When looking at the 100 cm segment, there is no apparent change in soil moisture after the precipitation events, while the 75 cm experiences a slight increase in the order of 0.20 % soil moisture from 16 to 25 September (Figure 50). The increase takes then place five days after the first precipitation event on 11 September.

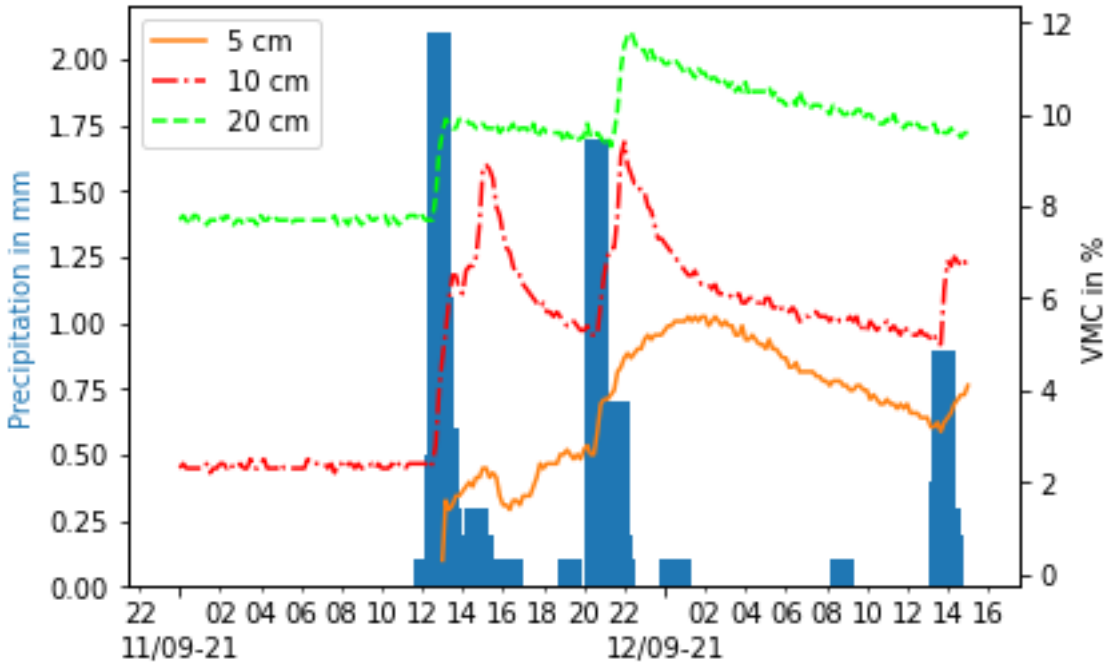

Figure 48: Precipitation displayed together with soil moisture measurements from the SoilVUE sensor at depths 5, 10 and 20 cm from the period 11 September to 12 September 2021. The red lines represent the soil moisture values while blue bars represent precipitation. Precipitation is measured on the left y-axis, while volumetric moisture content (VMC) is on the right y-axis.

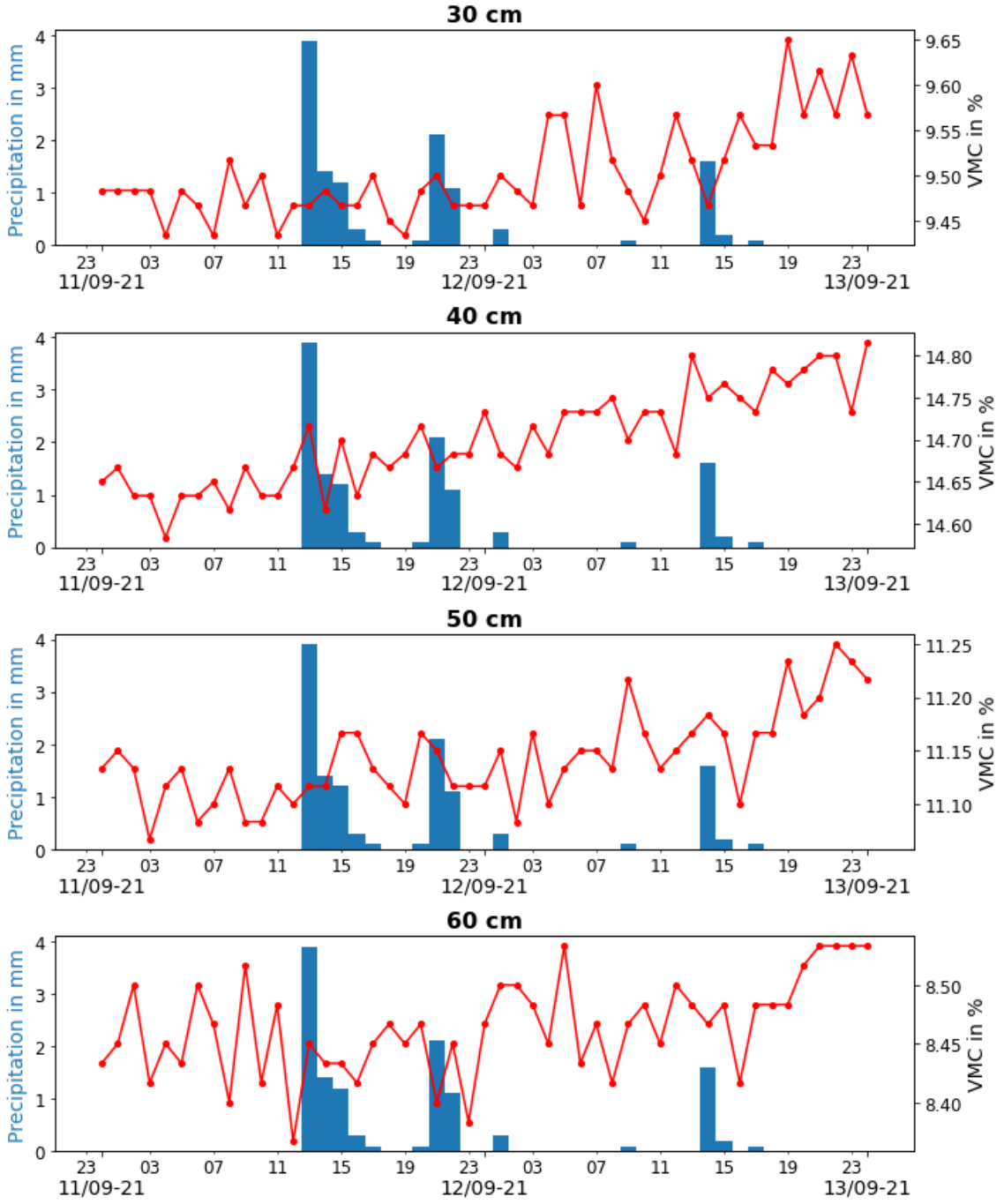

Figure 49: Hourly precipitation amount displayed together with hourly soil moisture measurements from the SoilVUE sensor at depths 30, 40, 50 and 60 cm from the period 11 September to 13 September 2021. The red lines represent the soil moisture values while blue bars represent precipitation. Precipitation is measured on the left y-axis, while volumetric moisture content (VMC) is on the right y-axis.

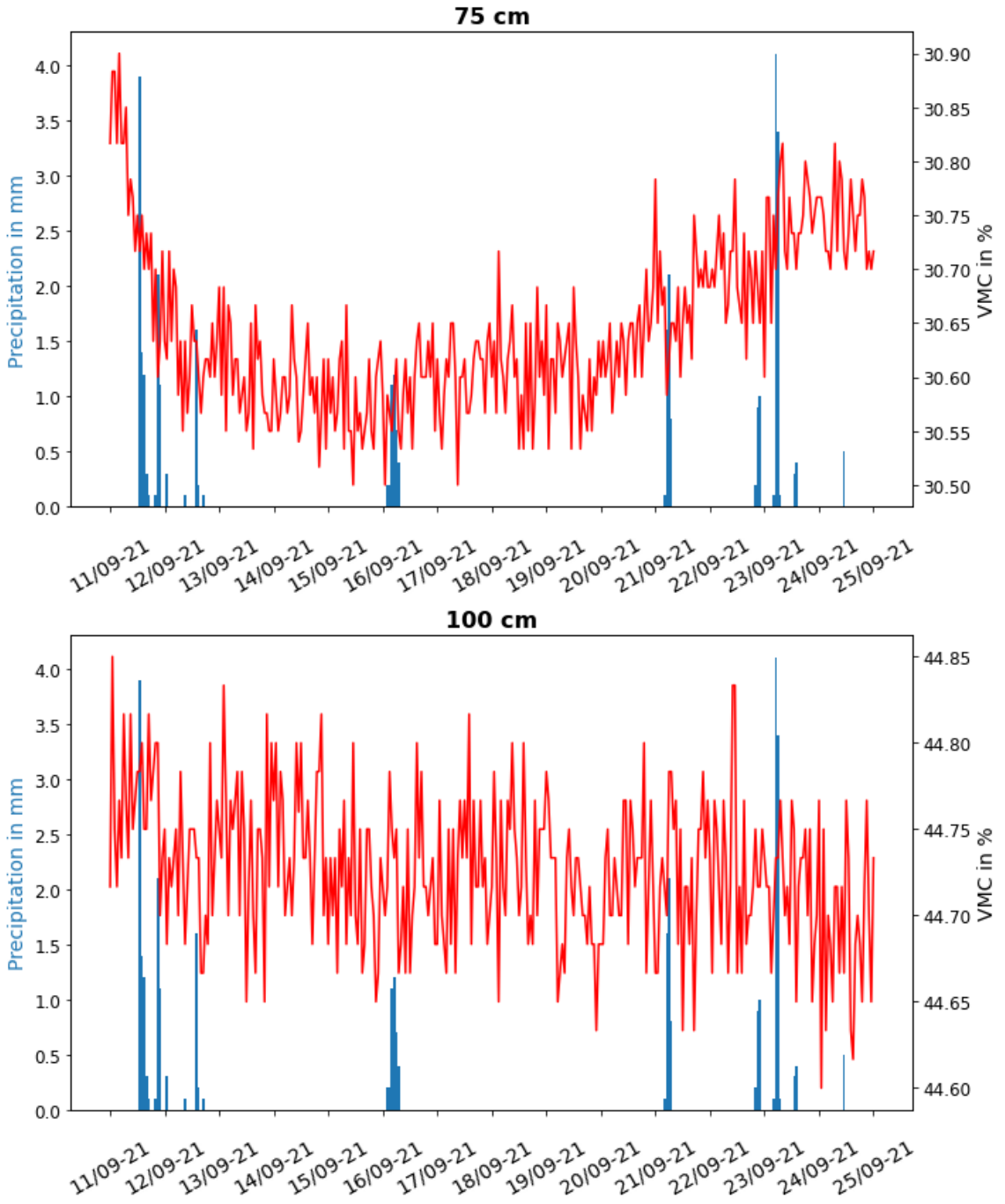

Figure 50: Hourly precipitation amount displayed together with hourly soil moisture measurements from the SoilVUE sensor at depths 75 and 100 cm from the period 11 September to 25 September 2021. The red lines represent the soil moisture values while blue bars represent precipitation. Precipitation is measured on the left y-axis, while volumetric moisture content (VMC) is on the right y-axis.

4.7 Calibration of GroPoint Profile sensor

In this section, the results from the soil-specific calibration of one GroPoint Profile sensor are presented.

The average of the five sensor readings taken at different moisture levels by the 5 cm and 25 cm segment of the GroPoint Profile sensor are displayed against the actual soil moisture values determined from the volumetric method in Figures 51a and 51b.

The equations from the fitted third-order polynomials are

$$y = 0.0006x^3 - 0.035x^2 + 1.6949x + 5.3881 \tag{13}$$

for the 5 cm segment and

$$y = 0.0004x^3 - 0.0294x^2 + 1.5696x + 5.0218 \tag{14}$$

for the 25 cm segment of the sensor.

The R^2 for the 5 cm and 25 cm segments are 0.994 and 0.999, respectively.

From Table 13, we see that the RMSE between the sensor readings and the soil moisture measurements from the volumetric method decrease when correcting the sensor readings using the coefficients in Equation 13 and 14.

Table 13: RMSE for the original and calibrated sensor readings.

Segment		RMSE (%)
5 cm	Original	9.77
	Calibrated	1.71
25 cm	Original	6.75
	Calibrated	0.89

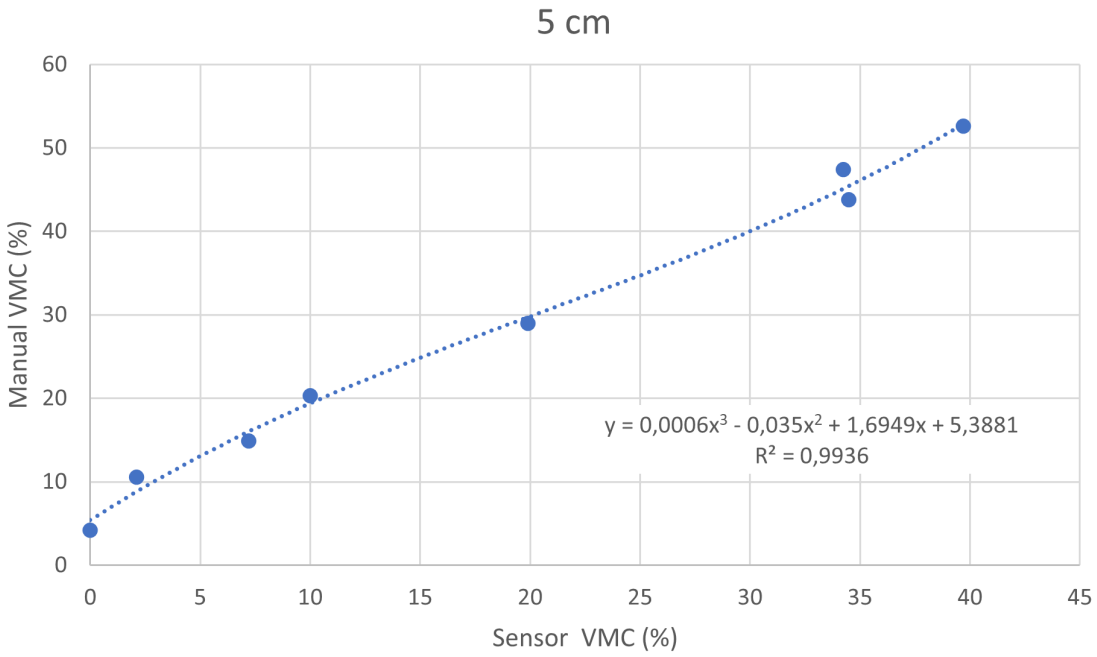

(a)

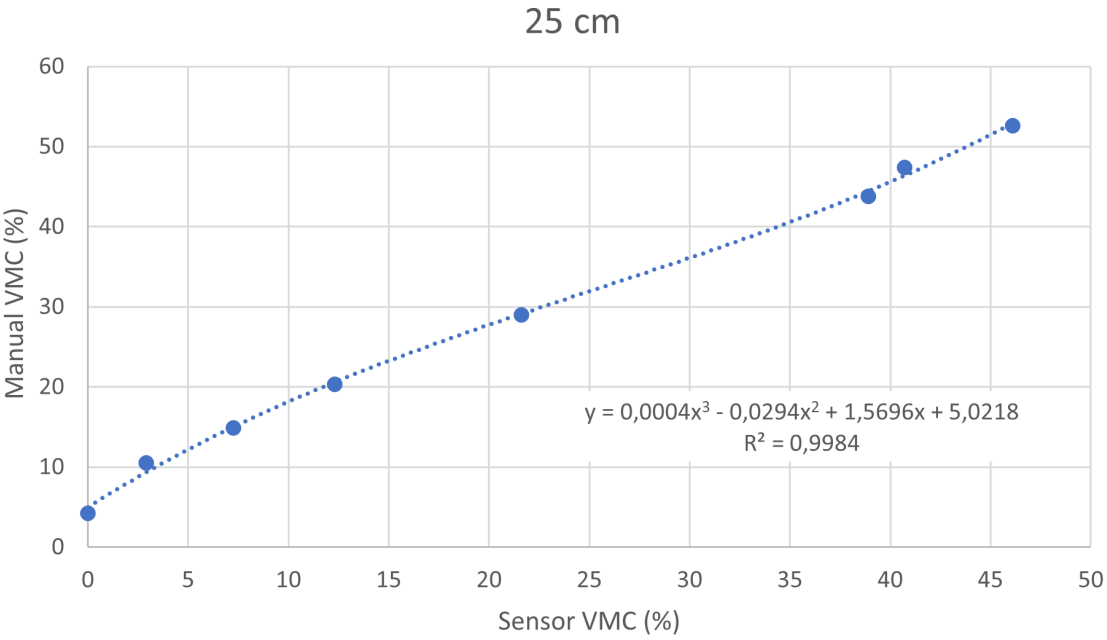

(b)

Figure 51: Scatter plots of soil moisture values obtained from volumetric method against the sensor readings from the *a)* 5 cm and *b)* 25 cm segment, together with a fitted third-order polynomial. The equation and R^2 values from the third-order polynomial are also displayed in the figures.

The result of displaying the sensor readings obtained during the calibration together with the values corrected with the third-order polynomial coefficients is shown in

Figure 52. We see that the corrected values are higher than the original sensor readings, both for the 5 and 25 cm segments. When soil moisture increases, the difference between the original and corrected values for the 5 cm segment also increases and is over 15 % at the most.

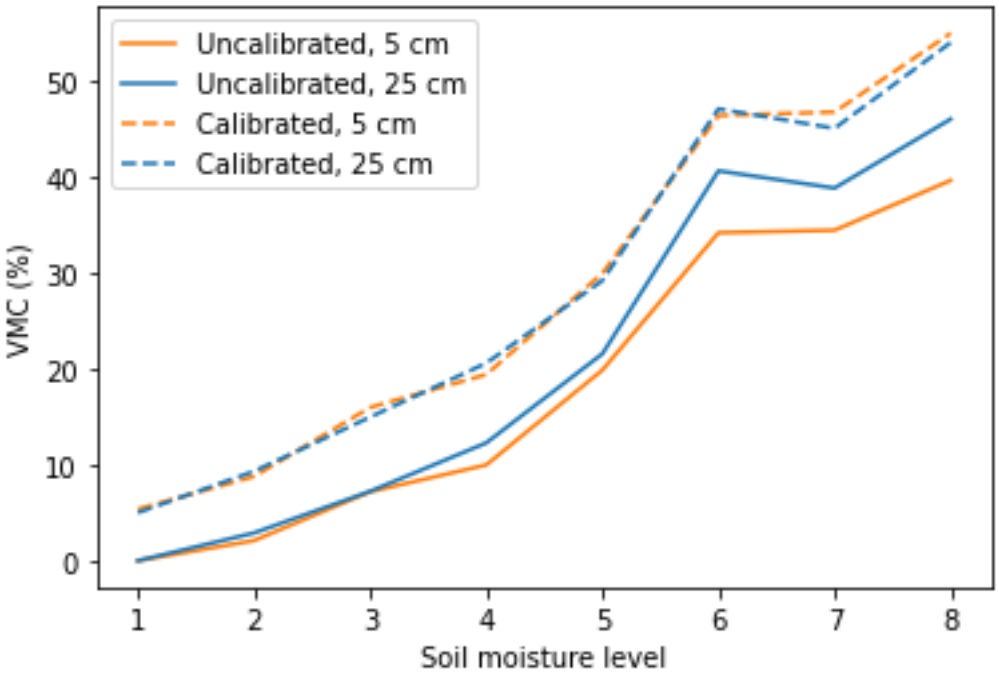

Figure 52: The sensor readings from the calibration process together with the corrected values using the third-order polynomial coefficients in Equations 13 and 14.

4.7.1 Comparison with permanently installed IoT sensors

The coefficients from Equations 13 and 14 were also used to update the other IoT sensors, and the original and corrected time series of the IoT 1 sensor are shown in Figure 53, while the two others are found in the Appendix. We see that the corrected time series generally have higher soil moisture values than the original. The difference between the original and corrected values for the 25 cm segments seems to be fairly constant, around 8 %, but for the 5 cm segments, the difference is around 10 % until the soil moisture rises, when the difference increases to over 20 %. The maximum of the corrected time series are 73 % and 58 % for the 5 and 25 cm segments, respectively.

4.7.2 Calibration with constant bulk density

During the sixth soil moisture level, the bulk density varied greatly compared to the previous soil moisture levels. At this stage, the standard deviation of the bulk density was 0.071 g/cm^3 compared to an average of 0.012 g/cm^3 for the previous stages. Therefore, the effect of varying bulk density was investigated by performing the same analysis while keeping the bulk density constant.

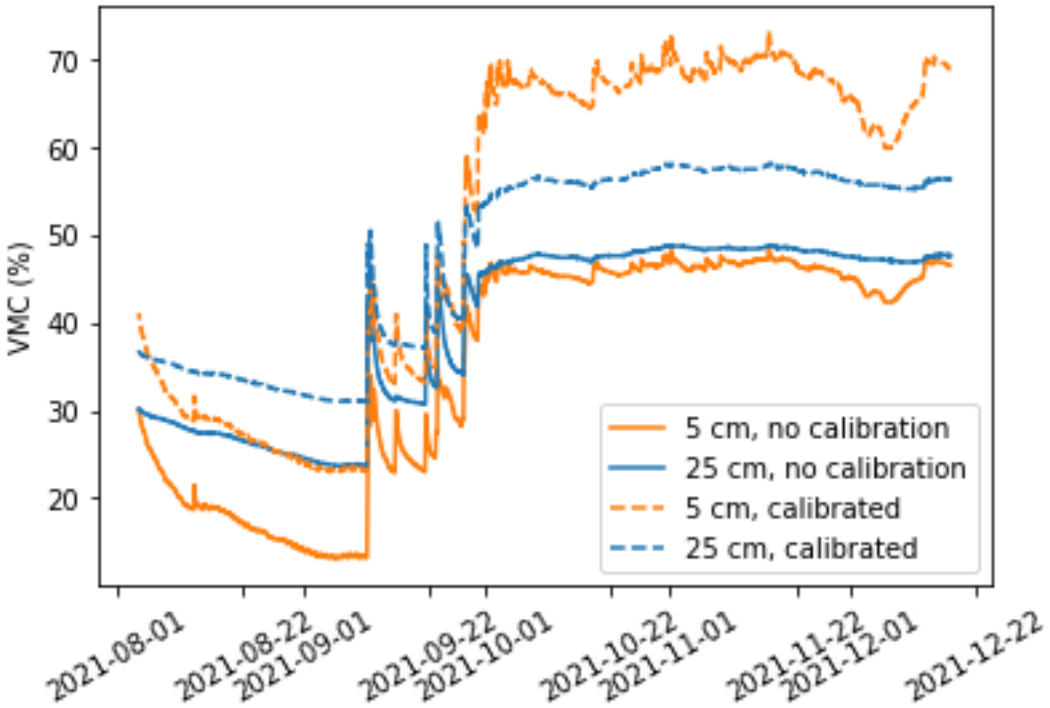

Figure 53: Soil moisture time series from the IoT 1 sensor, with original and corrected values using Equations 13 and 14.

When keeping the bulk density of the soil constant at 1.2 g/cm^3, the third-order polynomial equations became

$$y = 0.0014x^3 - 0.0959x^2 + 2.7302x + 4.0947$$

and

$$y = 0.0009x^3 - 0.0813x^2 + 2.4467x + 3.5928$$

and the R^2 values were 0.9864 and 0.9886.

From Table 14, we see that the RMSE between the sensor readings and the manual soil moisture measurements decreased when correcting the sensor readings for the 5 cm segment, but for the 25 cm, the RMSE increased after calibration.

Table 14: RMSE for the original and calibrated sensor readings with constant bulk density.

Segment		RMSE (%)
5 cm	Original	10.04
	Calibrated	2.33
25 cm	Original	7.53
	Calibrated	10.66

5 Discussion

The objective of this thesis was to investigate how soil moisture content varies in time and space across Søråsfeltet and how these variations are captured by different methods and instruments for measuring soil moisture. This chapter is therefore split in three main sections, where Sections 5.1 and 5.2 discuss the temporal and spatial variability in soil moisture in Søråsfeltet, while Section 5.3 provides a comparison of the soil moisture instrumentation used in the analysis. Lastly, Section 5.4 provides an evaluation of the calibration process of the GroPoint Profile sensor.

5.1 Temporal variability

From Section 4.1, we see that the soil moisture content varied greatly throughout the research period. We also see that the different instrumentation agreed upon the general trends in soil moisture. The changes in soil moisture corresponded well with the occurrence of precipitation, which is in line with what we know from theory and other related studies (Sehler et al., 2019). The effect of precipitation on soil moisture will be further discussed in Section 5.1.4.

Since the lengths of the measurement periods differ between the methods, direct comparison of the different time series is difficult. If possible, measurement periods should be made equal for a better comparison of the different methods of measuring soil moisture. For better representativity, longer time series of soil moisture measurements should be used. Periods longer than a year are preferable, as this enables us to detect seasonal variations in soil moisture. Other studies have used time series spanning over several decades, which in addition enables the climatic effects on soil moisture to be explored (Walker et al., 2004; Qing et al., 2014).

5.1.1 Diurnal variability

From Jackson (1973), it is known that soil moisture varies in a diurnal cycle, as the surface dries during the day and partially re-wets at night. The diurnal variations in soil moisture detected by sensor IoT 1 were less than 1 %, similar to what has been found by Heitman et al. (2003). Such small diurnal variations mean that potential irrigation could be performed regardless of the time of day and that plants on the site do not experience daily drought stress (Ehrnsperger, personal communication, 2022-04-25). However, since the minima in soil moisture occur around 0700 UTC and these variations are less than the instrument uncertainty, the diurnal variations could be due to measurement errors (Heitman et al., 2003).

5.1.2 SoilVUE

During the dry periods, SoilVUE measured soil moisture under 5 % and occasionally zero at 5 cm depth. At 60 cm depth, the minimum value of soil moisture was 8.4 %. These values are lower than what is expected in the area (Nemes, personal communication, 2022-04-26). Unfortunately, no other soil moisture sensors measure at the same depths as the SoilVUE sensor in Søråsfeltet. However, at an agricultural site approximately 8 km northeast of Søråsfeltet, soil moisture measurements have

been taken at depths 5-85 cm from October 2021 to April 2022 (Nemes, personal communication, 2022-04-26). From these measurements, soil moisture was never below 30 % for depths below 10 cm. Even though no dry periods equivalent to summer 2021 occurred in this time period, the measurements indicate that the deeper layers of the soil do not dry out.

Only sandy soils reach soil moisture down to 5 % at their permanent wilting point, when soil water is no longer available to plants (Hillel, 1982). In contrast, this point occurs between 15-20 % for clay soils (Cornell University, 2010). As the soil around Søråsfeltet contains 48 % clay and only 10 % sand (Section 3.1), such low values are unrealistic. The minimum values of the three IoT sensors were thus more realistic, ranging between 13.1 and 19.1 %.

During their study comparing the SoilVUE 10 to two other TDR sensors, Marek et al. (2021) found that the SoilVUE sensor generally reported lower values than the other sensors. These discrepancies were observed at shallow depths, and the performance of the SoilVUE sensor worsened as the soil dried out.

Marek et al. (2021) attribute the low values and poor performance of the SoilVUE sensor to problems with sensor-soil contact. During periods of little moisture, the sensor is surrounded by air, which has a lower dielectric constant than soil and water (Section 3.3). This leads to the measured values being lower than the actual soil moisture in the surrounding soil. It is reasonable to assume that this has contributed to the consequently lower values of the SoilVUE sensor in Søråsfeltet. Furthermore, since the soil in the area is rich in clay, it will also tend to shrink during dry periods, which will further decrease the contact between the sensor and the soil (Section 2.1). However, poor soil-sensor contact cannot explain why the sensor occasionally measured zero per cent soil moisture content. Such low values could, however, arise if the sensor is situated next to rocks (Nemes, personal communication, 2022-04-26).

In addition to these unrealistically low soil moisture values, the SoilVUE sensor also reported values exceeding the soil's porosity during the largest precipitation events. From physical inspection of the sensor, a hole next to the sensor was detected, which would facilitate preferential flow of water and thus give an over-representation of moisture.

According to Campbell Scientific, the threaded design of the SoilVUE 10 sensor is meant to both optimize soil contact and eliminate preferential flow (Dirk Baker, 2019). However, these benefits are not seen in practice. The absence of these benefits could be due to sensor design or have come from the installation process of the sensor. For example, the hole drilled prior to the sensor installation might have been too wide. The suboptimal performance of the SoilVUE sensor might also be partially attributed to conditions specific to the location of the sensor, which will be further discussed in Section 5.2.3.

To date, the research on the SoilVUE sensor is limited. Further testing of the sensor should be conducted to assess the causes of the suboptimal performance of the sensor and whether the sensor can provide reliable soil moisture measurements.

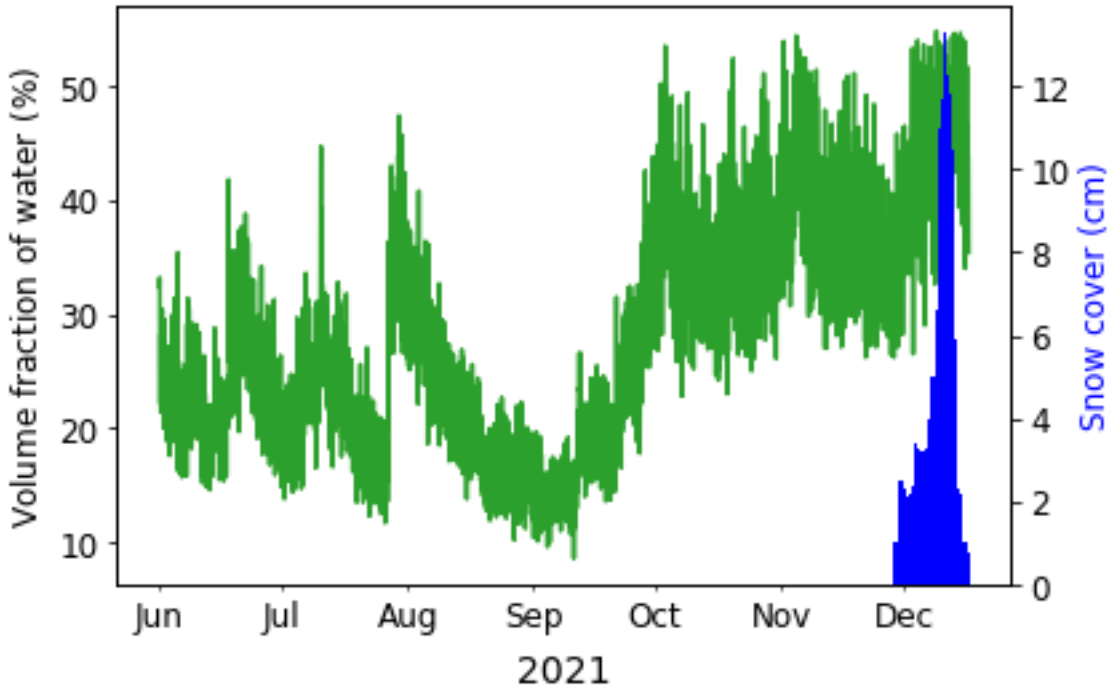

Figure 54: Soil moisture measurements from the COSMOS sensor from June to December 2021 together with hourly snow cover measurements from Søråsfeltet, represented by the blue bars. Note that the soil moisture content and snow depth are not measured in the exact same locations, but about 1.3 kilometers apart.

5.1.3 COSMOS

From the time series of the COSMOS measurements and precipitation in Figure 23, we see that from 26 November, the soil moisture increased even though there was very little rain. In Figure 54, we see the soil moisture measurements from the COSMOS sensor together with snow depth, and we see that the rise in soil moisture content corresponds with the increase in snow depth. Since the soil moisture content determined from the COSMOS sensor depends on the volume of H^+ ions in the area, snow will increase the measured values as it contributes to more H^+ ions (Section 3.3).

The effect of snow on soil moisture measurements from the COSMOS sensor can be corrected for, and one such correction method is under development by NVE (Mengistu, personal communication, 2022-03-08).

As found in Section 4.1, the variability in the soil moisture measurements from the COSMOS sensor varied between different periods and increased after the large precipitation event at the beginning of October 2021. To assess how this variability changes with increasing levels of soil moisture, the mean and standard deviation calculated over a two-day window are displayed against each other in Figure 55. The figure shows that the standard deviation increases with increasing soil moisture values, up to around 41 % soil moisture, after which it decreases. This indicates that soil moisture level influences the variability in the measurements.

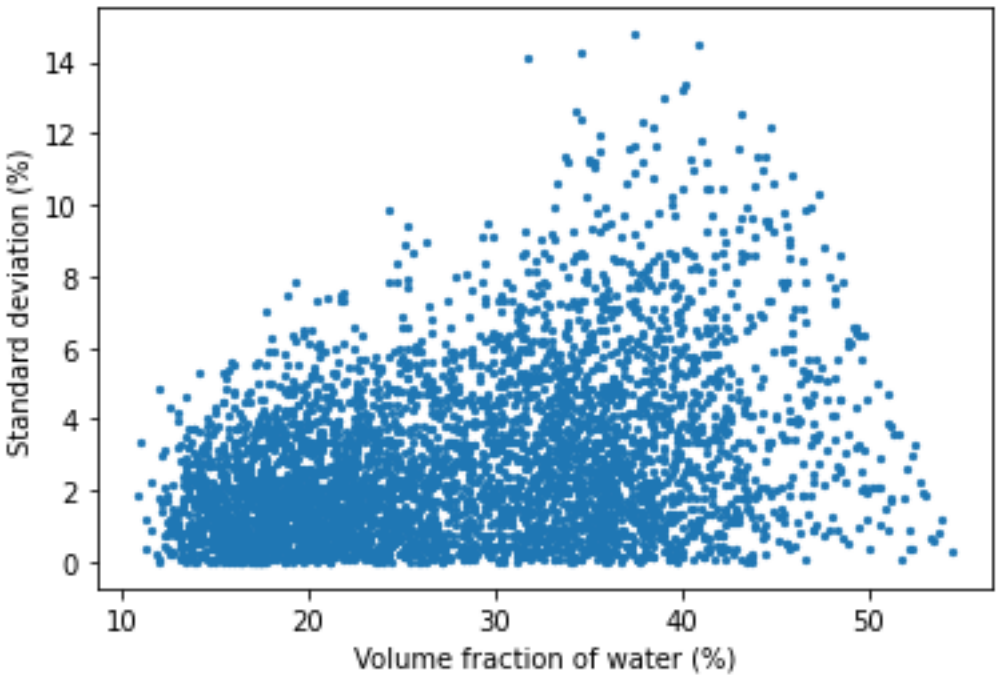

Figure 55: Scatter plot of standard deviation and mean of soil moisture measured by the COSMOS sensor, calculated over a two-day window.

Several other studies have also found the standard deviation as a function of mean soil moisture to have an upward convex shape, with peaks in intermediate soil moisture values (Teuling and Troch, 2005; Vereecken et al., 2007). 41 % soil moisture is, however, towards the higher end of the COSMOS measurements. The shift in this peak can come from a difference in soil types between the sites, the influence of snow on the COSMOS measurements, or simply differences in the windows used for calculating mean and standard deviation.

5.1.4 Effect of precipitation on soil moisture

In Section 4.6, it was found that the response time of soil moisture after precipitation events on 11 and 12 September 2021 was in the order of 0-2 hours, at depths 5-25 cm. The quick response to precipitation indicated that the soil did not become hydrophobic, i.e., water-repellent, during the 1.5 months of drought preceding these precipitation events. The equal response times for depths 5 and 25 cm indicate that infiltration and percolation in the shallower layers were rapid. This is reasonable, as we know from Section 2.1 that the shallower layers of the soil are less dense than the ones beneath and thus have more macropores which facilitate the downward movement of water. At depths deeper than 25 cm, soil moisture increased very slowly, which indicates that the percolation is slow in the deeper layers of the soil due to low permeability.

The slow responses of soil moisture to precipitation at depths below 25 cm might also be attributed to the amount of precipitation. Suppose the amount of precipitation is not enough to saturate the shallower layers of the soil. In that case, water will be

retained in these layers and transport to the deeper layers will only happen through preferential flow in subsurface channels. From Figure 45, it is evident that all depths except 100 cm respond quickly to the precipitation event on 02 October, when 58 mm of precipitation fell. In comparison, only 12.5 mm fell on 11 and 12 September.

Qing et al. (2014) have investigated how precipitation characteristics (amount, intensity, duration) and antecedent soil moisture affect response time and change in soil moisture. They found the degree of soil moisture change to be significantly influenced by precipitation amount and intensity and antecedent soil moisture in some cases. By taking these factors into account, we could better understand the effects of precipitation on soil moisture. This would require longer time series of soil moisture and precipitation measurements to have sufficient events within the different categories of, for example, low, intermediate and high values of soil moisture and precipitation amount.

Unfortunately, little information exists about the response time of clay soils, but in their study, Zhang et al. (2020) found that the response time of sandstone was 4-6 hours after a long drought period. In addition, they found that the response time was similar for depths 0-50 cm. The soil in the case of Zhang et al. (2020) could have become hydrophobic during the drought period, which could explain the long response time. Also, the greater permeability of sandstone than of clay could explain the difference in depths responding to precipitation (Duffield, 2019).

The quick response time of soil moisture to precipitation might also explain the bimodality seen in the distribution of the soil moisture measurements presented in Section 4.3.1. For both the IoT and SoilVUE sensors, some intermediate soil moisture levels have far lower counts than the higher and lower values. For the IoT sensors, these soil moisture levels lie between 30-40 % soil moisture. The low counts of these soil moisture levels indicate that the soil moisture rises rapidly from the lower to the higher values, indicating a high downward subsurface flow in these layers.

5.2 Spatial variability

Not only does soil moisture content vary greatly in time, but from the analysis, it is also evident that it has a large spatial variability across Søråsfeltet.

Spatial variability in soil moisture can result from natural variations in the soil or terrain. Baskan et al. (2013) have found soil texture, especially clay content, to have a large impact on the spatial variability of soil moisture. Yang et al. (2017) found a strong negative correlation between soil moisture and elevation, while Özkan and Gökbulak (2017) compared the effects of forest and herbaceous vegetation cover on soil moisture and found the removal of woody vegetation significantly increased the overall mean daily soil moisture.

5.2.1 Variability in ADR transect measurements

From Figure 25, we see that the variability in soil moisture measurements differs between the different ADR transects. A high variability is to be expected in these measurements, as over 100 measurements were taken across the field on each date.

As mentioned in Section 4.1, the northeast transect has a larger variability than the other transects on most dates. The large variability is on several of the dates due to point location NE6. This is also reflected in Figure 29, where we see that the soil moisture is always higher at this point location compared to the neighbouring locations and that this location has the highest values of soil moisture on several dates. This indicates that the conditions in this particular location are favourable for high soil moisture content.

When investigating the geographical location of the ADR measurements (Figure 15), we see that point location NE6 is situated close to the buildings in the upper right corner of Søråsfeltet. Since the buildings cast shadows, this location is less prone to evaporative water losses, which could explain the higher soil moisture values in this location than in the rest of the transect.

As identified in Section 4.2.1, several other point locations have consistently higher or lower values of soil moisture than their neighbouring locations, such as N5, N8, N13, W11 and W13. These anomalies might be due to any of the natural causes of spatial soil moisture heterogeneity mentioned earlier.

Since variations in, e.g. soil texture, elevation and vegetation cover have a strong impact on soil moisture, their distributions across Søråsfeltet should be further investigated, as this would increase the understanding of the spatial soil moisture heterogeneity.

5.2.2 Variability between IoT sensors

In Section 4.2.2, we saw that during the largest precipitation event of the research period, the IoT 2 sensor in the middle of Søråsfeltet experienced a larger variability in soil moisture than the two other sensors. In addition, Figure 22 showed that the 5 cm segment of the IoT 2 sensor experienced lower values of soil moisture than the others during most of the research period. This segment also experienced more rapid and large peaks in soil moisture from October to December 2021 than the other sensors. Together, these results could indicate that there might be poor contact between the sensor and the soil, as for the SoilVUE sensor (Section 5.1.2). Since both the IoT 2 and SoilVUE sensors, located within 1 meter of each other, deviate from the other instruments, conditions inherent to their location might also have impacted their performances. Therefore, the representability of their location will be discussed further in the following section.

5.2.3 Evaluation of soil measurement field

SoilVUE, IoT 2 and location ZERO of the volumetric method are all located in the same area, in the centre of Søråsfeltet. This area is dedicated to soil measurements, not only of soil moisture but also heat fluxes (Ehrnsperger, personal communication, 2022-04-25).

From Figure 24, we saw that the variability in the volumetric method measurements was distinctively lower in location ZERO than in the other locations during the research period. Since the SoilVUE, IoT, and volumetric method measurements

from this location all deviate from measurements from other parts of Søråsfeltet, the location might not be suitable for representative soil moisture measurements. The high and rapid peaks in soil moisture experienced by the permanently installed sensors are probably due to holes and channels directing water towards the sensors. Such channels might have been formed during the installation of the sensors or can be inherent to the area. Also, irregularities in topography might have contributed to the odd behaviour of these sensors.

By moving the sensors to another location, more representative measurements can be yielded. In this case, the extensive ADR measurements are helpful, as they extend over large parts of Søråsfeltet. Even though the measurements were conducted in a short period with relatively little rainfall, they are still valuable for assessing which locations are representative of the whole field. From the discussion in Section 5.2.1, we know that the soil moisture measurements in some locations are affected by external impacts, such as buildings, while other locations might not be suitable due to natural variations in the soil or terrain. Therefore, these locations should be avoided when moving the sensors. From Figure 29, it seems like the east, southeast, south, southwest, or northwest transects, except for the very start and end of the transects, are suitable alternatives to the current location of the sensors.

5.3 Comparison of soil moisture instrumentation

The range of soil moisture content of the time series measured differs between the instruments. A larger variation in soil moisture measurements from the ADR and COSMOS sensors is expected, as they measure soil moisture over a greater area than the other sensors. The SoilVUE, ADR and COSMOS sensors report values below 10 % during dry periods, while the volumetric method and IoT measurements are always around 15-20 % higher. However, the maximum value obtained from the volumetric method was only 32.5 %, while all other methods experienced soil moisture over 40 %.

The volumetric method and ADR measurements were only carried out from June to September 2021, the shortest measurement period used in this analysis. During the measurement campaign, the maximum daily precipitation was 19.8 mm, while all other instruments experienced the precipitation event in October when 58 mm fell on 02 October. Therefore, the volumetric method and ADR measurements are prone to biases in the soil moisture conditions, making them less representative of the site. This explains the low maxima of the volumetric method. From the histogram of the ADR measurements (Figure 34), the soil moisture measurements over 40 % constitute only a small portion of the total measurements. These extremes were often caused by site-specific conditions favouring high soil moisture, as discussed in Section 5.2.1.

5.3.1 Uncertainty of volumetric method

The volumetric method is often used as a standard for soil moisture measurements. In addition, it is used as a reference when calibrating soil moisture instruments, such as in the calibration of the GroPoint Profile sensor conducted in this thesis.

Therefore, the reliability of this method should be investigated.

One crucial factor for the reliability of the volumetric method is the bulk density of the soil. The standard deviation of the bulk density in each location across Søråsfeltet was 0.14 g/cm^3 on average. This is comparable to what is found in other studies. For example, Lestariningsih et al. (2013) found the standard deviation of the bulk density of clay loam to be 0.13 and 0.14 g/cm^3 at depths 1-10 and 10-20 cm, respectively. Table 7 shows how these variations in bulk density affect the soil moisture content calculated from this method. From the table, we see that the volumetric method measurements across Søråsfeltet, on average, deviate 2.64 % from values calculated using constant bulk densities. The variations in bulk density can arise for several reasons, some inherent to the method and others which can be diminished.

First and foremost, the soil samples were not taken in the exact same location each time. This is an inherent trait of the volumetric method, as it is invasive to the area it is applied in. This means that spatial variability in soil moisture due to natural factors such as soil structure, grass coverage and elevation might have contributed to parts of the differences in bulk density.

Bulk density is also sensitive to the depth at which the soil is located. According to (United States Department of Agriculture, 2019a), "subsurface layers are more compacted and have less organic matter, less aggregation, and less root penetration compared to surface layers, therefore contain less pore space". In general, ensuring that the samples were taken at equal depths was challenging due to the equipment used. By using soil augers instead of a shovel, the soil depth could be more easily controlled.

In addition, during the period in which the volumetric method measurements were conducted, the soil was generally dry and porous. This led to the soil simply running through the cylinder after it was hammered into the ground. Therefore, exactly filling the cylinder to 100 cm^3 was challenging. A different volume of soil would lead to a different soil moisture content being recorded.

Lastly, both the volumetric method and ADR measurements were taken by different people throughout the measurement period. In order to reduce measurement errors, the measurements should be sought to be conducted by the same person.

5.3.2 Comparison of SoilVUE and IoT sensor

The difference between the measurements from the 5 cm segments of the SoilVUE and IoT 2 sensors fluctuated between 15 and 20 % soil moisture content for most of the research period. The large difference observed at the beginning of the research period is likely due to wetting of the soil surrounding the IoT sensor during installation (Ehrnsperger, personal communication, 2022-03-22). However, the difference decreased during precipitation and was reduced to around zero during the largest precipitation events. The difference in soil moisture measured by the two sensors at 5 cm depth was similar both before and after the large precipitation event at the beginning of October. However, for the 20 and 25 cm segments, the difference between the two sensors drastically changed after the precipitation event. Before, the difference was between 20 to 25 %, while it dropped to less than 5 % after the event.

This is in line with what Marek et al. (2021) found in their studies; the performance of the SoilVUE sensor is poorer in dry periods when the contact with the soil is decreased.

For both the 5 and 20 cm segments of the SoilVUE sensor, the deviation from the IoT sensor was close to zero during the largest precipitation events, when both sensors experienced peaks in soil moisture. This is because the increase in the SoilVUE readings was higher than those of the IoT sensor, which indicates that the SoilVUE sensor is more prone to preferential flow than the IoT sensor, most likely due to the hole detected near the sensor. It is also potentially due to the larger diameter of the SoilVUE sensor causing greater disturbance to the surrounding soil.

5.3.3 Improvements of quality controls

To ensure reliable soil moisture measurements, adequate quality controls for the permanently installed soil moisture sensors should be in place.

As mentioned in Section 3.5, only measurements from the 5 cm segment of the SoilVUE sensor were marked with quality code 0, meaning OK after the quality control. According to Wolff (personal communication, 2022-04-09), if an instrument takes measurements at different depths, the quality control from MET is only performed on one of the sensor segments. For the SoilVUE sensor, this means that the quality control has only been performed on the 5 cm segment. To ensure reliable measurements from the sensor, this control should be performed on all segments.

As also discussed in Sections 3.5 and 5.1.2, the SoilVUE sensor occasionally reports unrealistically high and low values of soil moisture. For further improvement of the quality controls, physically meaningful thresholds for the minimum and maximum values of soil moisture should be set specifically for the area. Values outside of these thresholds should be flagged.

Electromagnetic sensors are also sensitive to ice formation as this changes the dielectric constant of the soil. Therefore, periods, where the soil temperature is below zero should also be flagged.

The measurements from the COSMOS sensor did not undergo any quality control before uploading to the server (Mengistu, personal communication, 2022-04-19). A simple check of whether the measurements are within the physical limits of 0-100 % should be in place, and flagging unrealistic values would further enhance the reliability of the measurements. Correcting the COSMOS measurements for snow or simply flagging soil moisture measurements during snow-covered periods would also increase the reliability of these measurements.

5.4 Evaluation of the calibration method for the GroPoint Profile sensor

As the soil texture largely determines the soil water movement, soil-specific calibration of sensors is recommended for obtaining highly accurate measurements (GroPoint, 2010). Therefore, one GroPoint Profile sensor was calibrated in soil from

Søråsfeltet, following the procedure provided by the manufacturer. This section will discuss the results of the process and its feasibility.

5.4.1 General evaluation

By updating the sensor readings using the third-order polynomial obtained from the calibration process, the RMSE values between the sensor and manual soil moisture measurements were diminished for both the 5 and 25 cm segments. When applying the same correction to the IoT sensors installed in the field, however, the corrected sensor readings yielded up to 73 % soil moisture content for sensor IoT 1 (Figure 53) and even more for IoT 2 (see Appendix), which is not realistic for the soil in the area. This suggests that each sensor should be calibrated individually.

A decrease in soil moisture was seen between the sixth and seventh soil moisture level of the calibration process. This was due to a large variation in bulk density at the sixth soil moisture level. New third-order polynomials were obtained using constant bulk density to see whether removing these variations could yield better results. This did not seem to have a positive effect, as the RMSE between sensor readings and manual soil moisture measurements were higher than for the calibration without constant bulk density. In addition, the RMSE of the 25 cm segment calibrated with constant bulk density was higher than for the original sensor readings. This was due to the last three soil moisture levels calculated using constant bulk density being far lower than that measured by the sensor.

The calibration process, as described in Section 4.7, is, in general, a tedious and time-consuming process, especially for soil with high clay content. Before starting the calibration, the soil must be extracted and dried until it contains less than 5 % soil moisture, which could take several weeks. Soil extraction is also limited to periods when the soil is not frozen. For each of the seven or eight soil moisture levels required, taking sensor measurements, soil samples for the volumetric method and increasing the soil moisture takes between 1.5 to 2 hours. After this, the soil must be left to equilibrate for a minimum of one hour. For soils with high clay content, this waiting time is even longer (GroPoint, 2010). Conducting the calibration process took approximately one week.

Another downside of this calibration method is that it is invasive of the area from which the soil is gathered. In this case, approximately 20 litres of soil was extracted from the area, which amongst other things, impacts the flow of water in the area, making it unsuitable for future soil moisture measurements.

5.4.2 Errors and uncertainties

During the several stages of the calibration process, errors and uncertainties that might have impacted the result of the process were introduced.

When preparing the soil before the calibration, the lumps formed were broken down into uniform pieces using hands and a hammer. When breaking down the soil, pores are destroyed, and the structural integrity of the soil is not retained. This means the soil sample is disturbed, i.e., not representative of the area it came from. This

further means that the amount of water needed to reach a certain soil moisture level will differ between the prepared soil and the soil in Søråsfeltet (Nemes, personal communication, 2022-04-26).

The degree of packing of the soil around the sensor significantly affected the sensor readings. Insufficient soil packing leads to air pockets between the sensor and the soil, again leading to the sensor reporting far lower values than expected. The difference between no packing and packing was tested and yielded a difference in around 9 % soil moisture. The medium wet soils are difficult to pack, as they form many lumps that are difficult to break up. Also, when the clay soil is very moist, it must not be packed too tightly around the sensor, as this will push some of the water out of the soil.

During the first five soil moisture levels, the bulk density of the three soil samples did not vary much, with an average standard deviation of 0.012 g/cm^3. However, on the sixth soil moisture level, the standard deviation of the bulk density increased to 0.071 g/cm^3. The standard deviation was 0.053 g/cm^3 for the last soil moisture level. The variable bulk density could arise because of insufficient mixing of the water throughout the soil, but it is more likely due to the loss of soil during the soil sampling. At high soil moisture levels, the clay soil stuck to everything, including the cylinder, which was used to determine the actual soil moisture content. The approximate effect of this loss of soil is a difference in 2.6 % soil moisture. This indicates that this particular calibration method is unsuitable for soils with high clay content.

5.4.3 Suggestions for improvement

An alternative to this calibration process would be to perform the calibration on site. This enables taking sensor readings and soil samples for the volumetric method in representative soil with undisturbed structure, thus giving more reliable results. When placing the sensor in the field, its location should be as representative of the whole field as possible. The spatial variability in the soil samples for the volumetric method should therefore not be a problem (Nemes, personal communication, 2022-04-26).

6 Conclusion & Outlook

During the research period from June to December 2021, soil moisture in Søråsfeltet was confirmed to have large temporal variations. These variations were larger for the shallower depths of the soil. At 100 cm depth, the soil moisture only varied by 1.5 % throughout the research period.

Precipitation was found to be an important driver of the temporal variations in soil moisture at depths down to 75 cm. At depths 5, 10, 20 and 30 cm, precipitation was found to be a statistically significant predictor of soil moisture ($P < 0.05$).

After a dry period of 1.5 months from July to September 2021, the response time of soil moisture to precipitation was on the order of 0-2 hours for depths 5-25 cm. For the intermediate and deeper layers, the increase in soil moisture was slow and small. However, after the largest precipitation event of the research period, these layers also experienced large and rapid increases in soil moisture, indicating that the amount of precipitation determined the rate and amount of change in soil moisture.

Even though Søråsfeltet is relatively homogeneous in vegetation cover and elevation, soil moisture also showed a considerable spatial variation across the site. On particular dates, measurements from the ThetaProbe ML2 sensor (ADR) of soil moisture varied up to 20 % across the field. A high variability in these measurements if expected as over 100 measurements were taken across the field on each date. From the ADR measurements, the spatial heterogeneity appears to be greater when soil moisture is higher. From the cosmic-ray (COSMOS) measurements, displaying the standard deviation as a function of the mean showed an upward convex shape, with a peak around 41 % soil moisture, when calculating the standard deviation and mean over a two-day window. This indicates that the variability in these measurements is also dependent on soil moisture level.

Some systematic variations in soil moisture across Søråsfeltet were detected from the ADR measurements. Measurements taken near buildings were consistently higher than the neighbouring locations, likely due to reduced evaporative losses from shadowing. A few other locations were also prone to higher or lower soil moisture levels, which might be due to natural variations in the soil and terrain.

Overall, the SoilVUE sensor did not show promising performance. Throughout the research period, it consistently measured lower values than the other instruments. All depths above 75 cm measured soil moisture below 15 % during dry periods, and at 60 cm depth, a minimum of 8.4 % soil moisture was recorded. This is unlikely for the soil type in Søråsfeltet and inconsistent with what is observed at other nearby locations. These unrealistically low values cannot be easily explained but could partially be due to rocks or underground structures in the area.

In addition, during the largest precipitation events of the research period, the 5 and 10 cm segments of the SoilVUE sensor recorded soil moisture values exceeding the soil's porosity. The over-representation of moisture during large precipitation events could be explained by holes near the sensor, which facilitate preferential flow of water.

The GroPoint Profile sensor located next to the SoilVUE sensor, IoT 2, also deviated

from the other GroPoint Profile sensors. IoT 2 showed similar behaviour to the SoilVUE sensor by almost consistently recording lower values, except during large precipitation events, when this sensor reported high peaks in soil moisture. Since the temporal variability in the measurements from IoT 1 and IoT 3 are similar, there is strong evidence that the location of the IoT 2 (and SoilVUE) sensor is not representative of Søråsfeltet. Therefore, before concluding on the performance of these sensors, they should be moved to a more representative location.

Before installing soil moisture sensors, it is recommended that the location be investigated using, e.g. ADR measurements to detect anomalies in soil moisture conditions and thus avoid unrepresentative locations.

The calibration method provided for the GroPoint Profile sensors does not facilitate sensor measurements in conditions representative of the area in which the sensor will be installed later. Using disturbed soil in the calibration method makes the results unreliable, as the behaviour of the soil will not be representative of the soil in the area of interest. In addition, the method introduces a range of uncertainties that make the results more unreliable. However, in order to see the results of the calibration in practice, the sensor should be updated with the coefficients obtained from the process and installed in the field.

The method is particularly unsuitable for soils with high clay content, like the soil in Søråsfeltet. As an alternative, a soil specific calibration could be performed on-site, where the sensor readings should be compared to manual measurements from soil samples extracted from the field.

6.1 Further work

Since other studies have found soil texture, especially clay content, to be an essential factor determining the spatial variability of soil moisture, the spatial distribution of texture and clay content in Søråsfeltet should be investigated. This would increase the understanding of the soil moisture variability.

Soil moisture sensors should also be installed across a larger area with differences in land use, soil texture and vegetation to investigate how these factors impact the spatiotemporal variations in soil moisture.

As the summer of 2021 was abnormally dry, the volumetric method and ADR measurements may not have been typical of the site. Therefore, these measurements should be repeated in more meteorologically representative periods. In addition, time series of ADR and volumetric method measurements should be made to overlap with the permanently installed sensors in order to compare the performances of the different instrumentations directly. As the volumetric method is associated with minor uncertainties, these measurements should be used to validate the performances of the other techniques.

To better representativity and detect seasonality in the soil moisture measurements, time series, preferably longer than a year, should be investigated. More extended time series of soil moisture would enable a more thorough investigation of the effects of

precipitation on soil moisture, as one could investigate to which extent precipitation amount, duration and intensity and antecedent soil moisture influence soil moisture.

In addition, remote-sensing measurements of soil moisture should be compared to the ground measurements to assess their accuracy and whether these measurements could be used to represent the soil moisture variations in an area like Søråsfeltet.

In order to ensure the reliability of soil moisture measurements, more adequate quality controls with physically meaningful thresholds should be developed. Information about the site-specific soil properties should be used in order to establish reasonable maximum and minimum values of soil moisture. As electromagnetic sensors are sensitive to ice formation and cosmic-ray sensors are impacted by snow cover, the impacts of these phenomena should be accounted for in the quality controls.

References

Oguz Baskan, Yakup Kosker, and G. Erpul. Spatial and temporal variation of moisture content in the soil profiles of two different agricultural fields of semi-arid region. *Environmental monitoring and assessment*, 185, 07 2013. doi: 10.1007/s10661-013-3343-8.

bioCEED, University of Bergen. Comparing two variances – Fisher's F test. `https://biostats.w.uib.no/1-comparing-two-variances/`. Retrieved 2022-03-29.

G.R. Blake. Particle density. *Encyclopedia of Soil Science*, 04 2008.

Luca Brocca, Luca Ciabatta, Christian Massari, Stefania Camici, and Angelica Tarpanelli. Soil Moisture for Hydrological Applications: Open Questions and New Opportunities. *Water*, 9(2), 2017. ISSN 2073-4441. doi: 10.3390/w9020140. URL `https://www.mdpi.com/2073-4441/9/2/140`.

Kaye L. Brubaker. *Nonlinear dynamics of water and energy balance in land-atmosphere interaction*. PhD thesis, Massachusetts Institute of Technology. Department of Civil and Environmental Engineering, 1995.

Campbell Scientific, Inc. *Product Manual SoilVUE10 Complete Soil Profiler*, 2 2021.

Campbell Scientific, Inc. SoilVUE10. `https://www.campbellsci.eu/soilvue10?gclid=CjwKCAjwve2TBhByEiwAaktM1Gxmw9gM7CU8RUDK1ItttLKzsiyo420EjKQXq8VThdiYUmYhBZN71RoCZksQAvD_BwE`, 2022. Retrieved 2022-05-11.

Mohammad Choker, Nicolas Baghdadi, Mehrez Zribi, Mohammad El Hajj, Simonetta Paloscia, Niko E. C. Verhoest, Hans Lievens, and Francesco Mattia. Evaluation of the Oh, Dubois and IEM Backscatter Models Using a Large Dataset of SAR Data and Experimental Soil Measurements. *Water*, 9(1), 2017. ISSN 2073-4441. doi: 10.3390/w9010038. URL `https://www.mdpi.com/2073-4441/9/1/38`.

Gabriela Civeira. Introductory Chapter: Soil Moisture. In *Soil Moisture*, chapter 1. IntechOpen, Rijeka, 2019. doi: 10.5772/intechopen.83603. URL `https://doi.org/10.5772/intechopen.83603`.

Cornell University. Field Capacity, Permanent Wilting Point and Available Water Capacity. `https://nrcca.cals.cornell.edu/soil/CA2/CA0212.1-3.php`, 2010. Retrieved 2022-06-04.

Wade T. Crow, Aaron A. Berg, Michael H. Cosh, Alexander Loew, Binayak P. Mohanty, Rocco Panciera, Patricia de Rosnay, Dongryeol Ryu, and Jeffrey P. Walker. Upscaling sparse ground-based soil moisture observations for the validation of coarse-resolution satellite soil moisture products. *Reviews of Geophysics*, 50(2), 2012. doi: https://doi.org/10.1029/2011RG000372. URL `https://agupubs.onlinelibrary.wiley.com/doi/abs/10.1029/2011RG000372`.

Delta-T Devices Ltd. *ThetaProbe Soil Moisture Sensor User Manual*, 3 1998.

Dirk Baker. Taking In-Situ Soil Measurements to New Performance Depths. https://www.campbellsci.cc/blog/in-situ-soil-measurements, 2019. Retrieved 2022-04-22.

Glenn M. Duffield. Representative Values of Hydraulic Properties. http://www.aqtesolv.com/aquifer-tests/aquifer_properties.htm, 2019. Retrieved 2022-05-10.

Laura Ehrnsperger, personal communication, 2022-03-22.

Laura Ehrnsperger, personal communication, 2022-04-25.

Dara Entekhabi, Eni G. Njoku, Peggy E. O'Neill, Kent H. Kellogg, Wade T. Crow, Wendy N. Edelstein, Jared K. Entin, Shawn D. Goodman, Thomas J. Jackson, Joel Johnson, John Kimball, Jeffrey R. Piepmeier, Randal D. Koster, Neil Martin, Kyle C. McDonald, Mahta Moghaddam, Susan Moran, Rolf Reichle, J. C. Shi, Michael W. Spencer, Samuel W. Thurman, Leung Tsang, and Jakob Van Zyl. The Soil Moisture Active Passive (SMAP) Mission. *Proceedings of the IEEE*, 98(5): 704–716, 2010. doi: 10.1109/JPROC.2010.2043918.

Michael Galarnyk. Understanding Boxplots. https://towardsdatascience.com/understanding-boxplots-5e2df7bcbd51, 2018. Retrieved 2022-03-21.

Rodger B. Grayson, Andrew W. Western, Francis H. S. Chiew, and Günter Blöschl. Preferred states in spatial soil moisture patterns: Local and nonlocal controls. *Water Resources Research*, 33(12):2897–2908, 1997. doi: https://doi.org/10.1029/97WR02174. URL https://agupubs.onlinelibrary.wiley.com/doi/abs/10.1029/97WR02174.

GroPoint. *GroPoint Profile Multi Segment Soil Moisture & Temperature Profiling Probe Operating Manual*, 12 2010.

Paul D. Hallett, Jörg Bachmann, Henryk Czachor, Emilia Urbanek, and Bin Zhang. *Hydrophobicity of Soil*, pages 378–384. Springer Netherlands, Dordrecht, 2011. ISBN 978-90-481-3585-1. doi: 10.1007/978-90-481-3585-1_195. URL https://doi.org/10.1007/978-90-481-3585-1_195.

R. J Hanks and G. L Ashcroft. *Applied Soil Physics*. Springer Science & Business Media, 1980. ISBN 978-1-4684-0184-4. doi: https://doi.org/10.1007/978-1-4684-0184-4.

Josh Heitman, J. Basinger, G. Kluitenberg, Jay Ham, J. Frank, and Philip Barnes. Field Evaluation of the Dual-Probe Heat-Pulse Method for Measuring Soil Water Content. *Vadose Zone Journal - VADOSE ZONE J*, 2:552–560, 11 2003. doi: 10.2113/2.4.552.

Daniel Hillel. *Introduction to Soil Physics*. Academic Press, San Diego, 1982. ISBN 978-0-08-091869-3. doi: https://doi.org/10.1016/B978-0-08-091869-3.50002-0. URL https://www.sciencedirect.com/science/article/pii/B9780080918693500020.

Ray D. Jackson. *Field Soil Water Regime*, chapter Diurnal Changes in Soil Water Content During Drying, pages 37–55. John Wiley & Sons, Ltd, 1973. ISBN 9780891189008. doi: https://doi.org/10.2136/sssaspecpub5.c3. URL https://acsess.onlinelibrary.wiley.com/doi/abs/10.2136/sssaspecpub5.c3.

A.I. Johnson. Methods of measuring soil moisture in the field. *Water Supply Paper*, 1619, 1962. doi: 10.3133/wsp1619U.

Y.H. Kerr, P. Waldteufel, J.-P. Wigneron, J. Martinuzzi, J. Font, and M. Berger. Soil moisture retrieval from space: the Soil Moisture and Ocean Salinity (SMOS) mission. *IEEE Transactions on Geoscience and Remote Sensing*, 39(8):1729–1735, 2001. doi: 10.1109/36.942551.

M. Krzic, T. Naugler, S. Dyanatkar, and C. Crowley. Time Domain Reflectometry. https://labmodules.soilweb.ca/team/, 2010. Retrieved 2022-03-29.

Miroslav Kutilek and Donald R. Nielsen. *Soil Hydrology*. Schweizerbart Science Publishers, Stuttgart, Germany, 01 1992. ISBN 9783510653874. URL http://www.schweizerbart.de//publications/detail/isbn/9783510653874/Kutilek_Nielsen_Soil_Hydrology_GeoEcol.

Iva Lestariningsih, Widianto, and Kurniatun Hairiah. Assessing Soil Compaction with Two Different Methods of Soil Bulk Density Measurement in Oil Palm Plantation Soil. *Procedia Environmental Sciences*, 17:172–178, 12 2013. doi: 10.1016/j.proenv.2013.02.026.

Keith Little, B. Metelerkamp, and C. Smith. A comparison of three methods of soil water content determination. *South African Journal of Plant and Soil*, 15:80–89, 05 1998. doi: 10.1080/02571862.1998.10635121.

G.W. Marek, S.R. Evett, T.H. Marek, K.R. Heflin, J. Bell, and D. Brauer. Field evaluation of conventional and downhole TDR soil water sensors for irrigation scheduling in a clay loam soil. ASABE Annual International Meeting, 7 2021. URL https://www.ars.usda.gov/research/publications/publication/?seqNo115=384408.

Zelalem Tadege Mengistu, personal communication, 2022-03-08.

Zelalem Tadege Mengistu, personal communication, 2022-04-19.

R. Muñoz-Carpena. Field Devices For Monitoring Soil Water Content. *Bull. Inst. Food Agric. Sci. Univ. Fla.*, 343, 01 2004. doi: 10.32473/edis-ae266-2004.

National Oceanic and Atmospheric Administration. Soil Moisture. https://www.drought.gov/topics/soil-moisture, 2022. Retrieved 2022-05-05.

Attila Nemes, personal communication, 2022-02-10.

Attila Nemes, personal communication, 2022-03-17.

Attila Nemes, personal communication, 2022-03-18.

Attila Nemes, personal communication, 2022-04-26.

Norwegian Meteorological Institute. Data Clarifications. https://frost.met.no/dataclarifications.html. Retrieved 2022-03-29.

Norwegian Meteorological Institute. Hydrometeorology to Operations (H2O). https://www.met.no/prosjekter/hydrometeorology-to-operations-h20, 2020. Internal document.

Norwegian University of Life Sciences. BIOKLIM. https://www.nmbu.no/fakultet/realtek/laboratorier/bioklim/om-fagklim, 2021. Retrieved 2022-02-07.

Viliam Novák. *Evapotranspiration in the Soil-Plant-Atmosphere System*. Springer Verlag, Berlin, 01 2012. ISBN 978-94-007-3839-3. doi: 10.1007/978-94-007-3840-9.

T.R. Oke. *Boundary Layer Climates*. Methuen & Co. Ltd, 1987. ISBN 978-0-415-04319-9.

Jian Peng and Alexander Loew. Recent advances in soil moisture estimation from remote sensing. *Water*, 9(7), 2017. ISSN 2073-4441. doi: 10.3390/w9070530. URL https://www.mdpi.com/2073-4441/9/7/530.

Jian Peng, Clement Albergel, Anna Balenzano, Luca Brocca, Oliver Cartus, Michael H. Cosh, Wade T. Crow, Katarzyna Dabrowska-Zielinska, Simon Dadson, Malcolm W.J. Davidson, Patricia de Rosnay, Wouter Dorigo, Alexander Gruber, Stefan Hagemann, Martin Hirschi, Yann H. Kerr, Francesco Lovergine, Miguel D. Mahecha, Philip Marzahn, Francesco Mattia, Jan Pawel Musial, Swantje Preuschmann, Rolf H. Reichle, Giuseppe Satalino, Martyn Silgram, Peter M. van Bodegom, Niko E.C. Verhoest, Wolfgang Wagner, Jeffrey P. Walker, Urs Wegmüller, and Alexander Loew. A roadmap for high-resolution satellite soil moisture applications – confronting product characteristics with user requirements. *Remote Sensing of Environment*, 252:112162, 2021. ISSN 0034-4257. doi: https://doi.org/10.1016/j.rse.2020.112162. URL https://www.sciencedirect.com/science/article/pii/S0034425720305356.

Amilcare Porporato, Edoardo Daly, and Ignacio Rodriguez-Iturbe. Soil water balance and ecosystem response to climate change. *The American Naturalist*, 164(5):625–632, 2004. doi: 10.1086/424970. URL https://doi.org/10.1086/424970. PMID: 15540152.

Zhu Qing, Xiaofei Nie, Xiaobo Zhou, Kaihua Liao, and Hengpeng Li. Soil moisture response to rainfall at different topographic positions along a mixed land-use hillslope. *Catena*, 119:61–70, 08 2014. doi: 10.1016/j.catena.2014.03.010.

S.G. Reynolds. The Gravimetric Method of Soil Moisture Determination. Part I. A Study of Equipment, and Methodological Problems. *Journal of Hydrology*, Volume 11:258–273, 1970.

Robin Sehler, Jingjing Li, JT Reager, and Hengchun Ye. Investigating Relationship Between Soil Moisture and Precipitation Globally Using Remote Sensing Observations. *Journal of Contemporary Water Research & Education*, 168(1):106–118,

2019. doi: https://doi.org/10.1111/j.1936-704X.2019.03324.x. URL https://onlinelibrary.wiley.com/doi/abs/10.1111/j.1936-704X.2019.03324.x.

Vivek Sharma. Methods and techniques for soil moisture monitoring. *Department of Plant Sciences, University of Wyoming*, 11 2018.

Igor Shiklomanov. *Water in Crisis: A Guide to the World's Fresh Water Resources*, chapter World fresh water resources. Oxford University Press, New York, 1993.

Soil Science Society of America. *Glossary of soil science terms*. Madison, WI, [rev. ed.] edition, 1997. ISBN 0891188274.

Adriaan J. Teuling and Peter A. Troch. Improved understanding of soil moisture variability dynamics. *Geophysical Research Letters*, 32(5), 2005. doi: https://doi.org/10.1029/2004GL021935. URL https://agupubs.onlinelibrary.wiley.com/doi/abs/10.1029/2004GL021935.

George Clarke Topp, J. les Davis, and A. Peter Annan. Electromagnetic determination of soil water content: Measurements in coaxial transmission lines. *Water Resources Research*, 16:574–582, 1980.

UK Centre for Ecology & Hydrology. Cosmic-ray soil moisture monitoring network. https://cosmos.ceh.ac.uk/. Retrieved 2022-05-04.

United States Department of Agriculture. Bulk Density. https://www.nrcs.usda.gov/Internet/FSE_DOCUMENTS/nrcs142p2_053256.pdf, 2008. Retrieved 2022-04-07.

United States Department of Agriculture. Bulk Density / Moisture / Aeration. https://www.nrcs.usda.gov/Internet/FSE_DOCUMENTS/nrcs142p2_050936.pdf, 2019a. Retrieved 2022-05-04.

United States Department of Agriculture. ROSETTA Class Average Hydraulic Parameters. https://www.ars.usda.gov/pacific-west-area/riverside-ca/agricultural-water-efficiency-and-salinity-research-unit/docs/model/rosetta-class-average-hydraulic-parameters/, 2019b. Retrieved 2022-01-19.

H. Vereecken, T. Kamai, T. Harter, R. Kasteel, J. Hopmans, and J. Vanderborght. Explaining soil moisture variability as a function of mean soil moisture: A stochastic unsaturated flow perspective. *Geophysical Research Letters*, 34(22), 2007. doi: https://doi.org/10.1029/2007GL031813. URL https://agupubs.onlinelibrary.wiley.com/doi/abs/10.1029/2007GL031813.

Jeffrey P. Walker, Garry R. Willgoose, and Jetse D Kalma. In situ measurement of soil moisture: a comparison of techniques. *Journal of Hydrology*, 293(1):85–99, 2004. ISSN 0022-1694. doi: https://doi.org/10.1016/j.jhydrol.2004.01.008. URL https://www.sciencedirect.com/science/article/pii/S0022169404000393.

Raymond Weil and Nyle Brady. *Elements of the Nature and Properties of Soils. 2nd edition*. Pearson Education, 2004. ISBN 978-0130480385.

Wikipedia. Soil horizon. https://en.wikipedia.org/wiki/Soil_horizon#cite_note-6, 2022. Retrieved 2022-04-07.

Mareile A. Wolff, personal communication, 2022-04-09.

Mareile A. Wolff and Arne A. Grimenes. Været på Ås 2021. *Institutt for Fysikk, NMBU*, 2021. ISSN 978-82-7636-035-6.

Yang Yang, Yanxing Dou, Dong Liu, and Shaoshan An. Spatial pattern and heterogeneity of soil moisture along a transect in a small catchment on the loess plateau. *Journal of Hydrology*, 550:466–477, 2017. ISSN 0022-1694. doi: https://doi.org/10.1016/j.jhydrol.2017.05.026. URL https://www.sciencedirect.com/science/article/pii/S0022169417303141.

P. Zhang, P. Xiao, and W. Yao. Profile distribution of soil moisture response to precipitation on the Pisha sandstone hillslopes of China. *Scientific Reports*, Volume 10, 06 2020.

Qing Zhu, Kaihua Liao, Yan Xu, Guishan Yang, Shaohua Wu, and Shenglu Zhou. Monitoring and prediction of soil moisture spatial-temporal variations from a hydropedological perspective: A review. *Soil Research*, 50:625, 01 2012. doi: 10.1071/SR12228.

M. Zreda, W. Shuttleworth, Xiangwu Zeng, Christopher Zweck, D. Desilets, T. Franz, and Rafael Rosolem. COSMOS: the COsmic-ray soil moisture observing system. *Hydrology and Earth System Sciences*, 16:4079–4099, 11 2012. doi: 10.5194/hess-16-4079-2012.

Ufuk Özkan and Ferhat Gökbulak. Effect of vegetation change from forest to herbaceous vegetation cover on soil moisture and temperature regimes and soil water chemistry. *CATENA*, 149:158–166, 2017. ISSN 0341-8162. doi: https://doi.org/10.1016/j.catena.2016.09.017. URL https://www.sciencedirect.com/science/article/pii/S0341816216303861.

Appendix

Table A.1: Descriptive statistics for the COSMOS instrument. Columns 25 %, 50 % and 75 % are the 25th, 50th, and 75th percentiles.

Mean (%)	**Std (%)**	**Min (%)**	**25 % (%)**	**50 % (%)**	**75 % (%)**	**Max (%)**
27.96	9.80	8.60	19.80	26.70	35.40	54.80

Table A.2: Descriptive statistics for the three IoT sensors in Søråsfeltet. Columns 25 %, 50 % and 75 % are the 25th, 50th, and 75th percentiles.

Number	**Depth (m)**	**Mean (%)**	**Std (%)**	**Min (%)**	**25 % (%)**	**50 % (%)**	**75 % (%)**	**Max (%)**
1	5	35.46	13.01	13.10	22.23	44.60	46.20	48.30
	25	39.98	9.76	23.70	28.90	47.00	47.90	48.80
2	5	32.81	11.77	14.40	19.90	38.90	43.60	51.90
	25	40.26	8.27	26.70	31.20	45.20	47.60	49.60
3	5	31.40	11.70	19.10	21.40	25.40	46.60	49.10
	25	33.67	10.48	24.50	25.40	26.200	47.70	49.30

Table A.3: Descriptive statistics for the volumetric method and ADR measurements at the different point locations in Søråsfeltet. Columns 25 %, 50 % and 75 % are the 25th, 50th, and 75th percentiles.

Location	**Instrument**	**Mean (%)**	**Std (%)**	**Min (%)**	**25 % (%)**	**50 % (%)**	**75 % (%)**	**Max (%)**
N	Volumetric	19.25	2.55	15.77	17.01	18.97	20.84	24.65
	ADR	16.31	7.96	4.67	8.80	16.23	20.07	34.23
E	Volumetric	20.56	4.04	14.89	18.44	20.42	21.90	32.50
	ADR	15.61	9.15	3.03	8.19	13.93	20.31	38.27
NE	Volumetric	22.44	4.41	14.82	19.39	22.14	24.43	31.25
	ADR	17.04	9.67	1.33	9.70	15.73	21.87	43.07
SE	Volumetric	20.01	3.72	13.16	18.54	19.85	21.42	28.2
	ADR	17.55	8.65	3.70	12.11	16.72	21.25	42.33
S	Volumetric	15.97	5.27	10.19	12.88	14.36	16.17	31.00
	ADR	17.66	9.08	3.17	11.89	15.87	22.68	37.63
SW	Volumetric	20.70	4.43	13.91	17.54	21.47	22.65	29.52
	ADR	18.12	9.10	3.77	11.80	15.90	24.00	38.00
W	Volumetric	20.88	3.79	12.25	18.83	21.14	22.85	29.31
	ADR	18.21	9.31	4.47	10.37	17.63	21.97	41.60
NW	Volumetric	21.33	3.12	15.12	19.72	20.66	22.57	26.73
	ADR	17.80	8.69	5.03	10.03	17.55	21.36	42.53

Table A.4: Descriptive statistics for the SoilVUE sensor, at all depths, after filtering out unrealistic values. Columns 25 %, 50 % and 75 % are the 25th, 50th, and 75th percentiles.

Depth (cm)	**Mean (%)**	**Std (%)**	**Min (%)**	**25 % (%)**	**50 % (%)**	**75 % (%)**	**Max (%)**
5	13.17	10.62	0	3.33	9.75	23.03	47.52
10	14.81	11.74	2.28	4.61	9.27	26.13	49.50
20	22.99	14.44	7.67	10.22	17.00	41.13	46.61
30	24.35	12.81	9.43	12.92	20.19	41.10	42.93
40	26.09	9.05	14.58	17.96	22.87	37.57	38.35
50	25.75	12.89	11.06	13.15	20.19	41.55	42.10
60	30.83	15.54	8.36	15.70	37.26	46.10	46.62
75	43.60	6.15	30.50	43.65	46.22	47.97	48.26
100	44.72	0.16	43.86	44.61	44.70	44.80	46.30

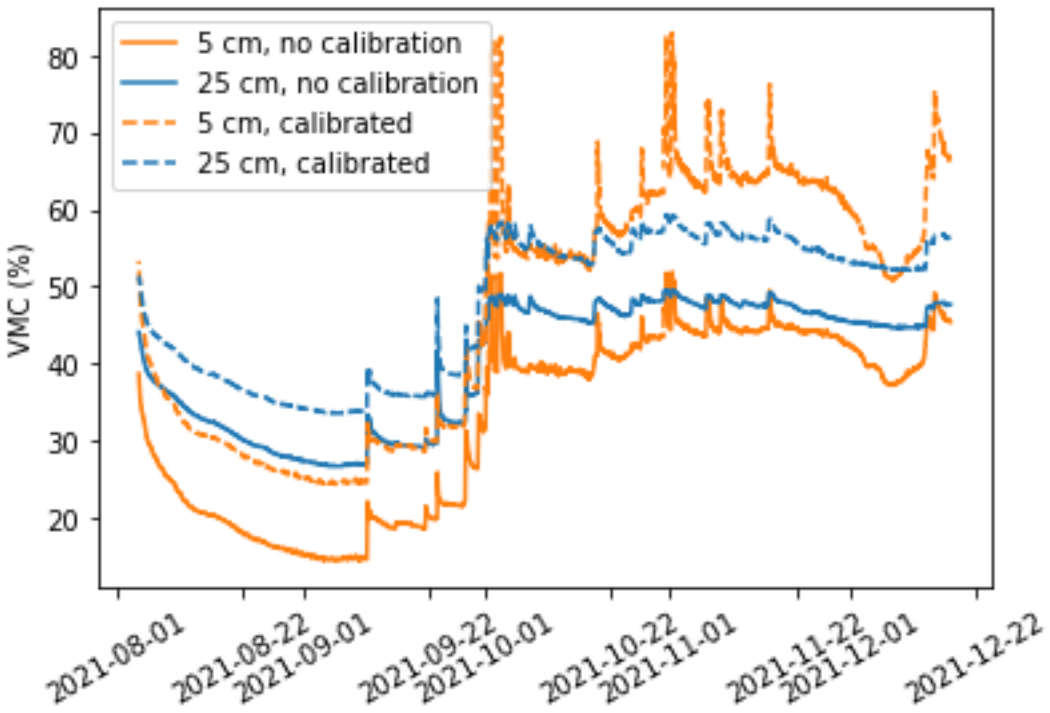

Figure A.1: Soil moisture time series from the IoT 2 sensor, with original and values corrected using the third-order polynomials obtained from the soil-specific calibration process.

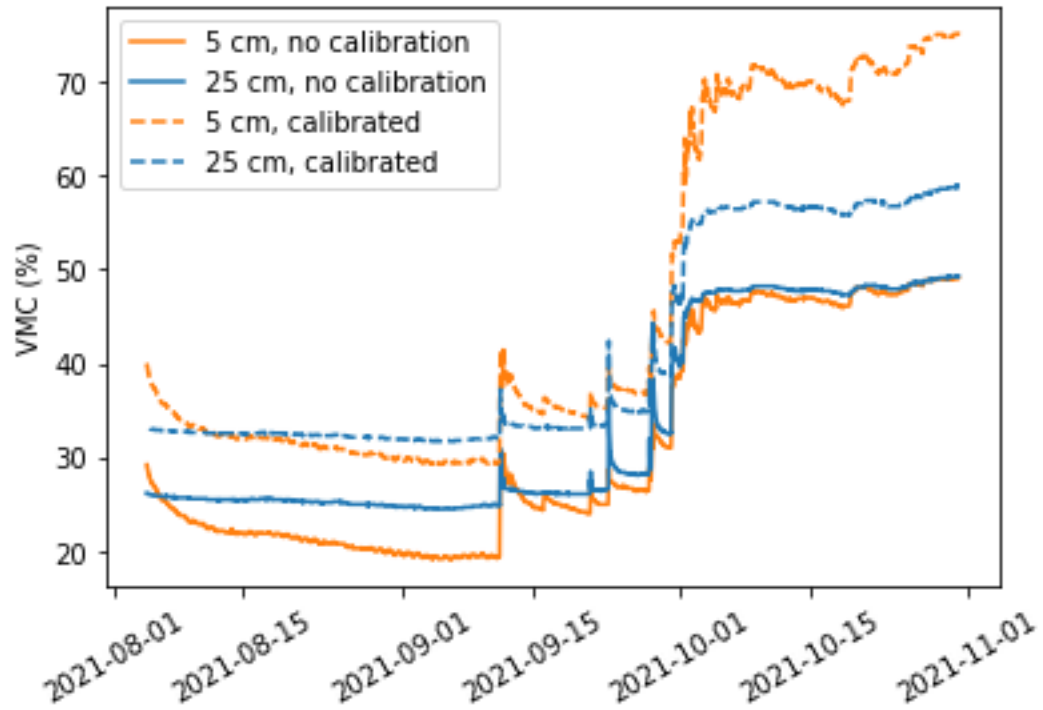

Figure A.2: Soil moisture time series from the IoT 3 sensor, with original and values corrected using the third-order polynomials obtained from the soil-specific calibration process.

Norges miljø- og biovitenskapelige universitet
Noregs miljø- og biovitskapelege universitet
Norwegian University of Life Sciences

Postboks 5003
NO-1432 Ås
Norway